Development of Tungsten Trioxide Nanoparticles for Catalytic and Water Remediation Applications

A thesis submitted towards partial

fulfilment of the requirements for

the degree of

Master of Technology in Nano science and Technology

Submitted by

Arnab Dhara

ROLL NO.: M4NST23017

REG. NO.: 160435

Dr. Sourav Sarkar

Associate Professor

School of Materials Science and Nanotechnology

Jadavpur University

Kolkata -700 032

Course affiliated to:

Faculty Council of Interdisciplinary Studies,

Law and Management, Jadavpur University

Kolkata-700 032, India

M. Tech. (Nanoscience and Technology)
Course affiliated to:
Faculty of Interdisciplinary Studies,
Law and Management
Jadavpur University
Kolkata, India

CERTIFICATE OF RECOMMENDATION

This is in order to certify that the thesis entitled "**Development of tungsten trioxide nanoparticles for catalytic and water remediation applications**" is a legitimate work done by **Arnab Dhara** under our supervision and guidance for the purposes of fulfilling the requirement for the degree of Master of Technology in Nanoscience and Technology in the School of Materials Science and Nanotechnology from the academic session 2021-2023.

Thesis advisor
Dr. Sourav Sarkar
School of Materials Science and Nanotechnology
Jadavpur University, Kolkata-700032

Director
School of Materials Science and Nanotechnology
Jadavpur University, Kolkata-700032

Dean
Faculty Council of Interdisciplinary studies, Law and Management
Jadavpur University, Kolkata-700032

M. Tech. (Nano science and Technology)
Course affiliated to:
Faculty Council of Interdisciplinary
Studies, Law and Management
Jadavpur University
Kolkata, India

CERTIFICATE OF APPROVAL **

This foregoing thesis is hereby approved as a credible study of an engineering subject carried out and presented in a manner satisfactorily to warranty its acceptance as a prerequisite to the degree for which it has been submitted. It is understood that by this approval the undersigned do not endorse or approve any statement made or opinion expressed or conclusion drawn therein but approve the thesis only for purpose for which it has been submitted.

Committee of final examination
for evaluation of Thesis

** Only in case the thesis is approved.

DECLARATION OF ORIGINALITY AND COMPLIANCE OF ACADEMIC ETHICS

I hereby declare that this thesis contains literature survey and original research work by the undersigned candidate, as part of his Master of Technology (Nanoscience and Technology) studies during academic session 2021-2023.

All information in this document has been obtained and presented in accordance with academic rules and ethical conduct.

I also declare that, as required by this rules and conduct, I have fully cited and referred all material and results that are not original to this work.

NAME: Arnab Dhara
ROLL NUMBER: M4NST23017
REG. NUMBER: 160435

THESIS TITLE: Development of tungsten trioxide nanoparticles for catalytic and water remediation applications.

SIGNATURE: **DATE:**

Dedicated to my

PARENTS

for their support and encouragement...

My Sincere gratitude to

All my teachers…

Acknowledgement

In the first place, I would like to express my profound gratitude to my supervisor Dr. Sourav Sarkar for his advice and guidance from the very early stage of this research as well as giving me extraordinary experiences throughout the work. Above all and the most needed, he provided me constant encouragement and support in various ways. Thank you also for the amicable environment conducive to extensive research work at Thin Film and Nanoscience Lab, in which you have welcomed me. All these provided me great support, helping me to confront the difficult periods of my project, which I do not think I would have completed it otherwise.

I want to extend my gratitude to my co-supervisor Dr. Ratna Sarkar for her advices, guidance, and crucial contribution throughout my work. Her involvement with her originality has triggered and nurtured my scholarly development that I will benefit from, for a long time to come. I really cannot value her support and generous cooperation.

I would also like to express my sincere thanks to Prof. (Dr). Kalyan Kumar Chattopadhyay, Dr. Chandan Kumar Ghosh, Dr. Mahua Ghosh Chowdhury for their help, support, encouragement, suggestion and advice during the course of the research. Their enthusiasm provided me a helpful and effective way of learning which in turn inspired me to follow the research project with great enthusiasm.

I extend my heartiest thanks to all my seniors of “Thin Film & Nano Science lab” especially Riyaz da, Dimitra di, Manas da, Nabamita di, Ankita di, Sreya di, and everyone in this lab for extending their helping hands. I would also like to thank all my friends Aaishiki, Gourav, Abhrajit, Sampurna, Soudip for their encouragement and cooperation.

In this context, I would like to thank the University with Potential for Excellence scheme (UPE-II), Department of Science and Technology (DST) and TEQIP programme for funding

various projects. Furthermore, I would wish to thanks the Department of Physics, Jadavpur University for throughout my Project's journey.

Most importantly, no word of thanks can sum up to the gratitude that I owe to my family members, especially my mother, father, brother, sister-in-law and my sweet niece. Their encouragement, patience, unconditional love, and blessings gave me the strength to complete this dissertation.

Finally, I would like to thank all my well-wishers, friends and teachers whom I will always keep in my mind throughout my life.

June 2023 Arnab Dhara

School of Materials Science and Nanotechnology

Jadavpur University

Kolkata -700 032

Abstract

Energy and fresh water are two of the most basic and essential elements of nature, and are two of the most rapidly depleting resources on the planet. This is due to extensive industrialization, excessive consumption, and overpopulation. Water is the basic need for life to survive, and approximately 70 % of the earth is covered with this precious component. However, it is very regrettable to discuss that less than 0.5 % of the earth is available as fresh water. Around 1.3 billion people on this planet face severe water scarcity because they lack access to fresh and drinkable water. As a result of rapid industrialization and irresponsible human activities, many different types of pollutants are being thrown directly into the water distribution system, including inorganics, organics, and biological. Fortunately, over the past few years, many researches and a variety of approaches have been explored to develop efficient and pollution-free technology to convert highly polluted and toxic water pollutants to non-toxic products for waste water management. Among many technologies, photocatalysis has emerged as one of the most efficient and eco-friendly, as it represents a green and economical way to demineralize pollutants by using sunlight energy or energy from an artificial source of light. As well as removing organic pollutants (like dyes, pesticides, herbicides, and phenolic compounds), heavy metals, and harmful bacteria and fungi, photocatalysis is also effective at removing heavy metals.

The removal of organic contaminants from water systems via photocatalytic degradation has gained popularity as a promising method. Using WO_3, ortho hydrated tungsten trioxide, WO_3/g-C_3N_4 (before and after annealing), and WO_3/exfoliated g-C_3N_4 (before and after annealing), the photocatalytic degradation of Rhodamine B (RhB) dye was examined in this study. The objective was to assess the effectiveness of photocatalysts in the degradation of hazardous RhB dye and explore the synergistic interactions between tungsten trioxide nanoparticles with graphitic carbon nitride and exfoliated graphitic carbon nitride. The

pristine tungsten trioxide and the nanocomposites were synthesized using a facile hydrothermal method. Powder X-ray diffraction (PXRD), Field emission scanning electron microscopy (FESEM), Fourier transform infrared spectroscopy (FTIR), Photoluminescence spectroscopy (PL), and UV-VIS DRS were used to assess the structural, morphological, compositional, and optical characteristics of the photocatalysts. The outcomes showed that the most improved photocatalytic activity was observed in tungsten trioxide/exfoliated graphitic carbon nitride photocatalyst about 89.13 % in 30 minutes duration. RhB dye degradation took place when it was exposed to visible light. The concentration of RhB dye was monitored at regular intervals using UV-Visible spectroscopy. According to the experimental findings, pristine tungsten trioxide and its nanocomposites both exhibited considerable photocatalytic activity towards the breakdown of RhB. Exfoliated graphitic carbon nitride may have synergistic effects with tungsten trioxide, as evidenced by the nanocomposite's improved degradation efficiency when compared to all other synthesized samples. The photocatalytic process followed pseudo first order kinetics and the degradation rate constants were determined. Thus, by incorporating exfoliated g-C_3N_4 with WO_3 enhances the photocatalytic performance indicating the potential of this nanocomposite for the treatment of organic pollutant in waste water treatment. The results of this study aid in the creation of effective and long-lasting photocatalytic materials for use in environmental remediation applications.

The synthesized samples have been considered to very active catalyst, because it can use visible light as an excitation source, it can also use solar radiation for future wastewater treatment and energy generation applications.

Keywords: Photocatalysis, Transition metal oxide, Tungsten tri-oxide (WO_3), Nano-composite, Water Remediation.

June 2023 Arnab Dhara

School of Materials Science and Nanotechnology

Jadavpur University

Kolkata -700 032

Table of Contents

Chapter 2: Review of past work

Chapter 3: Instruments and apparatus

Chapter 4: Synthesis process

Chapter 1

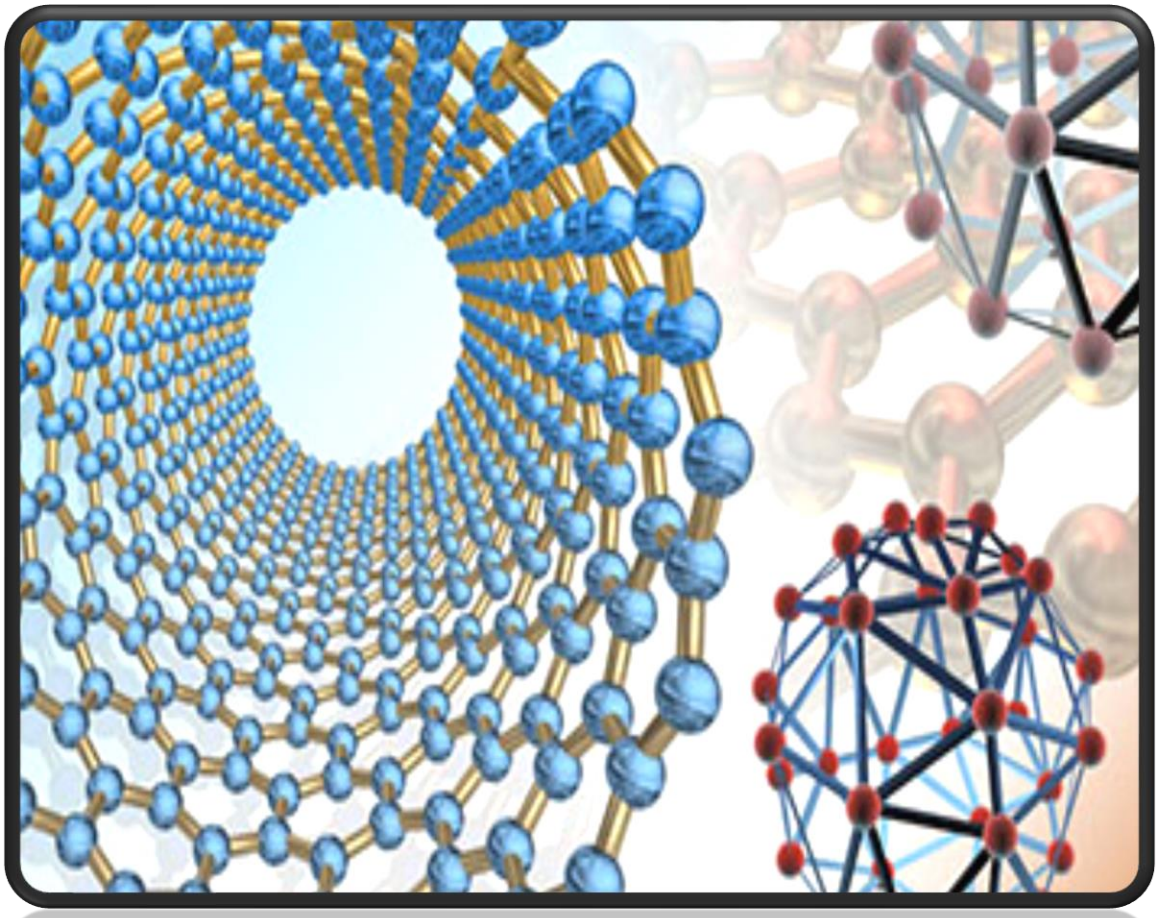

Introduction

1.1 Nanoscience

Nanoscience refers to the study of matter and their properties at nanoscale (1 nm = 10^{-9} m) [1]. As when the dimensions are converted from bulk to nanoscale due to the due to the increase of surface area to volume ratio which leads to the enhancement of mechanical properties, chemical reactivity, electrical and many other properties such as surface tension, catalytic property [2].

1.2 Nanomaterials

Nanomaterials are materials which consist of particles or constituents possessing minimum one of the external dimensions in the range of nanoscale (i.e., 1-100 nanometre) [2]. Nanomaterials can naturally occur or can be created as the by-products of combustion reactions it can be produced purposefully through various engineering procedures for specialised functions. This material, have enhanced physical and chemical properties from their bulk counterparts.

1.3 Nanotechnology

Nanotechnology refers to the branch of engineering science which deals with designing and producing structures and devices by manipulating atoms and molecules at nanoscale [3].

1.4 Benefits of nanomaterials over their bulk counterparts

- When the size of the material is converted from bulk to nano it leads to the increase in surface area to volume ratio which in turns increases the chemical reactivity of the material and open up possibilities for creation of new materials and facilitates the chemical processes [4].
- It can even notice the enhancement of thermal and catalytic properties of nanomaterials over their bulk counterparts. This is due to the fact that nanomaterials

possess high surface area which in turn shows that the surface atoms have pronouncing effect on physical and chemical properties of nanomaterials.

- The defects in the materials are removed in nanomaterials that cause reduction of mechanical failure and high mechanical strength is achieved.
- The electrical properties such as the electrical conductivity of nanomaterials such as carbon nanotube (CNT) and graphene oxide (GO) are tremendously increased [5].
- The nanomaterials have high porosity that leads to an increase in its demand for industrial purposes [6].
- Nanotechnology is prevalent in energy sector as they can provide or pave a pathway for efficient and cost-effective method for energy generation [7].
- Thus, in nanoscale the mechanical, electrical, chemical and optical properties of the materials are enhanced effectively from their bulk counterparts.

1.5 Disadvantages of Nanomaterials

- The synthesis of nanomaterials is bit more difficult and complex due to the lack of proper knowledge.
- Nanomaterials used in nanotechnology are unstable.
- They are hard to recycle.
- They may be toxic to humans.

1.6 Classification of nanomaterials based on dimensions

- Zero dimension-fullerenes, rings, quantum dots, atomic clusters.
- One dimension-nanotubes, whiskers and belts, fibres and filaments, spirals and springs.
- Two dimension-nano discs, nanolayers.
- Three dimension-embedded clusters, equiaxed crystallites.

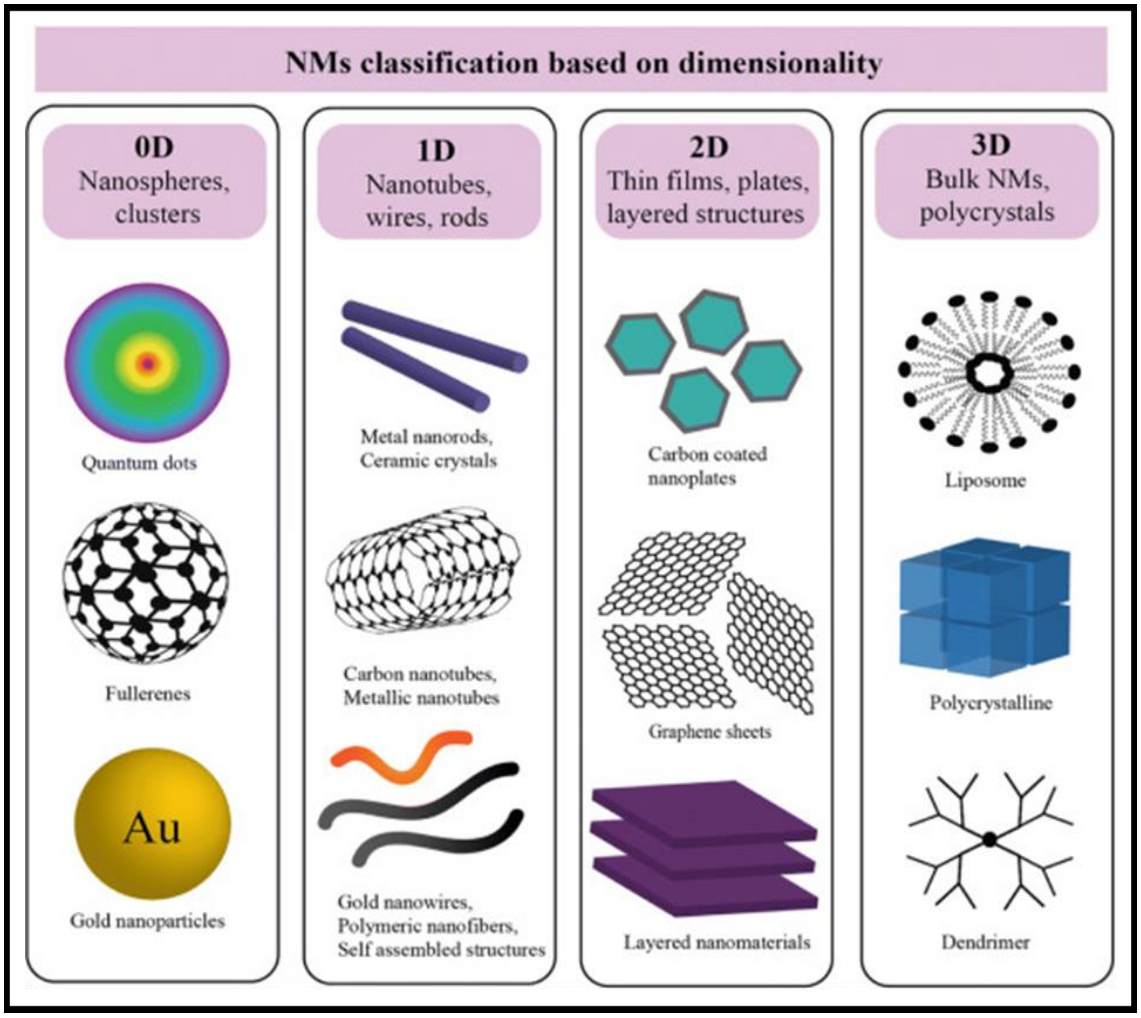

Fig. 1.1: Classification of nanomaterials based on dimensions

1.7 Classification of nanomaterials based on materials

- Carbon based nanomaterials, carbon based nanomaterials include-graphene oxide, fullerenes, carbon based quantum dots, and carbon nanotube (CNT).
- Organic based nanomaterials and comprises of chitosan, cationic quaternary polyelectrolytes, N-halamine compounds and quaternary ammonium compounds.
- Inorganic based nanomaterials and comprises of metal and nonmetal elements or taking the form of an oxide, chalcogenide, hydroxide or phosphate compound.
- Composite based nanomaterials and composite nanomaterials consist of two or more components of nanoscale with special chemical and physical properties [9].

1.8 Properties of nanomaterials

- Mechanical properties to the addition of nanoparticles of the common materials, leads to the refinement of grain structure and the formation of intergranular or an intragranular structure that in turn lead to the improvement of grain boundary structure thereby improving the mechanical properties [10].
- Electrical conductivity of nanoparticles such as graphene oxide and carbon nanotubes shows some of the highest electrical conductivities for their uses in the application of EMI [11].
- Piezo-electricity to the ability of a material to become polarized electrically when they are stimulated mechanically. They also undergo strain when applied an electric field across it [12].
- Chemical reactivity of the nanomaterials are chemically more reactive in nature because they are having high surface area and possess high surface energy.
- Optical properties such as absorption, reflection, light emission and transmission are dynamic in nature and vary significantly from their bulk counterparts.
- Surface tension of the nano-structure is greater than their bulk counterparts. It can increase the surface tension and convert the hydrophilic character of material to hydrophobic character by variation of size of the material.

1.9 Synthesis of Nanomaterials

The two basic approaches to nanomaterial synthesis are:

a. Top-down approach

In top-down approach the bulk material is converted to nanoparticles by mechanical process of crushing or breaking like ball milling.

b. Bottom-up approach

The approach in which the nanoscale dimensions particles is assembled to larger structures by physical or chemical forces [13].

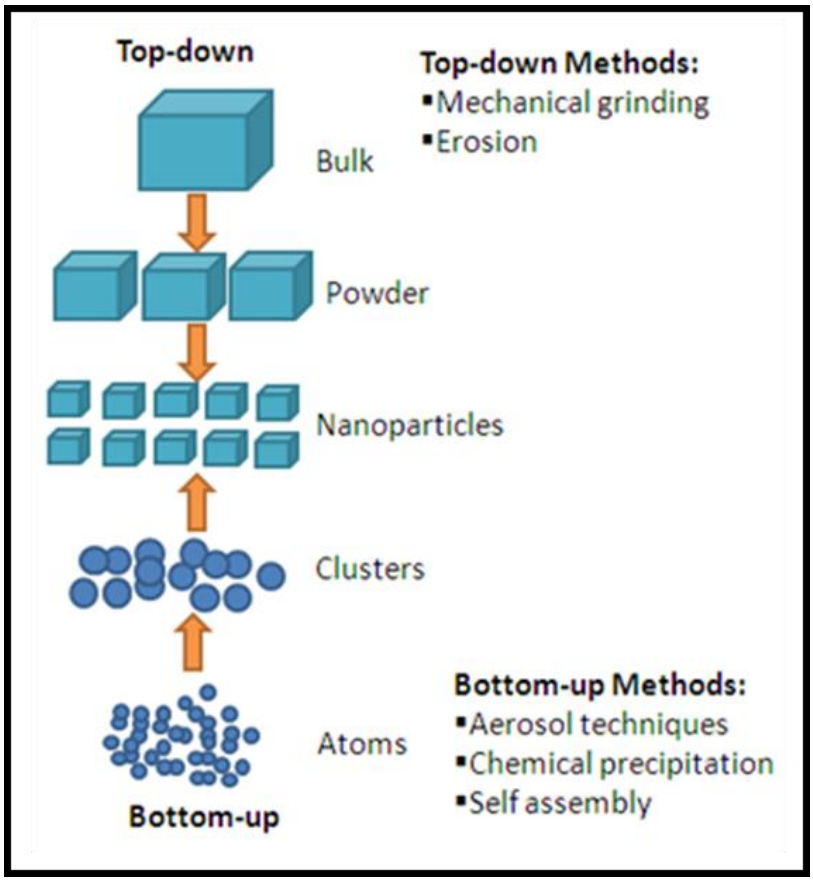

Fig. 1.2: Schematic diagram of synthesis of nanomaterials by top down and bottom approach

Various Synthesis processes are:

1.9.1 Ball milling

Ball milling is a method of production of nanomaterials. The process is used in the production of ceramic and metallic nanoparticles. The mills are equipped with grinding media composed of steel or wolfram carbide. The metallic ball is used to break the material from bulk to nanoscale. The fundamental principle of reduction in size in mechanical attrition devices lies in the energy imparted to the sample during impacts between the milling media.

The balls rotate around the horizontal axis partially filled with materials to be ground plus the grinding medium. The balls rotate with high energy inside a drum and then fall on the solid with gravity force and crush the solid into nanoparticles. The significant advantage of this method is that it can be used commercially. Ball milling are used to make boron nitride nanotubes and carbon nanotubes. Ball milling is a preferred for synthesis of metal oxide nano crystallites like zinc oxide and cerium oxide [15].

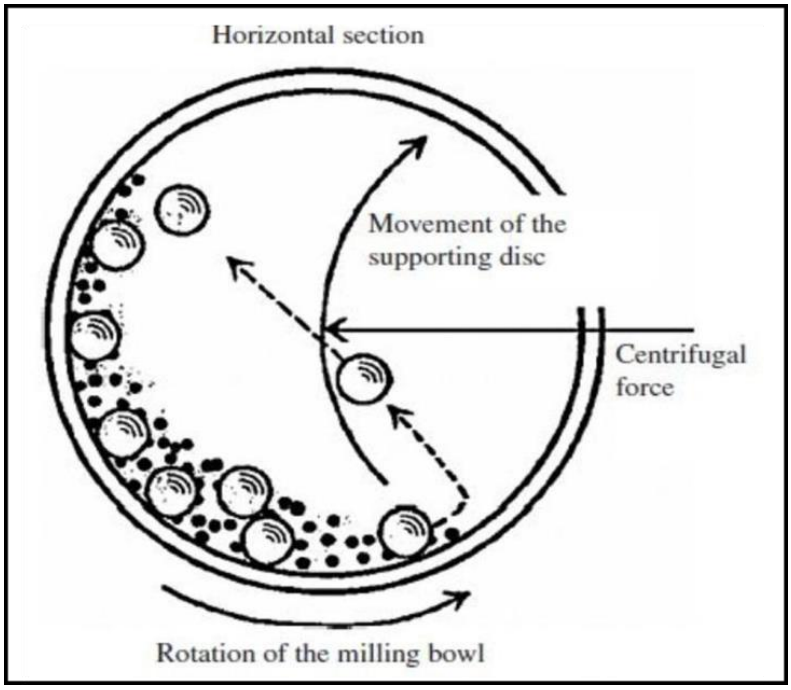

Fig. 1.3: Synthesis of nanomaterials by ball milling

1.9.2 Laser Ablation

The nanoparticle by laser ablation leads to the generation of nanoparticles by ablating on a solid target that lies in a gaseous or a liquid environment and we can get the nanoparticles in nano powder form or a colloidal solution. It is an easy and a fast method of nanoparticles synthesis as it does not have long reaction time or multiple reaction steps. It does not require any toxic chemical for its synthesis. Thus, it is environment friendly or green method. We can also add ligand to the particles after synthesis process or we can add suitable solvent itself so that it can be coated on the surface of nanoparticles [16].

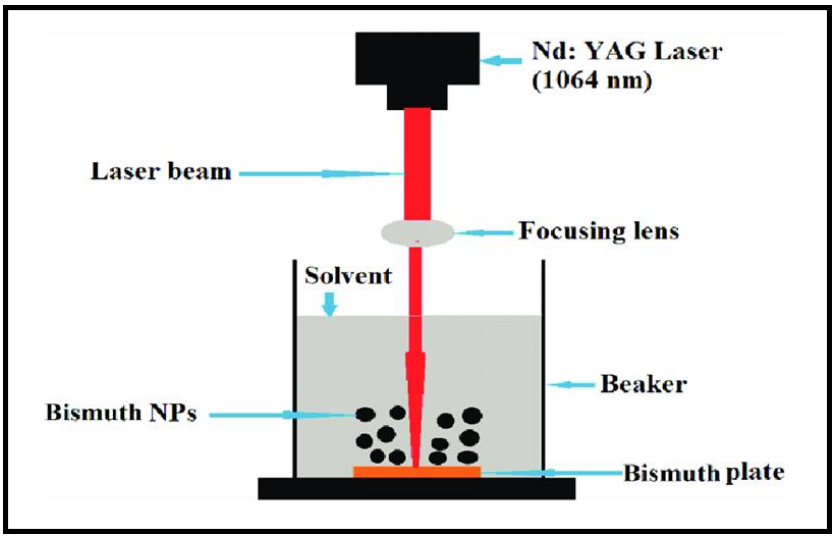

Fig. 1.4: Laser Ablation method for synthesis of nanoparticles

1.9.3 Chemical Vapour Deposition (CVD)

It is the formation of solid non-volatile film on the surface of the substrate by the reaction of vapour phase chemicals (reactants) that contain the required components. The reactants gases are introduced into a reaction chamber and reacted at the heated surface of the substrate to form the thin film. Fundamental principle is that a chemical reaction takes place between the source gases. The product of which is a solid material that condenses on the surface of the substrate inside the reactor. Precursors gases (often diluted in carrier gases) are delivered into the reaction chamber at approximately ambient temperature.

Sequential steps in CVD:

A. Transport of the reacting gases on the substrate surface.

B. The species are absorbed on the substrate surface.

C. The substrate surface catalyses heterogenous surface reaction.

D. Desorption of gaseous reaction by products takes place.

E. The reaction by products is transported away from the substrate.

- The above steps which take place at slowest rate will determine the rate of deposition and is termed as rate limiting step.

- If the deposition process is governed by step1. It is known as mass transport-controlled process.
- If the deposition is governed by step 2,3 or 4 it is known as surface-controlled process.
- Coatings provided by CVD process are fine grained, pure and impervious in nature.
- Energy sources for CVD processes are Resistive heating (Tube furnace), Radiant heating (halogen lamps), and Radio frequency heating (induction heating lasers).
- The precursors in CVD process must be volatile but at the same time it should be stable enough to be delivered to the reactor [17].

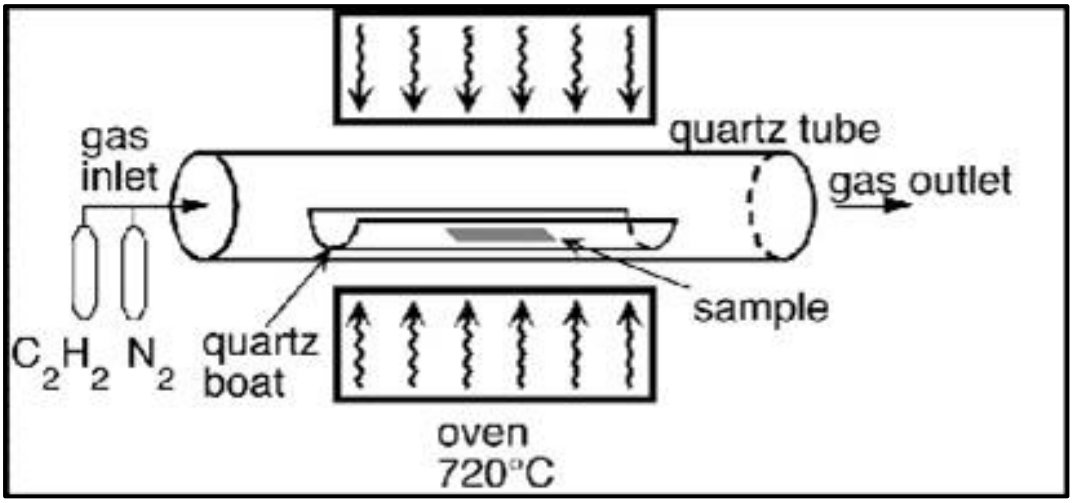

Fig. 1.5: Schematic diagram of CVD

1.9.4 Physical Vapour Deposition (PVD)

Physical vapour deposition is a process of deposition of thin film of material on the substrate surface. The materials are converted into vapour phase which are to be deposited on the substrate surface by physical means. A region of low pressure exists from source to substrate for transportation of the vapour. Condensation of vapours takes place on the substrate surface for the formation of the thin film. The main difference of PVD from CVD is that the deposition of thin film on the substrate surface occurs by condensation whereas in CVD it takes place by chemical reaction [19].

1.9.5 Sputtering

Sputtering is a deposition technique consists of the following steps:

a. Ions are generated and directed at the target material.

b. The ion sputter atom from the target material.

c. The sputter atoms get transported to the substrate surface through a region of reduced pressure.

d. This sputter atom condenses on the substrate forming a thin film [20].

Types of sputtering:

1.9.5.1 RF sputtering

- It allows sputtering of target that is electrical insulators.
- During one half of the cycle the argon ions are attracted towards the target.
- The electrons build up negative charges which act as the self-bias for attracting argon ions which does the sputtering.

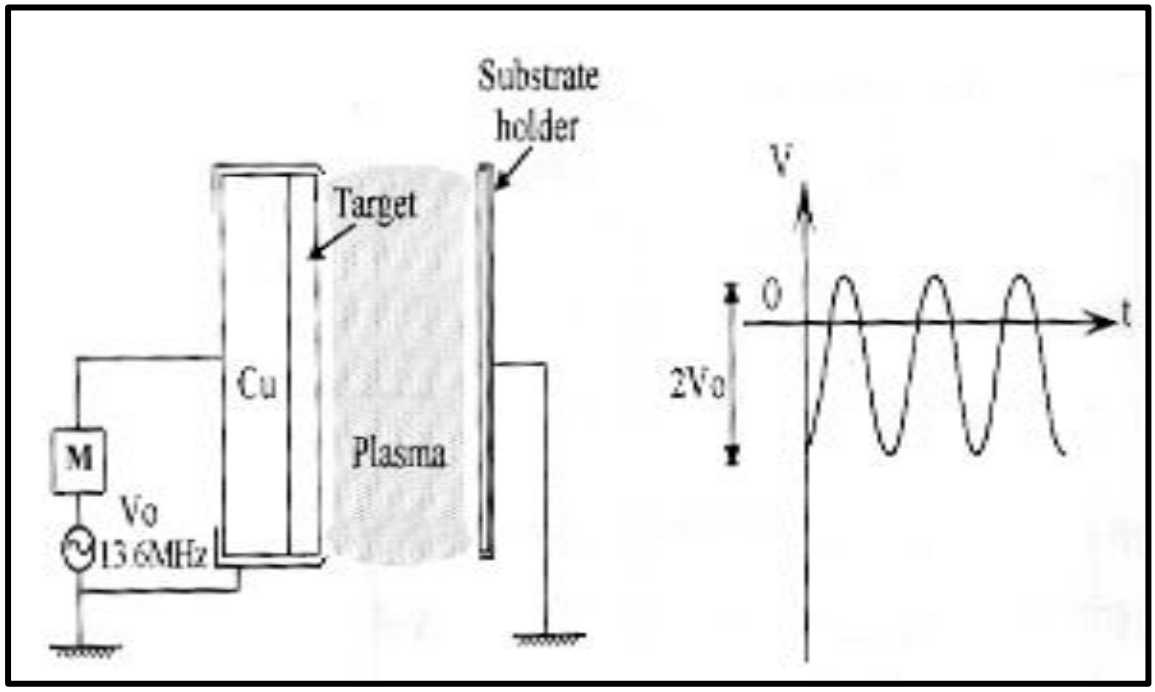

Fig. 1.6: Schematic diagram of RF sputtering

1.9.5.2 DC sputtering

- Sputtering can be done with the application of a large DC voltage (approximately 2000V).
- A plasma discharge is established and the argon ions will be attracted to an impact sputtering of the target atoms.
- In DC sputtering the target must be conductive electrically which in turn otherwise lead to the accumulation of ions and repel other argon ions.

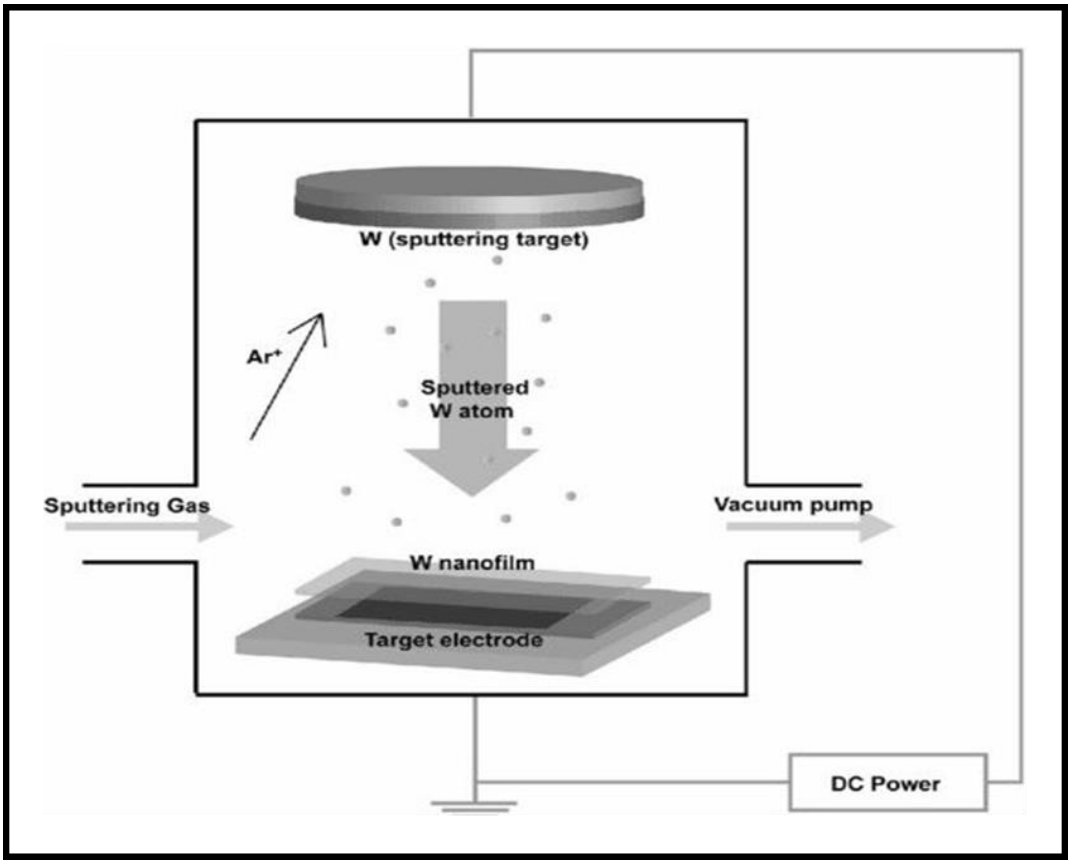

Fig. 1.7: Figure showing DC sputtering

1.9.5.3 Magnetron Sputtering

- The magnetic field is applied parallel to the surface of the target and is superimposed to the electric field applied so that secondary electrons which are emitted by the surface of the target during bombardment are trapped near the target surface.

- A single electron leads to the ionisation of several argon atoms before it is lost on the chamber walls by recombination.
- The ionization at the target surface increases which in turn increases the deposition rate.

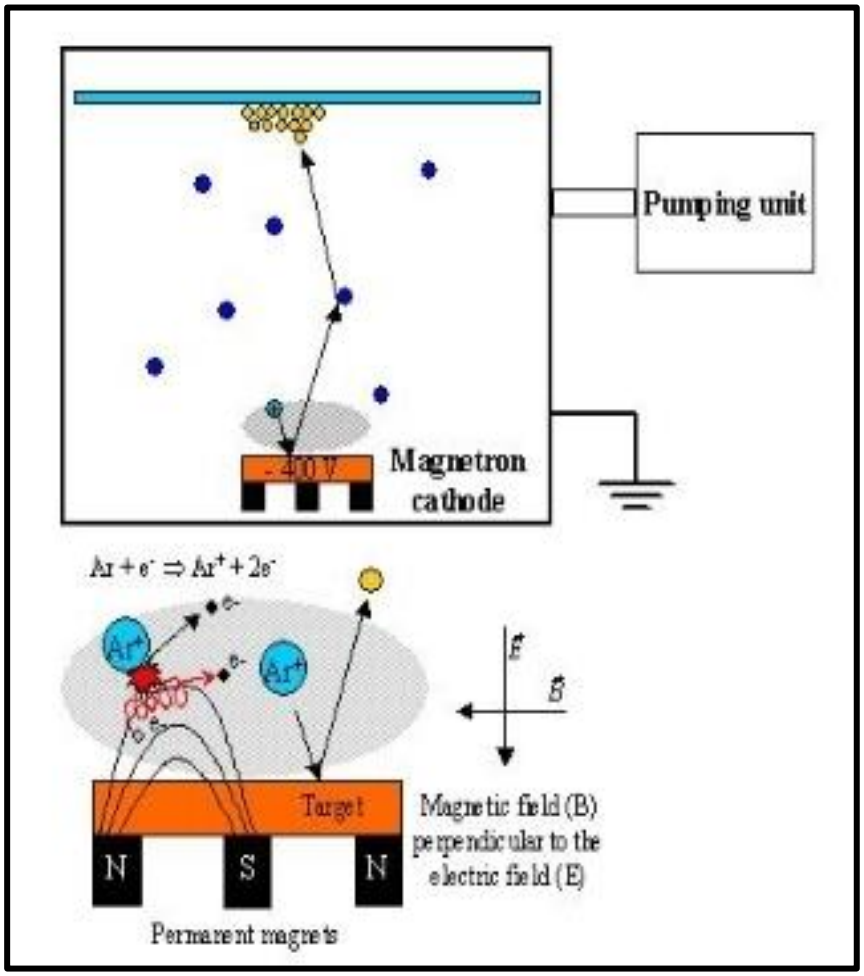

Fig. 1.8: Schematic diagram of magnetron sputtering

1.9.6 Sol-Gel technique

The sol is the name of a colloidal solution made of solid particles, few hundred nanometre in diameter, suspended in a liquid phase. The gel can be considered as a solid macromolecule immersed in a solvent. The sol gel technology is a well establish colloidal chemistry technology, which offers the possibility to produce various materials with novel, predefined

properties in a simple process and at relatively low cost. The main benefit of sol-gel is its high purity and uniform nanostructure available at low temperature [21].

1.9.7 Hydrothermal Synthesis

The hydrothermal synthesis uses aqueous medium as the reaction system in a reaction vessel which is specially closed to provide a reaction environment of high pressure and temperature by heating and pressurizing the system in oven. In hydrothermal synthesis the nanomaterials can be synthesized with a wide variation of temperature ranging from room temperature to very high temperature. The morphology of the material is controlled by the application of low or high pressure depending on the reaction composition vapour pressure. Nanomaterials having high vapour pressure can be produced with minimum material loss. In this case the aqueous mixture of precursor is heated in a sealed stainless-steel autoclave above the boiling point of water and consequently the pressure within the reaction is dramatically increased above the atmospheric pressure. The synergistic effect of high temperature and pressure provides a one-step synthesis process to produce high crystalline materials without the need of post annealing treatments. The technique is useful when it is difficult to dissolve the precursors at low temperatures or room temperature.

Instrumentation

- The hydrothermal process is carried out in a sealed reactor known as Autoclave, a high -pressure bomb or a pressure vessel.
- It is specific style of strong vessel that we intend to face up to better pressure and high temperature from within.
- The autoclave consists of cylindrical vessel which is thick and steel walled having hermetic sealing which allows it to bear high level of pressure and temperature with utmost safety.

- Mostly the hydrothermal reactors consist of Teflon or an extra container made of Teflon to give protection to the autoclave body from the highly corrosive solvents.

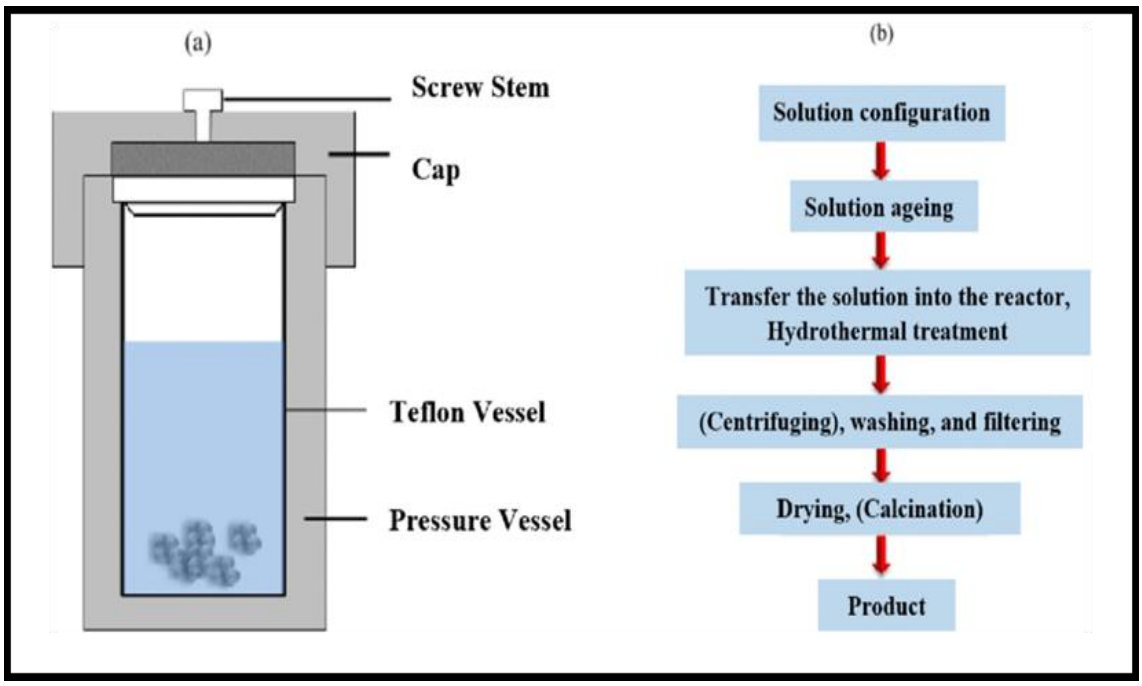

Fig 1.9: (a) Schematic diagram of the Teflon along with the stainless-steel autoclave, (b) Process flow of hydrothermal treatment

Mechanism of crystal growth by hydrothermal process

- Synthesis of nanomaterials by hydrothermal method is a crystallization process directly from solutions that usually involves two steps: crystal nucleation and subsequent crystal growth.
- Nucleation occurs when the solutes exceed the limit of solubility in the solution i.e., when the solution is supersaturated.
- It is an irreversible reaction, the solutes precipitates into clusters of crystals that leads to the growth in macroscopic size.
- Following nucleation, the crystals grow sequentially via a series of process involving the incorporation of growth units, having the composition same as crystal entities but possess the same or different structures from the bulk solution into existing crystal entities and causing increased size.

- The process can be categorized as follows: units are transported through the solutions, units are attached to the surface, movements of units on surface and attachment of units to the growth sites [22].

1.10 Application of nanotechnology

- Food industry-Polymers combined with silver nanoparticles are utilised for improving the quality of materials for packaging food which increases its lifetime. Thus, it will last for a longer duration of time.
- Electronics and Devices-Technological advancement from massive television or phone sets to sleek television or phones. The nanomaterials such as graphene have created light weight and higher quality screens of TV sets that consumes lesser electricity.
- Security/development of smart ink-Nanotechnology can be used in the development of security ink.
- Medicine-Significant side effects are undergone by patients from many drugs and therapies for chronic conditions such as brain tumour, cancer etc. Therefore, the nanoparticles are used for targeted delivery of drug to destroy the cancer cell without affecting the cells of the entire body.
- Solar cell-Nanotechnology can be applied for improving the efficiency of solar cell by enhancing the retention and absorption of sunlight.
- Automobiles-Vast application of nanotechnology can also be seen in automobile sector several nanocomposites of polymer are employed for manufacture of abrasion resistant tyres. Tungsten nanospheres are added to the automotive fluids to enhance their mechanical qualities.

- Improving the quality of water-The photocatalytic properties of nanoparticles helps in breaking the cationic or anionic dyes to carbon dioxide and water. Thus, the carcinogenic dyes are decomposed by the application of nanomaterials.
- Improving Air Quality-The membranes are coated with nanomaterials used for separation of contaminants from the air.
- Chemical sensors-Various chemical sensors are being developed by using nanomaterials like CNT, zinc oxide nanowire which can detect the smallest concentration of harmful compounds.
- A biosensors-Transducers material which is an important part for development of biosensors generally uses nanomaterials.

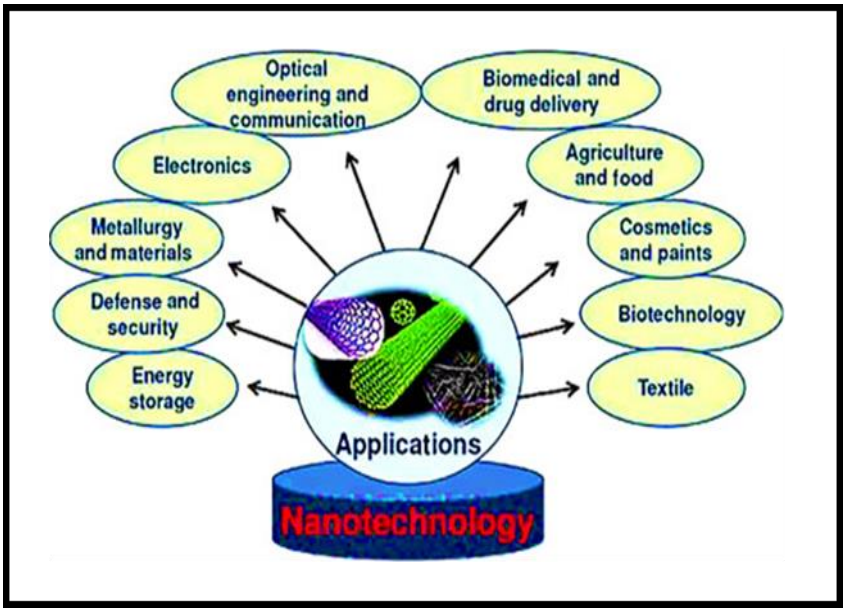

Fig. 1.10: Applications of nanotechnology

1.11 Catalysis

Catalysis is a process in which the rate of chemical reaction is increased due to the addition of a substance known as catalyst. The catalyst itself do not participate in the reaction process. With the addition of catalyst, the reaction occurs at a faster rate and with lesser consumption of energy [24].

1.11.1 Activation energy

The minimum energy required to promote or start a chemical reaction is called activation energy.

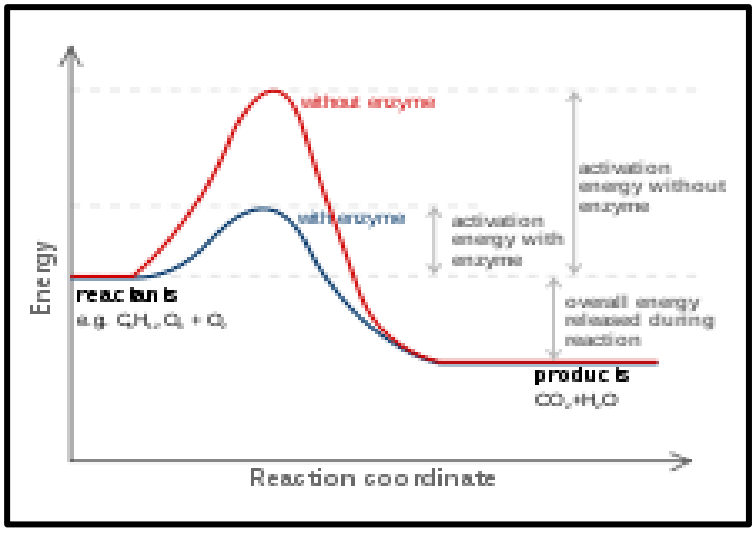

Fig 1.11: Activation energy barrier with and without the presence of the catalyst

1.11.2 Catalytic promoter

The substance that increases the efficiency of a catalyst is called a catalytic promoter.

1.11.3 Catalytic Inhibitor

The substance that decreases or inhibits the efficiency of a catalyst is called a catalytic inhibitor.

1.11.4 Types of catalyst

a. Positive catalyst

The catalyst that increases the rate of chemical reaction by decreasing the activation energy barrier is called positive catalyst.

$$\text{Example: } 2H_2O_2 \xrightarrow{Pt} 2H_2O+O_2$$

$$C_2H_4+H_2 \xrightarrow{Ni} C_2H_6$$

b. Negative catalyst

The catalyst that decreases the rate of chemical reaction by increasing the activation energy barrier is called negative catalyst.

Example: Cracking of petroleum by "Tetra Ethyl Lead".

c. Homogenous catalyst

The catalyst and the reactants are in the same phase or same physical state. The catalyst is called homogenous catalyst.

$$\text{Example: } 2CO(g)+O_2(g) \xrightarrow{NO(g)} 2CO_2(g)$$

d. Heterogenous catalyst

When the catalyst and the reactants in a chemical reaction are in different phases it is called a heterogenous catalyst.

$$\text{Example: } N_2(g)+3H_2(g) \xrightarrow{Fe(s)} 2NH_3$$

e. Heterogenous

Homogenous catalyst sometimes molecules of homogenous catalyst break the uniformity among catalyst and products by rendering separable state.

f. Auto catalyst

When one of the products formed during a reaction act as a catalyst itself is termed as auto catalyst.

$$\text{Example: } CH_3COOH_3+H_2O \xrightarrow{H+} CH_3COOH+CH_3OH$$

g. Bio catalyst

The chemical substance which increases or decreases the rate of reaction inside a living body is called a bio catalyst or an enzyme.

$$\text{Example-protein} \xrightarrow{pepsin} \text{peptides + peptones [25]}$$

1.11.5 Some of the catalysis process

a. Photocatalysis

Photocatalysis may be heterogenous or homogenous depending on the phase of the catalyst used. The substance that absorbs light and acts as a catalyst for driving a chemical reaction is known as photocatalyst and the process is known as photo-catalysis. Photocatalyst accelerates the rate of chemical conversion (oxidation and reduction) in the presence of visible light. During photocatalysis the photons leads to the generation of electron-hole pair. The electrons in the conduction band reduce oxygen to superoxide radical anion and the holes in the valence band oxidize water to hydroxyl radical. Thus, the generation of catalytically active species during photocatalysis lead to the degradation of harmful carcinogenic dye to simpler harmless products [26].

b. Sono-catalysis

The principle of Sono-catalysis is the diffusion and sorption of the components on a solid surface followed by a series of heterogenous chemical reaction on active sites. It uses powerful ultrasound radiations to makes the molecules undergo a chemical reaction at a faster rate.

c. Electro-catalysis

Modification of electrochemical reaction rate occurring at the electrode surface is known as Electro-catalysis.

d. Piezo-catalysis

It is the catalysis based on the piezo-electric material which relies on charge separation efficiency of the carriers.

1.12 Semiconductor

Solid substances have conductivity ranging between metal and insulator. It is caused due to doping of impurity or temperature effects.

1.12.1 P-type semiconductor

There are a number of semiconductors that have a large proportion of holes as charge carriers. It is obtained by doping of trivalent impurities such as Boron, Aluminium and gallium.

1.12.2 N-type semiconductor

This semiconductor is characterized by a large number of electrons as the main charge carriers. It is obtained by doping of pentavalent impurities such as Phosphorous, Antimony and Arsenic.

1.13 Reason for using semiconductors in photocatalysis instead of metals or insulators

As the band gap energy is zero electron volts in case of metals it does not show photocatalytic property. The band gap energy of insulator is greater than 5eV therefore it requires a large amount of energy for creation of electron hole pair in conduction and valence band which in turn helps in the decomposition of carcinogenic dyes by redox reactions into carbon dioxide and water. Thus, insulators are also not preferred for photocatalytic property. But in case of semiconductor the band gap energy ranges in between that of metal and insulator which is very much feasible for generation of electron hole pair and quite feasible material for photocatalysis.

The semiconductors are used for photocatalysis due to it's:

- High reactivity.

- Strong oxidizing and reducing ability.
- Chemical stability.
- Reduced cost.
- Low toxicity and
- photostability.

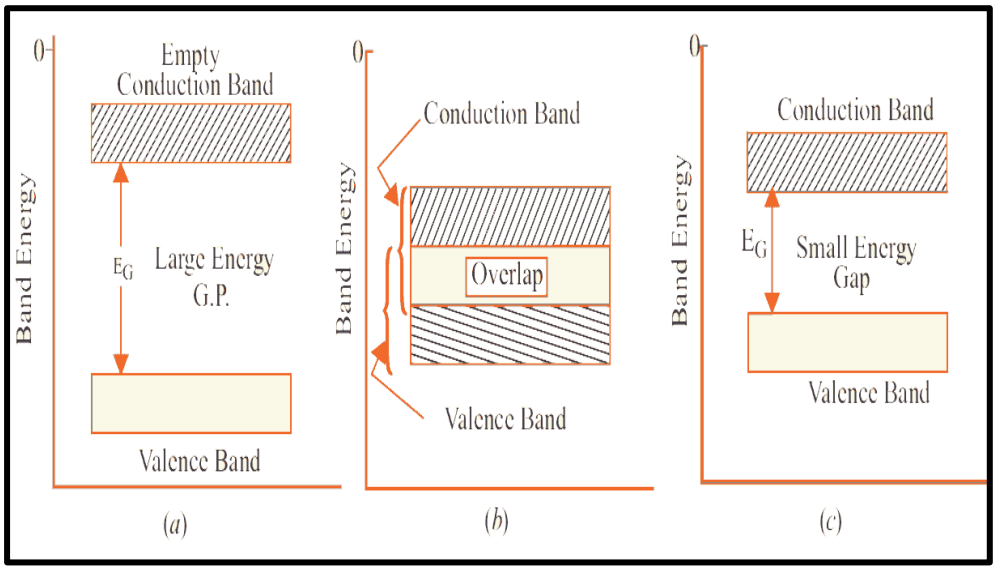

Fig. 1.12: Band diagram of (a) Insulator, (b) Metal and (c) Semiconductor

1.14 Nanomaterials used for photocatalytic property

1.14.1 Graphitic carbon nitride (g-C_3N_4)

- One of the most promising materials for photocatalytic processes, including the removal of organic pollutants from the environment and the reduction of CO_2 and water splitting, is known as graphitic carbon nitride (g-C_3N_4). On the other hand, in the area of field emission properties, carbon nitride also possesses exceptional qualities and broad application prospects.
- Wastewater, notably wastewater produced as a result of chemical industrialisation, is the main source of pollution because it contains a significant amount of big organic pieces, which are inherently harmful and carcinogenic.

- Prior to now, all kinds of organic and toxic wastewater were treated using environmental remediation technology, which consists of biological oxidation, adsorption, incineration and chemical oxidation.
- Photocatalysis is the term used to describe the acceleration of a photoreaction in the presence of a catalyst. The best-known media for photocatalysis reactions are aqueous solutions, pure organic liquid phases and gas phase media.
- Additionally, the optimum chemical degradation approach for regulating organic wastes, solar energy use, environmental treatment, and medicinal and sensing applications is frequently characterised as photocatalytic degradation via photons and a catalyst. Therefore, the development of solar light-driven photocatalysts like graphitic carbon nitride is responsible for the most advanced technology utilised for the treatment of organic wastewater and related applications.
- Semiconductor photocatalysts can be applied to the treatment of drinking water, environmental cleaning, industrial and health applications, as well as the removal of ambient concentrations of organic and inorganic species from aqueous or gas phase systems. This is because these semiconductors (g-C_3N_4, WO_3 and TiO_2) have a tremendous capacity for oxidizing organic and inorganic substrates in air and water through redox processes for their efficient application in solar energy utilization, wastewater treatment, environmental protection, and biomedical and sensing applications without any secondary pollution.
- In photocatalysis research, polymeric graphitic carbon nitride (g-C_3N_4) has taken precedence.
- Band gap energy of graphitic carbon nitride is 2.7 eV, thus it can act as a visible light driven photocatalyst. The energy location of conduction band and valence band via

hydrogen electrode is at -1.1 eV and 1.6 eV respectively. Graphitic carbon nitride is resistant towards attack from heat, strong alkaline and acid solution.

- g-C_3N_4 can be easily made by thermally poly condensing inexpensive N-rich precursors such urea, melamine, melamine cyanurate, dicyanamide, and cyanamide, as opposed to other metal-containing photocatalysts that need to be made with expensive metal salts.
- The usage of this prospective g-C_3N_4 in water splitting, CO_2 photo reduction, organic pollutants purification, catalytic organic synthesis, and fuel cells is more efficient and effective as a result of its exceptional features.
- The easiest way to describe photocatalysis is the activation of a catalyst that speeds up chemical transformations (oxidations and reductions). This reaction, which can result in the photocatalytic transformation of a pollutant, utilizes a semiconductor either alone or in combination with metal, organic, or organometallic promoters by light absorption, followed by charge or energy transfer to be adsorbed.

1.14.2 Structure of graphitic carbon nitride (g-C_3N_4)

There are two primary varieties of g-C_3N_4 structural polymorphs as a result of the proper precursor selection and condensation techniques. The first is the g-C_3N_4 that is composed of condensed s-triazine units (a ring of C_3N_3) with a periodic array of single-carbon vacancies. The second form of g-C_3N_4 has more periodic vacancies in the lattice because it is made up of condensed tri-s-triazine (tri-ring of C_6N_7) subunits connected through planar tertiary amino groups. In contrast to the melamine-based arrangements (the first type structure; this compose of the s-triazine), the g-C_3N_4 networks primarily consisting of melon-based segments (the second type structure; this consists of the tri-s-triazine unit) are thermodynamically more stable [27].

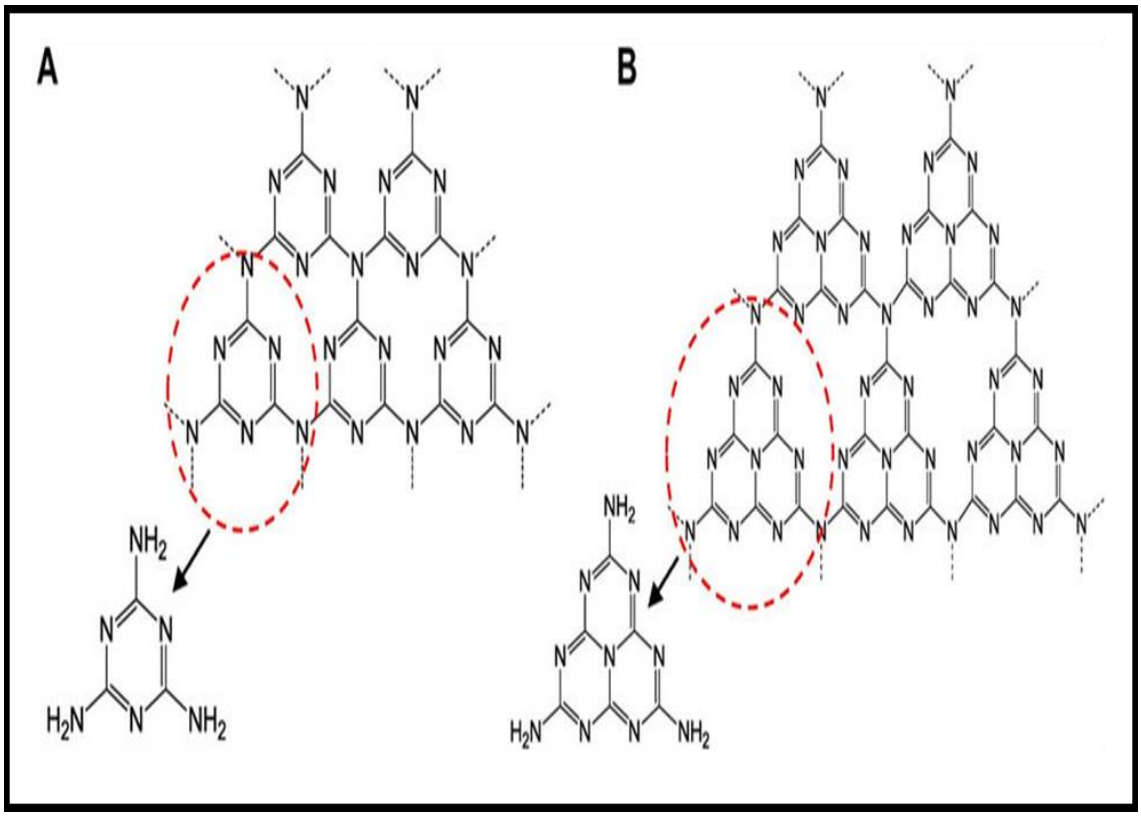

Fig. 1.13: (a) Triazine and (b) Tri-s-triazine structure of graphitic carbon nitride (g-C_3N_4)

1.14.3 Various techniques for synthesis of graphitic carbon nitride

The gC_3N_4 synthesis started in 1834 when Berzelius developed a polymeric derivative called melon by Liebig. This is the first synthetic polymer reported so far [28]. However, it was not until 1922 that the detailed structure came to light, suggesting that a mixture of variable sizes and shapes of polymers should adequately describe the material's structure. Since then, intense research has been done on the basic understanding of synthesis methods and the structure-property relationship of the material. In most cases, different carbon- and nitrogen-rich compounds are chosen as starting materials for synthesis. The average temperature for synthesis varies between 400 and 600 ºC. In addition, the coming section will highlight that the material's building block has a planar structure; thus, most of the methods resulted in the development of g-C_3N_4 with distorted 2-dimensional sheet-like structures, but there are reports of other morphologies also, like tube, rod, or other.

For instance, an amorphous phase of g-CN was developed by Kouvetakis et al. from melamine precursors in the temperature range of 450–600 ºC [29]. It has also been shown that extreme conditions like 800 ºC temperature, 2.5 GPa pressure, and hydrogen presence resulted in a g-C_3N_4 structure with almost perfect graphite stacking; however, the high temperature associated with the high temperature causes a relatively low abundance of nitrogen, and the carbon to nitrogen ratio is not perfect.

A high-pressure, high-temperature approach and 2-amino-4, 6-dichloro triazine as precursors can result in the formation of crystalline g-C_3N_4 planar structures through HCl elimination. Here, the HCl generated in situ during the reaction played a crucial role in the proper development of the g-C_3N_4 stacking structure [30]. The concept of "high molecular weight melon" and the synthesis of highly ordered and properly stacked 2 D g-C_3N_4 was introduced by Komatsu and the group in 2001 and can be considered a work of importance [31].

In this field, Schnick et al. also reported a landmark work where they separated an intermediate compound, 2,5,8-triaminotris-triazine, or melem ($C_6N_{10}H_6$), which is a very stable intermediate [32]. When carried forward, it was determined that a temperature range between 500 and 600 ºC is ideal for phase formation [33]. g-C_3N_4 may also be synthesized at a temperature as low as 200 °C by the solvothermal reaction when cyanurchloride-sodium amide and cyanurchloride-sodium azide are taken as precursors [34,35]. However, the graphitic nature of the as-developed sample was not so pronounced, mainly due to the lesser reaction temperature.

1.14.4 Applications of graphitic carbon nitride (g-C_3N_4)

This graphitic carbon nitride has a number of newly emerging uses, including sensing, biological applications, wastewater and environmental treatment, solar energy usage, and device manufacturing.

1.14.5 Tungsten tri-oxide (WO_3)

- Tungsten tri-oxide also known as Tungsten (VI) oxide which is chemical compound comprises of the transition metal tungsten and oxygen with a chemical formula of WO_3.
- Tungsten tri-oxide has temperature dependent crystal structure. It is monoclinic in the temperature ranging from 17 ℃ to 330 ℃, Orthorhombic in the range of 330 to 740 ℃, tetragonal at a temperature above 740 ℃, triclinic from -50 to 17 ℃ and monoclinic again at a temperature ranging below -50 ℃. The most common structure of WO_3 is monoclinic [36].
- Industrial preparation: When tungsten is extracted from its mineral tungsten trioxide is produced as an intermediate step. Alkalis can be used to process tungsten ores to create soluble tungstate. Alternately, scheelite or $CaWO_4$, is allowed to react with HCl to create tungstic acid which at higher temperature breaks down into WO_3 and water.

  $CaWO_4 + 2HCl \rightarrow CaCl_2 + H_2WO_4$

  $H_2WO_4 \rightarrow WO_3 + H_2O$

- Laboratory preparation: Calcination of Ammonium para tungstate leads to the synthesis of WO_3 under oxidizing conditions.
- The band gap energy of tungsten tri-oxide varies from 2.6 to 3 eV. The conduction band and the valence band potential of tungsten tri-oxide are 0.77 eV and 3.41 eV respectively.
- The valence band is formed by the filled O 2p orbital, whereas the conduction band is created by the empty W 5d orbital. Although WO_3 has a lower conduction band and its potential is not sufficiently negative to reduce water to hydrogen, its valence band's oxidation potential is sufficiently positive to oxidize water to oxygen [37].

1.14.6 Applications of tungsten tri-oxide (WO_3)

The production of tungstate begins with tungsten tri-oxide, X-ray screen phosphors are made of barium tungstate. Other prospective or existing applications include:

A. Fire resistant fabrics.

B. Water splitting using photocatalysis.

C. Sensors for gases and humidity.

D. Ceramic glazes, where it produces a deep yellow hue.

E. Electrochromic glass, like that seen in smart windows, whose transparency is adjustable by the application of voltage.

1.15 Types of Dyes

Various types of dyes are released into the water bodies from the industries. The dyes are categorized mainly into two types:

- **Cationic Dye**

Cationic dyes are materials consisting of components that make them to dissociate into positively charged ions in an aqueous solution. They are alkaline or basic in nature.

Example: Methylene Blue (MB), Rhodamine B (RhB).

- **Anionic Dye**

Anionic dyes are materials consisting of components that make them dissociate into negatively charged ions in an aqueous solution. They are acidic in nature.

Example: Methyl orange (MO), Orange G (OG).

- **Non-Ionic Dye**

Non-Ionic dyes are materials consisting of components that make them dissociate into neutral charged ions in an aqueous solution. They are neutral in nature.

Example: Green 97 (G97), Disperse Red 60 (DR60).

1.16 Photocatalytic Activity of tungsten tri-oxide (WO_3)

- Dyes released from the textile industries or leather industries serve as the major pollutants in waste water. We know that the volume of water consumed by textile industry is quite large and nearly ninety percent of the waste water is released.
- The waste water released from the industries to various water bodies consists of dyes which are very harmful and carcinogenic in nature. It poses threat to human life as well as the ecological system. So various effective methods are adopted for removal of pollutants to supply clean water.
- Photocatalysis is considered as one of the most efficient techniques in treatment of waste water and its ability to decompose toxic compounds to simpler harmless products.
- We know that titanium dioxide acts as an efficient photocatalyst due to its nontoxicity, degradation efficiency and thermal stability. However, it is a wide band gap material having band gap energy of 3.2 eV which provides a limitation for absorption of visible light.
- Therefore, Tungsten trioxide is used as an effective material for degradation of Rhodamine B dye which is carcinogenic in nature and poses threat to human life as tungsten trioxide is a visible light driven photocatalyst with a band gap energy of 2.6-2.8 eV. It is also non-toxic in nature.
- However pure tungsten trioxide does not serve the purpose of an efficient photocatalyst and its photocatalytic activity is quite low due to the rapid recombination rate of electron hole pair and having conductive band level relatively low.

- Therefore, for enhancement of photocatalytic activity of tungsten trioxide is undergone by coupling it with graphitic carbon nitride having band gap energy of 2.7 eV. Thus, the tungsten trioxide/graphitic carbon nitride nanocomposite acts as an efficient photocatalyst in visible light range for degradation of Rhodamine B dye.
- The increase in photocatalytic efficiency of the nanocomposite is due to the decrease of recombination rate or increase in separation efficiency of electron hole pair in conduction band and the valence band of the material respectively.
- The variation in the morphology of graphitic carbon nitride is undergone to compare its degradation efficiency with tungsten trioxide and tungsten trioxide/graphitic [38].

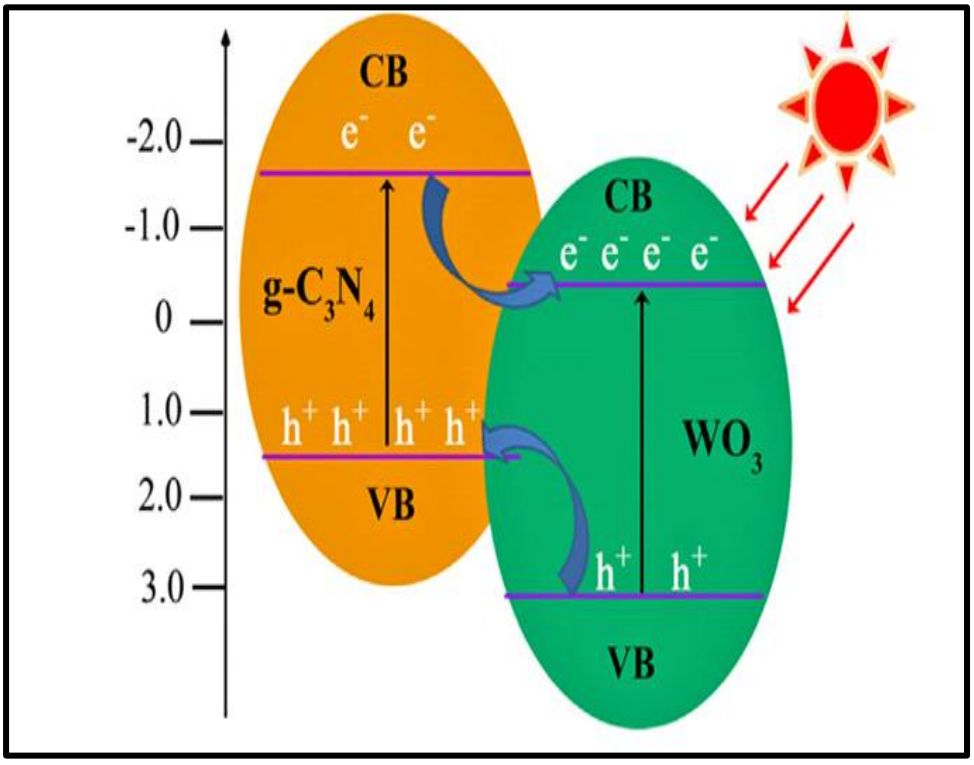

Fig. 1.12: Schematic diagram proposing the photocatalytic mechanism of Tungsten trioxide/Graphitic carbon nitride nanocomposite for the degradation of Rhodamine B dye

1.17 Objective

We are aware of the fact that the textile and leather industries releases waste water in water bodies like rivers, ponds and lakes which consists of various carcinogenic dyes like

Rhodamine B and Methylene Blue, that poses serious threat to human life and also the ecological system. We have synthesized semiconductor nanoparticles (Tungsten trioxide nanospheres and tungsten trioxide/Graphitic Carbon Nitride nanocomposites) which act as a visible light driven photocatalyst. On illumination with the visible light, it leads to the generation of electron and hole pair in conduction and valence band respectively which in turn leads to the degradation of hazardous dyes to simpler harmless products, thus providing an effective way in removal of pollutants from waste water and rendering it clean for supply.

1.18 References

1.https://www.google.com/search?q=define+nanoscience&oq=define+nan&aqs=chrome.2.69i57j35i39i650l2j69i59j0i20i263i512j0i512l5.5520j0j15&sourceid=chrome&ie=UTF-8

2. Jeevanandam, J., Barhoum, A., Chan, Y.S., Dufresne, A. and Danquah, M.K., 2018. Review on nanoparticles and nanostructured materials: history, sources, toxicity and regulations. *Beilstein journal of nanotechnology*, *9*(1), 1050-1074.

3. https://ec.europa.eu/health/scientific_committees/opinions_layman/en/nanotechnologies/l-2/1-introduction.htm

4. https://www.rsc.org/cpd/teachers/content/filerepository/frg/pdf/Nanoparticles.pdf

5. Wang, Y. and Weng, G.J., 2018. Electrical conductivity of carbon nanotube-and graphene-based nanocomposites. *Micromechanics and nanomechanics of composite solids*, 123-156.

6. Yadav, A.A., Hunge, Y.M. and Kang, S.W., 2021. Porous nanoplate-like tungsten trioxide/reduced graphene oxide catalyst for sonocatalytic degradation and photocatalytic hydrogen production. *Surfaces and Interfaces*, *24*, 101075.

7. Zhang, Q., Uchaker, E., Candelaria, S.L. and Cao, G., 2013. Nanomaterials for energy conversion and storage.

8. Alkaç, İ.M., Çerçi, B., Timuralp, Ç. and Şen, F., 2021. Nanomaterials and their classification. In *Nanomaterials for Direct Alcohol Fuel Cells* (17-33). Elsevier.

9. https://www.researchgate.net/figure/Schematic-diagram-showed-the-basic-classification-of-nanomaterials_fig2_344148908

10. Meyers, M.A., Mishra, A. and Benson, D.J., 2006. Mechanical properties of nanocrystalline materials. *Progress in materials science*, *51*(4), 427-556.

11. Cai, D., Song, M. and Xu, C., 2008. Highly conductive carbon-nanotube/graphite-oxide hybrid films. *Advanced Materials*, *20*(9), 1706-1709.

12. Nie, G., Yao, Y., Duan, X., Xiao, L. and Wang, S., 2021. Advances of piezoelectric nanomaterials for applications in advanced oxidation technologies. *Current Opinion in Chemical Engineering*, *33*, 100693.

13. Abid, N., Khan, A.M., Shujait, S., Chaudhary, K., Ikram, M., Imran, M., Haider, J., Khan, M., Khan, Q. and Maqbool, M., 2022. Synthesis of nanomaterials using various top-down and bottom-up approaches, influencing factors, advantages, and disadvantages: A review. *Advances in Colloid and Interface Science*, *300*, 102597.

14. https://www.ques10.com/p/29063/what-are-the-methods-used-in-nano-material-synthes/

15. Fecht, H.J., Hellstern, E., Fu, Z. and Johnson, W.L., 1990. Nanocrystalline metals prepared by high-energy ball milling. *Metallurgical Transactions A*, *21*, 2333-2337.

16. Semaltianos, N.G., 2010. Nanoparticles by laser ablation. *Critical reviews in solid state and materials sciences*, *35*(2), 105-124.

17. https://www.youtube.com/results?search_query=cvd+process+sequention+steps

18.https://www.google.com/search?q=Schematic+diagram+of+CVD.&oq=Schematic+diagram+of+CVD.&aqs=chrome..69i57j33i160l4.420j0j15&sourceid=chrome&ie=UTF-8#imgrc=h8ac7f9tPEnZDM

19.https://www.google.com/search?q=pvd+process+steps&oq=pvd+process+&aqs=chrome.1.69i57j0i512l4j0i22i30l5.5685j0j15&sourceid=chrome&ie=UTF-8

20. https://www.researchgate.net/figure/Schematic-of-sputtering-process-Basically-the-steps-of-sputtering-process-are-the_fig5_221917882#:~:text=Basically%20the%20steps%20of%20sputtering%20process%20are%20the%20following%3A%20(i,the%20cathode%20sheath%3B%20(iii)

21.https://www.youtube.com/results?search_query=sol+gel+method+for+nanoparticle+synthesis

22. hydrothermal synthesis principles (you tube).

23.https://www.google.com/search?q=application+of+nanotechnology+pictures&oq=&aqs=chrome.2.46i39i199i362i465j35i39i362l7.665332643j0j15&sourceid=chrome&ie=UTF-8

24.https://www.google.com/search?q=catalysis&oq=catalysis&aqs=chrome..69i57j0i512j69i64j0i512l5.3479j0j15&sourceid=chrome&ie=UTF-8

25. https://www.youtube.com/results?search_query=types+of+catalysis+in+details

26. Li, X., Song, X., Ma, C., Cheng, Y., Shen, D., Zhang, S., Liu, W., Huo, P. and Wang, H., 2020. Direct Z-scheme WO_3/graphitic carbon nitride nanocomposites for the photoreduction of CO_2. *ACS Applied Nano Materials*, *3*(2), 1298-1306.

27. https://www.researchgate.net/figure/Structure-of-a-s-triazine-and-s-triazine-based-g-C_3N_4-and-b-tri-s-triazine-and_fig10_303627507

28. Hussen, A., 2021. Review on gC_3N_4 Based Fluorescence Chemical Sensor for Detection of Heavy Metal Ions. *Asian Journal of Basic Science & Research*, 3(1), 69-84.

29. Kouvetakis, J., Todd, M., Wilkens, B., Bandari, A. and Cave, N., 1994. Novel synthetic routes to carbon-nitrogen thin films. *Chemistry of materials*, 6(6), 811-814.

30. Zhang, Z., Leinenweber, K., Bauer, M., Garvie, L.A., McMillan, P.F. and Wolf, G.H., 2001. High-Pressure Bulk Synthesis of Crystalline $C_6N_9H_3$•HCl: A Novel C_3N_4 Graphitic Derivative. *Journal of the American Chemical Society*, 123(32), 7788-7796.

31. Komatsu, T., 2001. Prototype carbon nitrides similar to the symmetric triangular form of melon. *Journal of Materials Chemistry*, 11(3), 802-803.

32. Jürgens, B., Irran, E., Senker, J., Kroll, P., Müller, H. and Schnick, W., 2003. Melem (2, 5, 8-triamino-tri-s-triazine), an important intermediate during condensation of melamine rings to graphitic carbon nitride: Synthesis, structure determination by X-ray powder diffractometry, solid-state NMR, and theoretical studies. *Journal of the American Chemical Society*, *125*(34), 10288-10300.

33. Gu, Y., Chen, L., Shi, L., Ma, J., Yang, Z. and Qian, Y., 2003. Synthesis of C_3N_4 and graphite by reacting cyanuric chloride with calcium cyanamide. *Carbon*, *41*(13), 2674-2676.

34. Guo, Q., Xie, Y., Wang, X., Lv, S., Hou, T. and Liu, X., 2003. Characterization of well-crystallized graphitic carbon nitride nanocrystallites via a benzene-thermal route at low temperatures. *Chemical Physics Letters*, *380*(1-2), 84-87.

35. Guo, Q., Xie, Y., Wang, X., Zhang, S., Hou, T. and Lv, S., 2004. Synthesis of carbon nitride nanotubes with the C_3N_4 stoichiometry via a benzene-thermal process at low temperatures. *Chemical communications*, (1), 26-27.

36. H. A. Wriedt (1898): "The O-W (oxygen-tungsten) system". *Bulletin of Alloy Phase Diagrams.*, volume 10, 368–384. doi:10.1007/BF02877593

37. https://www.researchgate.net/figure/Edges-of-valence-and-conduction-bands-of-WO-3-versus-the-standard-hydrogen-electrode_fig4_332770726

38. Zhao, J., Ji, Z., Shen, X., Zhou, H. and Ma, L., 2015. Facile synthesis of WO_3 nanorods/g-C_3N_4 composites with enhanced photocatalytic activity. *Ceramics International*, *41*(4), 5600-5606.

Chapter 2

Review of Past Work

2.1 General Idea

The chapter review focuses on the research already done on transition metal oxides and their photocatalytic capabilities. Due to their potential applications in numerous areas, such as environmental clean-up [1], energy conversion, and water splitting [2-3], transition metal oxides have drawn a lot of attention. In the introduction, a thorough survey of transition metal oxides is given. This survey emphasizes both their distinctive electronic and structural characteristics as well as their potential as photocatalytic candidates. It examines several transition metal oxides and discusses their crystal structures, band gaps, and other pertinent characteristics. Examples include titanium dioxide (TiO_2), zinc oxide (ZnO), and tungsten trioxide (WO_3). The review delves into the photocatalytic mechanisms of transition metal oxides, clarifying the procedures involved in light absorption, charge separation, and the production of reactive species. It investigates how surface changes, co-catalysts, and dopants can improve the photocatalytic performance of transition metal oxides. It addresses the important factors, such as crystallinity, particle size, and surface area, that affect photocatalytic performance. The review also conducts a comprehensive assessment of the literature on the photocatalytic uses of transition metal oxides, emphasizing the effectiveness of these materials in degrading organic pollutants [4], producing hydrogen through water splitting [5], and storing solar energy for use in generating electricity [6]. It analyses the difficulties encountered in actual implementation and offers alternative solutions. This, chapter review concludes with a thorough and insightful critique of earlier work on transition metal oxides as photocatalysts [7]. It lays the groundwork for further developments in this area by providing insightful information about their fundamental characteristics, photocatalytic mechanisms, characterization methods, and prospective applications.

2.2 Transition metal oxide

A transition metal element is joined to oxygen to form a compound known as a transition metal oxide. These oxides are flexible and desirable materials in many domains because of the vast variety of physical and chemical characteristics they exhibit. Transition metal oxides frequently have distinctive electrical, magnetic, and catalytic properties that are impacted by things like the metal's composition, oxidation state, and crystal structure. Numerous fields, such as catalysis, energy storage and conversion, electronics, and sensors, use these oxides. Iron oxide (Fe_2O_3), tungsten oxide (WO_3), and titanium dioxide (TiO_2) are a few examples of transition metal oxides. Each has unique properties and uses.

2.2.1 Application of transition metal oxide

In the examination of prior work, the use of transition metal oxides in numerous disciplines has been thoroughly investigated and documented. These adaptable materials have unique properties that make them useful in a variety of applications. As said in the overview, the study will explore the use of transition metal oxides in catalysis, energy storage and conversion, electronics, and sensors.

2.2.1.1 Catalysis

Transition metal oxides are frequently utilized as catalysts in a wide range of chemical processes. For its photocatalytic capabilities, titanium dioxide (TiO_2) is a notable example and has received considerable research. It is used in water and air filtration systems to degrade contaminants such chemical dyes and volatile organic compounds. The oxidation processes, ammonia synthesis, and methane conversion all benefit from the excellent catalytic activity of transition metal oxides such as tungsten oxide (WO_3) [8].

2.2.1.2 Energy storage and conversion

Devices for storing and converting energy rely heavily on transition metal oxides. For effective energy storage and release, lithium-ion batteries use transition metal oxide cathodes like lithium cobalt oxide ($LiCoO_2$) and lithium iron phosphate ($LiFePO_4$) [9-10]. Due to their high capacity and stability, transition metal oxides including titanium oxide (TiO_2) and vanadium oxide (VO_2) are also being researched as anode materials for lithium-ion batteries [11].

2.2.1.3 Solar energy conversion

Transition metal oxides are used as photoelectrodes for dye-sensitized solar cells (DSSCs) [12] and perovskite solar cells in the field of solar energy conversion [13]. DSSCs frequently use titanium dioxide (TiO_2) as a mesoporous scaffold because of its superior electron transport capabilities. In order to improve the photoconversion efficiency of these devices, researchers have also looked at additional transition metal oxides, such as tungsten oxide (WO_3) and bismuth vanadate ($BiVO_4$).

2.2.1.4 Electronics

Applications for transition metal oxides can be found in electronic parts and components. For instance, transparent electrodes made of indium tin oxide (ITO), a transparent conductive oxide, are frequently used in touchscreens, displays, and solar cells [14]. It demonstrates outstanding optical transparency along with strong electrical conductivity. Molybdenum oxide (MoO_3) and vanadium pentoxide (V_2O_5) are two more transition metal oxides being investigated for use as charge transport layers in organic electronic devices including organic light-emitting diodes (OLEDs) and organic photovoltaics (OPVs) [15].

2.2.1.5 Sensors

The ability of transition metal oxides to detect gases has received substantial research. When exposed to the target gases, metal oxide-based gas sensors look for changes in electrical conductivity. For instance, sensors made of tungsten oxide (WO_3) and tin dioxide (SnO_2) are frequently used to detect gases like nitrogen dioxide (NO_2) and carbon monoxide (CO) [16-17]. These sensors are used in environmental monitoring, industrial safety, and vehicle exhaust monitoring.

The analysis of prior research demonstrates the numerous uses of transition metal oxides in catalysis, energy storage and conversion, electronics, and sensors. They are valuable materials in a variety of industries due to their unique characteristics, which include catalytic activity, high capacity, electrical conductivity, and gas detecting abilities. Continued research and development in this area hold great potential for further advancements and the discovery of new applications for transition metal oxides.

2.2.2 Report on morphological changes of transition metal oxide

Previous studies examined closely at the morphological alterations of transition metal oxides and how they affect numerous industries, offering insightful information for uses in catalysis, energy storage, electronics, and sensing. The analysis of these report clarifies how important morphological control is to enhancing the functionality of transition metal oxide materials.

The surface area, active sites, and diffusion paths of transition metal oxides are strongly influenced by their morphology in catalysis, which in turn affects the catalytic activity. By increasing the surface area and encouraging light absorption, for instance, controlled morphological modifications in titanium dioxide (TiO_2) nanoparticles have been seen to improve photocatalytic effectiveness [18]. Similar to this, tungsten oxide catalysts' morphology can be tuned to improve catalytic performance in processes like oxidation and ammonia production [19].

The electrochemical performance of transition metal oxide electrodes in energy storage applications is directly influenced by their morphology. According to the studies, the morphology of transition metal oxide nanomaterials, such as hierarchical structures, nanowires, and nanosheets, can increase the specific surface area and reduce ion diffusion paths, improving the capacity for energy storage. Lithium-ion batteries, supercapacitors, and other energy storage technologies have used morphology-controlled transition metal oxides with success [20].

In the field of electronics, where it affects the charge transport characteristics and device performance, the morphology of transition metal oxides is also essential. As an illustration, it has been demonstrated that the controlled growth of zinc oxide nanowires increases charge carrier mobility, making them excellent candidates for field-effect transistors and other electronic devices [21]. To enhance the electrical conductivity and interface properties of transition metal oxide thin films in optoelectronic devices including solar cells and light-emitting diodes, morphological alterations have also been investigated.

Additionally, the effects of morphological changes on sensing applications in transition metal oxide materials have been researched. Metal oxide-based gas sensors' surface shape and structure have an impact on gas adsorption and reaction processes, which ultimately affects the sensing performance. Metal oxide sensors' gas sensing sensitivity and response times have been proven to be improved by controlled morphological alterations such as porous architectures, nanoparticles, or nanowires [22].

The significance of morphology control in numerous sectors has been underlined in previous reports on the morphological alterations of transition metal oxides. Transition metal oxides' surface area, active sites, charge transport properties, and gas sensing capabilities can all be tailored for particular purposes by modifying their morphology. It will be able to use morphological control to improve the performance of transition metal oxide materials in

catalysis, energy storage, electronics, and sensing applications as long as this research is conducted.

2.2.3 Report on surface modification of transition metals

In order to improve the characteristics and performance of transition metal oxides in a variety of applications, surface modification has become an essential method. The effects of various surface modification approaches on catalysis, energy storage, electronics, and sensing have been thoroughly examined in other reports. The analysis of these paper sheds light on how important surface modification is for enhancing the performance of transition metal oxide materials.

Surface modification of transition metal oxides in catalysis can increase their stability, selectivity, and catalytic activity. Doping or adding heteroatoms to the surface of the transition metal oxide is a typical method of surface modification. For instance, by encouraging charge separation and lowering recombination, doping titanium dioxide (TiO_2) with metals like silver (Ag) or platinum (Pt) improves its photocatalytic activity [23]. It has also been investigated to modify surfaces with metal nanoparticles or clusters in order to generate active sites and enhance catalytic performance in processes like hydrogenation and oxidation.

In energy storage technologies like lithium-ion batteries and supercapacitors, surface modification of transition metal oxide electrodes is essential. To improve the electrical conductivity and ion transport kinetics, a variety of techniques have been used, such as covering the surface with conductive polymers, carbon compounds, or metal oxides. Such changes boost the electrodes' charge transport characteristics and electrochemical performance, which improves energy storage capacity and cycling stability [24].

To customize interface qualities, increase charge carrier mobility, and boost device performance in electronics, transition metal oxide surfaces are modified. For instance, self-

assembled monolayers (SAMs) or polymers can be used to increase the stability and work function of indium tin oxide (ITO) electrodes [25], allowing for effective charge injection or extraction in organic electronic devices. The creation of functionalized surfaces for particular uses has also been explored through surface alterations, such as the insertion of functional groups onto transition metal oxide surfaces for biofunctionalization or selective chemical sensing.

In sensing applications, surface modification of transition metal oxides is important as well [26]. The selectivity and sensitivity of gas sensors can be improved by immobilizing specific receptors or ligands on metal oxide surfaces. The performance of gas sensing has been enhanced by surface modifications, such as the addition of metal nanoparticles or nanostructures, which produce catalytically active sites.

The analysis of earlier work on surface modification of transition metal oxides shows the significance of this strategy in enhancing their characteristics and functionality. Catalytic activity, energy storage capacity, charge transport characteristics, and sensing performance can all be considerably improved by surface modifications such as doping, coating, and functionalization. The development and implementation of transition metal oxide materials in catalysis, energy storage, electronics, and sensing applications will benefit from ongoing study and investigation of novel surface modification techniques.

2.2.4 Review of the mechanical properties of Transition metal oxides

The analysis of the mechanical characteristics of transition metal oxides has attracted the attention of many academic works. These investigations shed light on these materials' structural integrity, stability, and strength—aspects that are essential for their use in a variety of applications. Here, summarize the several important conclusions about the mechanical characteristics of transition metal oxides from the literature.

Determining the elastic characteristics of transition metal oxides has been one area of focus. Studies have used methods like atomic force microscopy and nanoindentation to measure characteristics like Young's modulus and hardness. Studies on titanium dioxide (TiO_2), for instance, have revealed that the elastic modulus of the material can change depending on a number of variables, including crystal structure, phase, and doping [27]. The mechanical properties of other transition metal oxides, such as zinc oxide (ZnO) and tungsten oxide (WO_3), have also been the subject of study.

Researchers have also examined the strength and fracture toughness of transition metal oxides. Strength determines a material's capacity to endure external forces without deforming or failing, whereas measures of fracture toughness reveal how resistant a substance is to crack propagation. Tantalum oxide (Ta_2O_5) and zirconium oxide (ZrO_2), for example, have been research because their high fracture toughness makes them appropriate for uses requiring resistance to mechanical stress.

It has also been investigated how size and shape affect the mechanical characteristics of transition metal oxides. Studies, for instance, have looked into how particle size and shape affect the mechanical properties of nanoscale transition metal oxide materials. Reducing the size of transition metal oxide nanoparticles has been found to increase hardness and strengthen mechanically. Furthermore, compared to their bulk equivalents, controlled production of transition metal oxide nanostructures, such as nanowires and nanosheets, has shown improved mechanical properties.

Additionally, it has been studied how transition metal oxides' mechanical characteristics change with changes in temperature and humidity. Certain researches have demonstrated how the environmental factors affect certain materials mechanically. For instance, research on tungsten oxide (WO_3) has revealed that phase transitions and thermal expansion cause changes in the material's mechanical properties at high temperatures.

In studies on the mechanical characteristics of transition metal oxides have revealed important information on their elastic properties, strength, and the effects of size, morphology, and environmental factors. For these materials to be successfully used in areas like structural materials, sensors, and microelectromechanical systems (MEMS), it is essential to understand their mechanical behaviour. The design and optimization of transition metal oxide-based materials with customized mechanical properties for particular applications would benefit from further research in this field.

2.2.5 Review of electrical properties of transition metal oxides

The fascinating electrical characteristics of transition metal oxides (TMOs), which make them excellent candidates for a variety of applications including catalysis, energy storage, and electronics, have drawn considerable interest in the field of materials research. Based on articles that have been published, and it will examine the electrical characteristics of TMOs in this review.

The adjustable conductivity of transition metal oxide is one of the significant electrical characteristics. The conductivity of transition metal oxide can be modified by adjusting external stimuli like temperature, pressure, or doping. For instance, an electric field can regulate the conductivity of vanadium dioxide (VO_2). VO_2 experiences a metal-to-insulator transition at a threshold temperature, which significantly alters conductivity [28]. Potential uses for this characteristic include switches and sensors in electronic equipment.

Transition metal oxides also display a variety of electronic ordering phenomena. For example, the interaction of charge, spin, and orbital degrees of freedom in perovskite-type transition metal oxides results in fascinating phenomena like high-temperature superconductivity and enormous magnetoresistance. In a study it is looked that the electronic ordering of manganite-based perovskites and found that when temperature decreased, there was a significant decrease in conductivity and a transition from a ferromagnetic metal to an

antiferromagnetic insulator [29]. This transition results in complex phase diagrams and unusual electrical characteristics because of the delicate balance between electron-electron interactions and lattice distortions.

Furthermore, their distinct redox characteristics, transition metal oxides have showed potential in energy storage applications. Lithium-ion batteries frequently use transition metal oxides as cathode materials, such as lithium cobalt oxide ($LiCoO_2$) [30]. Lithium ions can be intercalated and deintercalated inside the crystal structure of TMOs, which promotes reversible redox processes and effective energy storage. A novel manganese oxide-based material with improved capacity and stability for sodium-ion batteries was synthesized creating new opportunities for next-generation energy storage technologies [31].

In transition metal oxides have a wide range of rich and varied electrical characteristics. They are very appealing for a variety of applications due to their adjustable conductivity, electronic ordering phenomena, and redox characteristics. The studies covered in this review demonstrate how adaptable and useful TMOs are for a variety of applications, including energy storage and electronics. Unlocking the full potential of these materials and discovering unique phenomena that could completely alter a variety of technical fields are both possible with more research in this area.

2.2.6 Review of chemical properties of transition metal oxides

Transition metal oxides (TMOs) are flexible materials with a wide range of exciting chemical properties that make them useful in a variety of industries, including catalysis, energy storage, and electronics. Based on earlier findings, it will examine the chemical characteristics of TMOs in this review.

The redox activity of transition metal oxides is a crucial chemical characteristic. Because they may undergo reversible oxidation and reduction reactions, a lot of transition metal oxides are useful for energy storage applications. For instance, in a study of the redox properties of

cobalt oxide (Co_3O_4), which is used as an anode material in lithium-ion batteries [32]. Due to its multi-electron redox processes, Co_3O_4 has shown to have a high specific capacity and good cycling stability, making it a suitable option for next-generation energy storage devices.

Additionally, because of their distinct surface structures and electrical topologies, transition metal oxides frequently display a variety of catalytic capabilities. One well-known catalyst utilized in numerous applications is titanium dioxide (TiO_2). The catalytic capabilities of TiO_2 in the breakdown of organic contaminants was examined [33]. It was evident that TiO_2's catalytic activity was considerably influenced by its chemical composition, crystal structure, and surface area, underscoring the need of comprehending the chemical features for improving catalytic performance.

Transition metal oxides can also go through ion exchange and intercalation processes, which let foreign ions or molecules be incorporated into their structures. This feature creates possibilities for ion storage and sensor applications. The ion exchange behaviour of tungsten oxide (WO_3) for electrochromic applications was investigated [34]. They were able to generate tunable colour changes in the material by managing the intercalation of protons and lithium ions, opening the door to possible uses in smart windows and displays.

Additionally, a key factor in determining the practical application of transition metal oxides is their chemical stability. Transition metal oxides can display different levels of chemical reactivity, oxidation resistance, and corrosion resistance. These characteristics may be affected by elements such the crystal structure, surface termination, and environmental exposure. To ensure TMOs' long-term effectiveness in applications like coatings and corrosion protection, it is crucial to comprehend their chemical stability [35]. To develop methods for increasing the stability and toughness of transition metal oxide-based materials, more study in this area is required.

The numerous and significant chemical characteristics of transition metal oxides are summarized in this chapter. They are extremely desirable for a variety of applications due to their high redox activity, catalytic abilities, ion exchange behaviour, and chemical stability. The studies covered in this review underline the significance of comprehending and modifying the chemical characteristics of transition metal oxides for the creation of new materials with improved functionality and performance. Continued study in this area has the potential to open up new applications and further advancing the field of materials science.

2.3 Classification of tungsten tri-oxide (WO_3)

The chemical compound combining oxygen and the transition metal tungsten, having the formula WO_3, is tungsten (VI) oxide, commonly referred to as tungsten trioxide. Due to its close kinship to tungstic acid H_2WO_4, the substance is sometimes known as tungstic anhydride. It is a crystalline solid that is light yellow. In nature tungsten (VI) oxide is found as hydrates of the minerals tungstite ($WO_3.H_2O$), meymacite ($WO_3.2H_2O$), and hydro tungstite (which has the same chemical composition as meymacite but is occasionally abbreviated as H_2WO_4). These secondary tungsten minerals are extremely rare.

Temperature affects tungsten trioxide's crystal structure. At temperatures over 740 °C, it is tetragonal; between 330 and 740 °C, orthorhombic; between 17 and 330 °C, monoclinic; between -50 and 17 °C, triclinic; and below -50 °C, monoclinic once more. The monoclinic form of WO_3 is the most stable [36].

2.4 Properties of tungsten tri-oxide (WO_3)

The compound tungsten trioxide (WO_3) has a variety of characteristics that make it a valuable material for many different uses. Here are some of tungsten trioxide's main characteristics based on survey of the literature:

2.4.1 Catalytic properties

The catalyst tungsten trioxide works well for a variety of reactions. It is recognized for its catalytic activity in the oxidation of organic substances, including alcohols, hydrocarbons, and volatile chemical molecules [37]. Tungsten trioxide has a special surface structure and redox characteristics that enhance its catalytic activity.

2.4.2 Mechanical and thermal properties

High melting point, strong thermal stability, and exceptional mechanical qualities are all characteristics of tungsten trioxide. Due of these qualities, it can be used in high-temperature applications including thermal barrier coatings and refractory materials [38].

2.4.3 Electrical properties

A semiconductor with a broad bandgap, usually between 2.5 and 3.0 eV, is tungsten trioxide. This bandgap allows for efficient absorption of visible light and makes it suitable for optoelectronic applications [39].

2.4.4 Optical properties

Particularly in the visible and near-infrared spectrums, tungsten trioxide demonstrates intriguing optical characteristics. For optical coatings and anti-reflection coatings, its high refractive index makes it beneficial. Additionally, tungsten trioxide exhibits electrochromic behaviour [40], making it appropriate for use in smart windows and display devices since it can alter its colour and optical transmittance in reaction to an external electric field.

In tungsten trioxide has a variety of qualities that make it helpful in a variety of applications. It is an advantageous material for applications ranging from optics and electronics to energy and environmental technologies because of its optical, electrical, catalytic, energy storage, gas sensing, photocatalytic, and mechanical capabilities.

2.5 Review of Various synthesis methods of tungsten trioxide

2.5.1 Solid state synthesis

Ammonium meta tungstate served as the precursor for the preparation of the hexagonal phase of WO_3 in high yield (approximately 95 % of the precursor). A quartz plate that had been previously dispersed with ammonium meta tungstate was then put into the centre of a horizontal tube furnace. When the temperature reached 500, 600, 700, 800, or 900 °C, an argon gas flow was started and maintained for three hours [41].

$$\text{Ammonium meta tungstate} \xrightarrow{500℃} 6NH_3\uparrow + (n+4)\,H_2O + 12WO_3 \xrightarrow{600℃} \text{m-}WO_3 \xrightarrow{700-800℃} \text{c-}WO_3 \xrightarrow{900℃} \text{h-}WO_3$$

2.5.2 Sol-gel method

In the sol-gel process, metal precursors are hydrolysed and condensed to create a sol, which is then heated to produce the required oxide. Tungsten alkoxides or tungsten chloride can be employed as precursor materials in the manufacture of WO_3. This process provides good control over the morphology and content of the final WO_3. The WO_3 nanoparticles, thin films, and other nanostructures have all been synthesized using it. The sol-gel method allows for tailoring the properties of WO_3 by modifying the synthesis parameters and dopants [42].

2.5.3 Hydrothermal method

The synthesis of tungsten trioxide nanoparticles uses tungsten hexachloride as a precursor. The reaction was carried out by combining 0.05 M tungsten hexachloride and 0.05 M urea in a 40 mL solution of ethanol. Using a magnetic stirrer, the solution was continuously stirred until it took on a dark blue hue. It was then moved to a stainless steel autoclave with teflon lining, where it was kept at 180 ℃ for 12 hours. To get rid of the untreated species, the

finished product was washed and rinsed many times with distilled water and ethanol. The precipitate was then collected and dried for 24 hours in an oven set to 60 ℃. To form pristine WO_3, the resultant solid products were annealed at 450 ℃ for three hours. The resulting WO_3's particle size, morphology, and crystallinity can be controlled by adjusting the reaction parameters, which include temperature, pressure, and reaction time [43].

2.5.4 Precipitation method

In the precipitation method, tungsten compounds are precipitated from a solution and then subjected to a further heat process to transform them into WO_3. Starting materials frequently include tungstate salts like sodium tungstate or ammonium tungstate. By modifying the precipitation circumstances and post-treatment procedures, this method allows for scalability, simplicity, and the possibility of changing particle size and shape. The WO_3 that has precipitated can then be treated further to produce the required results, such as nanoparticles, films, or bulk materials [44].

2.5.5 Thermal decomposition method

The thermal decomposition process entails the thermal decomposition of tungsten compounds at high temperatures, such as ammonium meta-tungstate (AMT). This method has been used to produce WO_3 nanoparticles, thin films, and nanowires. High purity and crystallinity are typical characteristics of the resultant WO_3. By altering the precursor concentration, reaction temperature, and environment, one may control the particle size and morphology [45].

2.5.6 Chemical Vapour Deposition (CVD)

Chemical vapour deposition is the process of depositing a solid coating onto a substrate by breaking down volatile precursor molecules in a gas phase. The tungsten precursor in the CVD technique is typically tungsten hexafluoride (WF_6). Thin films of WO_3 with regulated thickness and morphology can be produced by modifying the deposition parameters such as

temperature, pressure, and precursor flow rate. WO_3 may be deposited via CVD with precise control over the film's characteristics on a variety of substrates [46].

2.5.7 Electrodeposition method

By using pulsed electrodeposition, high surface area, porous, nanoparticulate tungsten oxide has been successfully synthesized. Pulse length has the ability to regulate particle size; as pulse duration reduced, particle size also reduces, and this effect was unaffected by the deposition voltage. Nanoparticulate tungsten oxide had higher photoactivity and current density for hydrogen intercalation compared to tungsten oxide films made using continuous electrodeposition. higher light absorbance, improved charge transport, and higher surface redox activity are the results of the nanocrystalline tungsten oxide's reduced particle size and larger surface area [47].

Other synthesis techniques have been investigated for WO_3 in addition to the ones previously listed, such as spray pyrolysis [48], and template-assisted.

2.6 Applications of tungsten trioxide (WO_3)

A versatile and extensively researched transition metal oxide, tungsten trioxide (WO_3) has several uses in a variety of industries. It is suitable for a variety of technological developments due to its special characteristics, which include tunable electrical conductivity, photochromic behaviour, and catalytic activity. The various uses of tungsten trioxide are examined in this literature review, with an emphasis on its importance in energy storage, optoelectronics, gas sensing, and smart windows.

2.6.1 Photocatalysis

Due to its photocatalytic capabilities, tungsten trioxide may use solar energy in a variety of ways. It is suitable for water splitting, pollutant degradation, and hydrogen production because it can produce charge carriers in response to light irradiation. Photocatalysts based on

tungsten trioxide have demonstrated good performance in the degradation of organic dyes [49], water purification, and overall solar energy conversion efficiency [50].

2.6.2 Energy storage

For use as an electrode material in energy storage systems like lithium-ion batteries and supercapacitors, tungsten trioxide has attracted attention [51]. It is a viable contender for high-performance battery applications due to its capacity to intercalate lithium ions and its charge/discharge cycling stability. Additionally, a supercapacitor's increased energy storage capacity is made possible by the material's enormous surface area and high electrochemical activity.

2.6.3 Optoelectronics

Due to its exceptional optical and electrical characteristics, tungsten trioxide is the perfect substance for optoelectronic devices. Its use in electrochromic devices (ECDs) and smart windows has been thoroughly researched [52]. Reversible colour changes provided by ECDs based on tungsten trioxide allow for dynamic regulation of light transmission, which is useful for energy-efficient windows and smart glass applications.

2.6.4 Gas sensing

It has been widely investigated how tungsten trioxide can be used in gas sensing applications to detect gases including nitrogen dioxide (NO_2) [53], carbon monoxide (CO), and volatile organic compounds (VOCs). The high specific surface area and distinctive surface chemistry of this material enable effective gas adsorption and detection. High selectivity, sensitivity, and quick response times of tungsten trioxide-based gas sensors have made them suitable for application in environmental monitoring, industrial safety, and air quality control.

2.6.5 Nanoelectronics

For nano-electronic applications, the unique electrical characteristics of tungsten trioxide at the nanoscale have garnered considerable interest. Field-effect transistors, resistive random-access memory (RRAM), and nanowires have all benefited from its use. Due to their exceptional stability, high electron mobility, and compatibility with complementary metal-oxide-semiconductor (CMOS) technology, tungsten trioxide nanowires hold promise as a foundation for future nano-electronic devices.

A versatile material with numerous uses in energy storage, optoelectronics, gas sensing, photocatalysis, and nanoelectronics is tungsten trioxide (WO_3). It is a prospective contender for a number of technological breakthroughs due to its distinctive qualities, which include variable electrical conductivity, photochromic behaviour, and catalytic activity. For tungsten trioxide to reach its full potential and grow its range of uses across various industries, further research and development are required in this area. Tungsten trioxide is expected to play a significant role in determining the future of advanced electronics, environmental monitoring, and energy-efficient technologies.

2.7 Application of tungsten tri-oxide based material in photocatalysis

Materials based on tungsten trioxide (WO_3) have drawn a lot of interest in the field of photocatalysis because of their distinctive characteristics and potential for effective solar energy conversion. Water splitting, the degradation of pollutants, and the production of hydrogen are all common applications for the process known as photocatalysis, in which a catalyst absorbs light and starts a chemical reaction. Given this situation, WO_3-based materials provide a number of benefits that make them strong contenders for photocatalytic applications.

Firstly, tungsten trioxide has an optimal bandgap energy (2.6–2.8 eV) that enables it to effectively absorb visible light. This makes it more effective than substances that solely

absorb ultraviolet (UV) light because it can use a wider range of the solar spectrum for catalytic processes. Visible light can be used for a variety of solar-powered applications because visible light makes up the majority of solar energy [54].

Secondly, WO_3-based materials have great charge separation efficiency and high charge carrier mobility, both of which are necessary for effective photocatalysis. The separation of these charges is essential to avoid recombination and optimize the use of photoexcited electrons for catalytic reactions. WO_3 produces electron-hole pairs when exposed to light. Tungsten tri-oxide based material has a distinctive electronic structure that makes charge transfer effective and allows for increased photocatalytic activity.

Thirdly, exceptional stability and resistance to photo-corrosion are displayed by tungsten trioxide, which is necessary for long-term photocatalytic applications. Under continuous light exposure, several photocatalysts have a tendency to deteriorate or undergo structural changes, which restricts their usefulness. However, under photocatalytic circumstances, WO_3-based materials have demonstrated good stability, ensuring their longevity and long-term performance.

Tungsten trioxide has been used in a variety of photocatalytic reactions. For instance, WO_3-based catalysts have been utilized to split water into hydrogen and oxygen with the help of solar radiation. The creation of hydrogen fuel and the production of renewable energy are both significantly impacted by this process [55].

Additionally, WO_3-based photocatalysts were proven to function exceptionally well in the oxidative photocatalytic oxidation of organic contaminants such as dyes and pharmaceuticals. The effective breakdown of organic pollutants is facilitated by the reactive oxygen species produced by tungsten trioxide, which aids in environmental clean-up.

This materials based on tungsten trioxide have demonstrated significant promise for photocatalytic applications. They make ideal candidates for solar-driven water splitting,

pollutant degradation, and hydrogen production due to their high charge carrier mobility, outstanding stability, efficient absorption of visible light, resistance to photo-corrosion, and resistance to photodegradation. For tungsten trioxide-based photocatalysts to be widely used in renewable energy and environmental applications, continued research and development in this field are essential for increasing their effectiveness and comprehending the underlying mechanisms.

2.8 Conclusions

The literature study has shown the several uses of tungsten trioxide (WO_3) and its importance in photocatalysis, optoelectronics, gas sensing, and energy storage. WO_3 is a special kind of material because of its tunable electrical conductivity, photochromic activity, and special features. The study also discusses the several synthesis techniques used to synthesize tungsten trioxide, such as solid-state synthesis, sol-gel techniques, hydrothermal synthesis, and chemical vapor deposition. These synthesis techniques contribute to the development of tailored WO_3 structures with optimized properties for specific applications.

2.9 References

1. Koli, P.B., Kapadnis, K.H. and Deshpande, U.G., 2019. Transition metal decorated Ferrosoferric oxide (Fe_3O_4): An expeditious catalyst for photodegradation of Carbol Fuchsin in environmental remediation. *Journal of Environmental Chemical Engineering*, *7*(5), 103373.

2. Zhao, H., Jian, L., Gong, M., Jing, M., Li, H., Mao, Q., Lu, T., Guo, Y., Ji, R., Chi, W. and Dong, Y., 2022. Transition-metal-based cocatalysts for photocatalytic water splitting. *Small Structures*, *3*(7), 2100229.

3. Toroker, M.C. and Carter, E.A., 2013. Transition metal oxide alloys as potential solar energy conversion materials. *Journal of Materials Chemistry A*, *1*(7), 2474-2484.

4. Khaki, M.R.D., Shafeeyan, M.S., Raman, A.A.A. and Daud, W.M.A.W., 2017. Application of doped photocatalysts for organic pollutant degradation-A review. *Journal of environmental management*, *198*, 78-94.

5. Pattanayak, P., Singh, P., Bansal, N.K., Paul, M., Dixit, H., Porwal, S., Mishra, S. and Singh, T., 2022. Recent progress in perovskite transition metal oxide-based photocatalyst and photoelectrode materials for solar-driven water splitting. *Journal of Environmental Chemical Engineering*, 108429.

6. Da, Y. and Zhou, J., 2022. Decorating Calcium-Based Materials with Transition Metal Elements for Directly Capturing and Storing Solar Energy. *ACS omega*.

7. Zhuang, G., Yan, J., Wen, Y., Zhuang, Z. and Yu, Y., 2021. Two-dimensional transition metal oxides and chalcogenides for advanced photocatalysis: progress, challenges, and opportunities. *Solar RRL*, *5*(6), 2000403.

8. Abasaeed, A.E., Lanre, M.S., Kasim, S.O., Ibrahim, A.A., Osman, A.I., Fakeeha, A.H., Alkhalifa, A., Arasheed, R., Albaqi, F., Kumar, N.S. and Khan, W.U., 2022. Syngas production from methane dry reforming via optimization of tungsten trioxide-promoted mesoporous γ-alumina supported nickel catalyst. *International Journal of Hydrogen Energy*.

9. Chen, H., Qiu, X., Zhu, W. and Hagenmuller, P., 2002. Synthesis and high rate properties of nanoparticled lithium cobalt oxides as the cathode material for lithium-ion battery. *Electrochemistry communications*, *4*(6), 488-491.

10. Hassoun, J., Bonaccorso, F., Agostini, M., Angelucci, M., Betti, M.G., Cingolani, R., Gemmi, M., Mariani, C., Panero, S., Pellegrini, V. and Scrosati, B., 2014. An advanced lithium-ion battery based on a graphene anode and a lithium iron phosphate cathode. *Nano letters*, *14*(8), 4901-4906.

11. Yang, M.C., Lee, Y.Y., Xu, B., Powers, K. and Meng, Y.S., 2012. TiO_2 flakes as anode materials for Li-ion-batteries. *Journal of Power Sources*, *207*, 166-172.

12. Unal, F.A., Ok, S., Unal, M., Topal, S., Cellat, K. and Şen, F., 2020. Synthesis, characterization, and application of transition metals (Ni, Zr, and Fe) doped TiO_2 photoelectrodes for dye-sensitized solar cells. *Journal of Molecular Liquids*, *299*, 112177.

13. Moore, K. and Wei, W., 2021. Applications of carbon nanomaterials in perovskite solar cells for solar energy conversion. *Nano Materials Science*, *3*(3), 276-290.

14. Wu, C.C., 2018. Highly flexible touch screen panel fabricated with silver-inserted transparent ITO triple-layer structures. *RSC advances*, *8*(22), 11862-11870.

15. Wang, F., Qiao, X., Xiong, T. and Ma, D., 2008. The role of molybdenum oxide as anode interfacial modification in the improvement of efficiency and stability in organic light-emitting diodes. *Organic Electronics*, *9*(6), 985-993.

16. Ganbavle, V.V., Mohite, S.V., Agawane, G.L., Kim, J.H. and Rajpure, K.Y., 2015. Nitrogen dioxide sensing properties of sprayed tungsten oxide thin film sensor: effect of film thickness. *Journal of colloid and interface science*, *451*, 245-254.

17. Mahajan, S. and Jagtap, S., 2020. Metal-oxide semiconductors for carbon monoxide (CO) gas sensing: A review. *Applied materials today*, *18*, 100483.

18. Gelover, S., Mondragón, P. and Jiménez, A., 2004. Titanium dioxide sol–gel deposited over glass and its application as a photocatalyst for water decontamination. *Journal of Photochemistry and Photobiology A: Chemistry*, *165*(1-3), 241-246.

19. Endoh, E., Leland, J.K. and Bard, A.J., 1986. Heterogeneous photoreduction of nitrogen to ammonia on tungsten oxide. *The Journal of Physical Chemistry*, *90*(23), 6223-6226.

20. Tan, H.T., Sun, W., Wang, L. and Yan, Q., 2016. 2D transition metal oxides/hydroxides for energy-storage applications. *ChemNanoMat*, *2*(7), 562-577.

21. Chang, P.C., Fan, Z., Chien, C.J., Stichtenoth, D., Ronning, C. and Lu, J.G., 2006. High-performance ZnO nanowire field effect transistors. *Applied physics letters*, *89*(13),133113.

22. Korotcenkov, G., 2008. The role of morphology and crystallographic structure of metal oxides in response of conductometric-type gas sensors. *Materials Science and Engineering: R: Reports*, *61*(1-6), 1-39.

23. Loganathan, K., Bommusamy, P., Muthaiahpillai, P. and Velayutham, M., 2011. The syntheses, characterizations, and photocatalytic activities of silver, platinum, and gold doped TiO_2 nanoparticles. *Environmental Engineering Research*, *16*(2), 81-90.

24. Chaudhary, M., Tyagi, S., Gupta, R.K., Singh, B.P. and Singhal, R., 2021. Surface modification of cathode materials for energy storage devices: A review. *Surface and Coatings Technology*, *412*, 127009.

25. Benneckendorf, F.S., Hillebrandt, S., Ullrich, F., Rohnacher, V., Hietzschold, S., Jänsch, D., Freudenberg, J., Beck, S., Mankel, E., Jaegermann, W. and Pucci, A., 2018. Structure–property relationship of phenylene-based self-assembled monolayers for record low work function of indium tin oxide. *The Journal of Physical Chemistry Letters*, *9*(13), 3731-3737.

26. Viter, R. and Iatsunskyi, I., 2019. Metal oxide nanostructures in sensing. In *Nanomaterials Design for Sensing Applications* (41-91). Elsevier.

27. Ma, X.G., Liang, P., Miao, L., Bie, S.W., Zhang, C.K., Xu, L. and Jiang, J.J., 2009. Pressure-induced phase transition and elastic properties of TiO_2 polymorphs. *physica status solidi (b)*, *246*(9), 2132-2139.

28. Chudnovskiy, F., Luryi, S. and Spivak, B., 2002. Switching device based on first-order metal-insulator transition induced by external electric field. *Future trends in microelectronics: the nano millennium*, *148*.

29. Tanaka, H., Zhang, J. and Kawai, T., 2001. Giant electric field modulation of double exchange ferromagnetism at room temperature in the perovskite manganite/titanate p− n junction. *Physical review letters*, *88*(2), 027204.

30. Liu, Q., Su, X., Lei, D., Qin, Y., Wen, J., Guo, F., Wu, Y.A., Rong, Y., Kou, R., Xiao, X. and Aguesse, F., 2018. Approaching the capacity limit of lithium cobalt oxide in lithium ion batteries via lanthanum and aluminium doping. *Nature Energy*, *3*(11),936-943.

31. Fang, S., Bresser, D. and Passerini, S., 2022. Transition metal oxide anodes for electrochemical energy storage in lithium-and sodium-ion batteries. *Transition Metal Oxides for Electrochemical Energy Storage*, 55-99.

32. Wang, G.X., Chen, Y., Konstantinov, K., Lindsay, M., Liu, H.K. and Dou, S.X., 2002. Investigation of cobalt oxides as anode materials for Li-ion batteries. *Journal of Power Sources*, *109*(1), 142-147.

33. Nakata, K. and Fujishima, A., 2012. TiO_2 photocatalysis: Design and applications. *Journal of photochemistry and photobiology C: Photochemistry Reviews*, *13*(3), 169-189.

34. Zeb, S., Sun, G., Nie, Y., Xu, H., Cui, Y. and Jiang, X., 2021. Advanced developments in nonstoichiometric tungsten oxides for electrochromic applications. *Materials Advances*, *2*(21), 6839-6884.

35. Gulbiński, W., Suszko, T., Sienicki, W. and Warcholiński, B., 2003. Tribological properties of silver-and copper-doped transition metal oxide coatings. *Wear*, *254*(1-2), 129-135.

36. https://en.wikipedia.org/wiki/Tungsten_trioxide

37. Abe, R., Takami, H., Murakami, N. and Ohtani, B., 2008. Pristine simple oxides as visible light driven photocatalysts: highly efficient decomposition of organic compounds over platinum-loaded tungsten oxide. *Journal of the American Chemical Society*, *130*(25), 7780-7781.

38.https://www.google.com/search?q=mechanical+properties+of+tungsten+trioxide&oq=mechanical+properties+of+tungsten+trioxide&aqs=chrome..69i57j0i22i30j0i390i650l5.11532j0j15&sourceid=chrome&ie=UTF-8

39. Cong, S., Geng, F. and Zhao, Z., 2016. Tungsten oxide materials for optoelectronic applications. *Advanced Materials*, *28*(47), 10518-10528.

40. Wei, H., Yan, X., Wang, Q., Wu, S., Mao, Y., Luo, Z., Chen, H., Sun, L., Wei, S. and Guo, Z., 2013. Electrochemical properties and electrochromic behaviors of the sol–gel derived tungsten trioxide thin films. *Energy and Environment Focus*, *2*(2), 112-120.

41. Mu, W., Xie, X., Li, X., Zhang, R., Yu, Q., Lv, K., Wei, H. and Jian, Y., 2015. Solid-state synthesis of hexagonal tungsten trioxide nanorods. *Materials Letters*, *138*, 107-109.

42. Susanti, D., Diputra, A.G.P., Tananta, L., Purwaningsih, H., Kusuma, G.E., Wang, C., Shih, S. and Huang, Y., 2014. WO_3 nanomaterials synthesized via a sol-gel method and calcination for use as a CO gas sensor. *Frontiers of Chemical Science and Engineering*, *8*, 179-187.

43. Jeevitha, G., Abhinayaa, R., Mangalaraj, D. and Ponpandian, N., 2018. Tungsten oxide-graphene oxide (WO_3-GO) nanocomposite as an efficient photocatalyst, antibacterial and anticancer agent. *Journal of Physics and Chemistry of Solids*, *116*, 137-147.

44. Rezaee, O., Mahmoudi Chenari, H. and Ghodsi, F.E., 2016. Precipitation synthesis of tungsten oxide nanoparticles: X-ray line broadening analysis and photocatalytic efficiency study. *Journal of Sol-Gel Science and Technology*, *80*, 109-118.

45. Hunyadi, D., Sajó, I. and Szilágyi, I.M., 2014. Structure and thermal decomposition of ammonium metatungstate. *Journal of Thermal Analysis and Calorimetry*, *116*, 329-337.

46. Kirss, R.U. and Meda, L., 1998. Chemical vapor deposition of tungsten oxide. *Applied organometallic chemistry*, *12*(3), 155-160.

47. Baeck, S.H., Jaramillo, T., Stucky, G.D. and McFarland, E.W., 2002. Controlled electrodeposition of nanoparticulate tungsten oxide. *Nano Letters*, *2*(8), 831-834.

48. Nakakura, S., Arif, A.F., Rinaldi, F.G., Hirano, T., Tanabe, E., Balgis, R. and Ogi, T., 2019. Direct synthesis of highly crystalline single-phase hexagonal tungsten oxide nanorods by spray pyrolysis. *Advanced Powder Technology*, *30*(1), 6-12.

49. Palanisamy, G., Bhuvaneswari, K., Pazhanivel, T. and Bharathi, G., 2020. Enriched photocatalytic activity of Rhodamine B dye from aqueous solution using hollow sphere tungsten trioxide nanoparticles. *Optik*, *204*, 164171.

50. Wang, Y., Tian, W., Chen, C., Xu, W. and Li, L., 2019. Tungsten trioxide nanostructures for photoelectrochemical water splitting: material engineering and charge carrier dynamic manipulation. *Advanced Functional Materials*, *29*(23), p.1809036.

51. Xing, L.L., Huang, K.J. and Fang, L.X., 2016. Preparation of layered graphene and tungsten oxide hybrids for enhanced performance supercapacitors. *Dalton Transactions*, *45*(43), 17439-17446.

52. Djaoued, Y., Balaji, S. and Brüning, R., 2012. Electrochromic devices based on porous tungsten oxide thin films. *Journal of Nanomaterials*, *2012*, 7-7.

53. Shen, Y., Wang, W., Chen, X., Zhang, B., Wei, D., Gao, S. and Cui, B., 2016. Nitrogen dioxide sensing using tungsten oxide microspheres with hierarchical nanorod-assembled architectures by a complexing surfactant-mediated hydrothermal route. *Journal of Materials Chemistry A*, *4*(4), 1345-1352.

54. Palanisamy, G., Bhuvaneswari, K., Pazhanivel, T. and Bharathi, G., 2020. Enriched photocatalytic activity of Rhodamine B dye from aqueous solution using hollow sphere tungsten trioxide nanoparticles. *Optik*, *204*, 164171.

55. Yadav, A.A., Hunge, Y.M. and Kang, S.W., 2021. Porous nanoplate-like tungsten trioxide/reduced graphene oxide catalyst for sonocatalytic degradation and photocatalytic hydrogen production. *Surfaces and Interfaces*, *24*, 101075.

Chapter 3

Instruments and Apparatus

3.1. General description of synthesis methods of nanomaterials

In the current times, the synthesis of nanostructured materials has received significant attention which can be achieved by suitable physical and chemical techniques. The shape, size as well as the functionality of basic structural units of the nanomaterials to be synthesized can be controlled efficiently. Although, the synthesis of nanostructured materials can be done in several ways but generally, they can be classified into two main approaches: the top-down and the bottom-up. In top-down approach, the size of bulk material is reduced to nano-sized particle or structure with the help of physical processes like grinding, crushing, milling, electron-beam lithography etc. The greatest disadvantage of this method is the imperfection of crystallographic and surface structure. On the other hand, bottom-up approach involves gradual building of a nanomaterial from the bottom by assembling atom-by-atom or molecule-by-molecule. This method is very much economical as well as the shape and size distribution of the units of nanomaterials can be controlled easily. It includes chemical methods such as hydrothermal method, solid-state synthesis, colloidal precipitation, electrodeposition etc. The methods we have used for the synthesis of nanostructured materials (pure and hydrated WO3, gC_3N_4, composite of WO_3 with gC_3N_4) are described below:

3.1.1. Hydrothermal set-up

Hydrothermal method is a technique for synthesizing pure, hydrated and nano-composite materials. It is a non-conventional method of growing nanoparticles in an aqueous solution at high temperature (> room temperature)

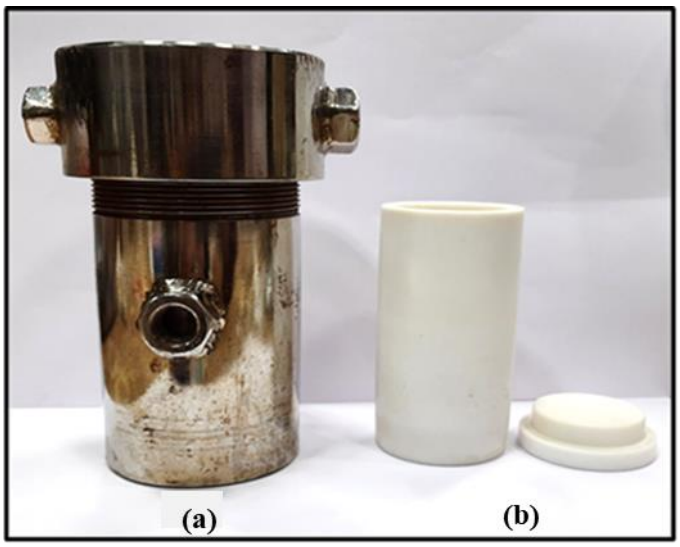

Fig. 3.1: Digital image of (a) autoclave setup and (b) the teflon tube in the autoclave

and pressure (> 1-2 atm) in an autoclave. Hydrothermal process has various advantages beginning from high product purity to homogeneity. In 21st century, this method has become a frontline technology in the developing field of advanced material processing. For material processing, hydrothermal technique requires a robust, non-reactive vessel known as autoclave as shown in **Fig. 3.1**. An autoclave is a pressurized device which is teflon-lined from inner side and outer side is made from stainless steel. In this device, the heating of aqueous solution or organic solvents take place above their boiling point at a pressure higher than normal atmospheric pressure. Basically, an autoclave is a cylindrical iron chamber which is fitted with an iron screw cap. To withstand very high pressure during the reaction, the iron screw cap may be fitted very tightly with the iron chamber. Inside the iron chamber, a cylindrical teflon tube with a teflon cap is fitted which serves as the inert reaction chamber.

3.2. General description of major synthesis apparatus

3.2.1. Hot Air Oven

The working theory is based on fine gravity air convection in a heated chamber by electricity. A number of parts are included in the machine to guarantee even heating throughout the chamber. The machine operates effectively and returns to normal temperature once the test process is complete due to features like the two jackets design, automatic control unit, PID controlled, PT 100 sensors, and temperature pre-set. It has been designed to simplify the process of dry sterilization and pre-treatment of various materials, such as rubber, plastic, and others. Forced circulation of the air inside the chamber enables proper heat distribution inside the space. The hotter the air inside the chamber gets the lighter and upward-moving it becomes. The fan inside the chamber pulls it back to the bottom as it reaches the top. This causes the air to circulate continuously in a circular motion inside the cabinet, finally resulting in the ideal temperature being reached. Always be careful not to remove items from

the oven too soon after placing them inside. The items are removed after the oven has reached a regular temperature.

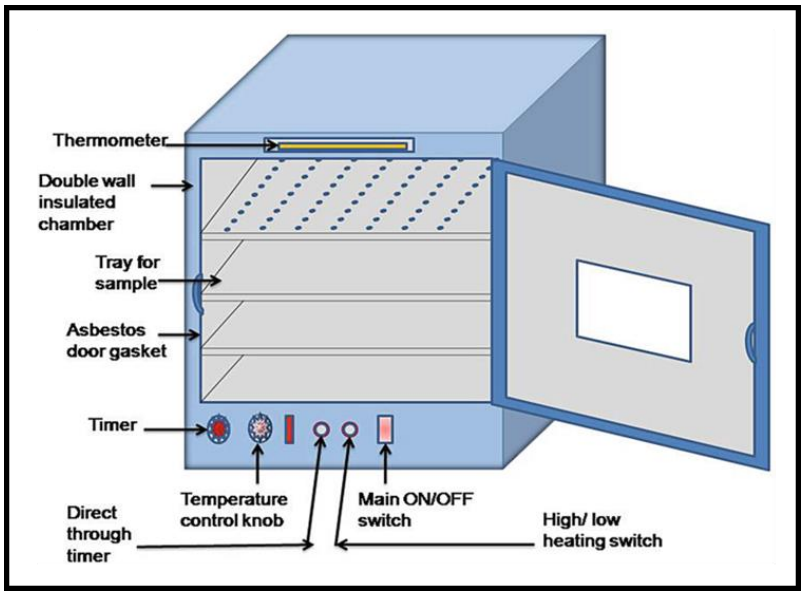

Fig. 3.2: Schematic diagram of a hot air oven

3.2.2 Weighing balance

An instrument used to calculate an object's weight or mass is a weighing balance. It is necessary equipment in laboratories, commercial kitchens, and pharmacies and is available in a variety of sizes with various weighing capacities.

Fig. 3.3: Digital weighing machine

3.2.3 Magnetic stirrer

In order to stir a non-magnetic liquid in a container, a magnetic stirrer uses a rotating magnetic field. A magnet installed on the stirrer under the container produces the revolving field. A revolving magnetic field that extends into the liquid is produced when the magnet spins.

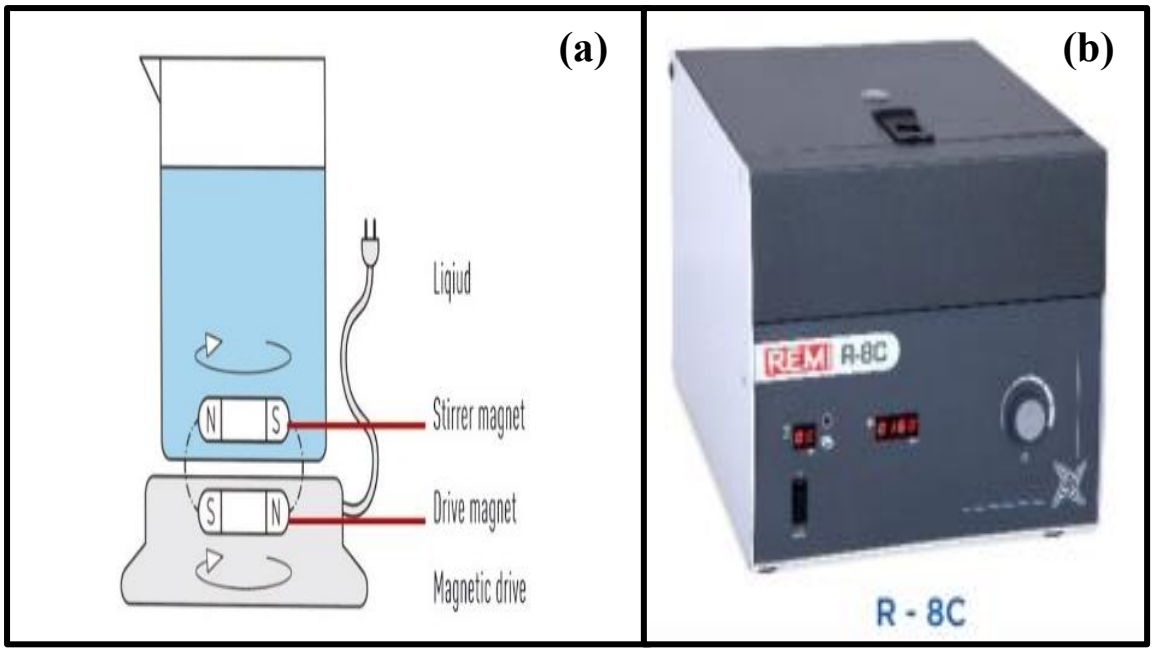

Fig. 3.4: Figure showing a magnetic stirrer (a) and **c**entrifuge machine (b)

3.2.4 Centrifuge

A centrifuge is a device that uses centrifugal force to apply a certain constant force to a specimen, such as to separate different fluid components. This is accomplished by rapidly spinning the fluid inside a container to separate liquids from solids or fluids with varying densities (such as cream from milk). Denser materials and particles travel outward in a radial direction as a result of its action. Less dense objects are also transported to the centre and dispersed at the same time. Due to the radial acceleration denser particles sink to the bottom of sample tubes used in laboratory centrifuges while low-density materials ascend to the top. Using a centrifuge as a filter to remove pollutants can be highly successful.

3.3. Characterization Tools

3.3.1 X-ray Diffractometer

X-ray diffraction is an important technique for determining the structure of the crystals. The German physicist Roentgen discovered X-ray in the year 1895 and it the term X-ray was given due to its unknown nature at that time. X-Ray shows more penetrating nature than that of light. The exact diffraction phenomenon of X-rays by the atomic planes of the crystal and its nature were properly discovered in the year of 1912. The theory behind XRD is a result of pioneering works of Bragg. The discovery showed the wave nature of X-rays and a new direction for investigation of structure of matter was explored. Solid matter can be classified as follows: Amorphous and Crystalline.

- **Amorphous**

  The arrangement of atoms is in random manner similar to the disorder we find in a liquid. Glass is an amorphous material.

- **Crystalline**

  The arrangement of atoms is periodic and repetitive in nature. One smallest volume of element by its repetition in three dimensions describes the crystal. This smallest volume of element is called a unit cell.

X-rays are electromagnetic radiation having shorter wavelength than that of light (0.01 to 10 nanometres). For analytical purpose 0.07 to 0.2 nm is most powerful. X-ray lies in the region of spectrum between gamma rays and ultraviolet rays.

3.3.1.1 X-ray Diffraction

X-ray diffraction method is based on scattering of X-rays by crystals. By using this method analyst can easily identify the crystal structure of any solid compound (sample) with high

degree of specificity and accuracy. XRD is extremely an important method as compared to others X-ray spectroscopy.

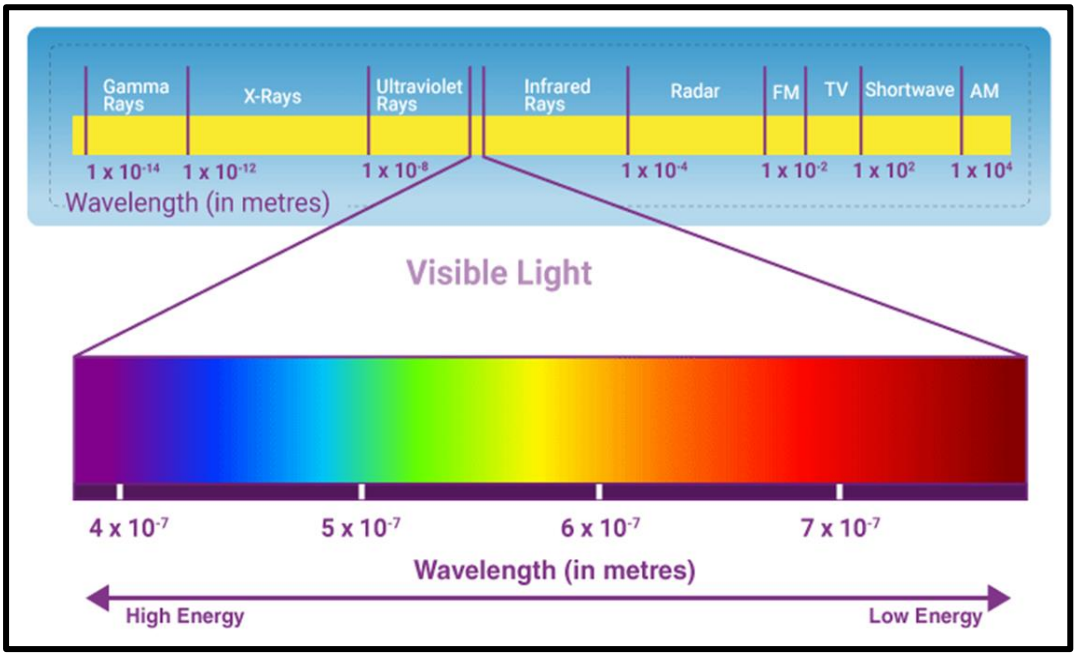

Fig. 3.5: Visible light spectrum - the electromagnetic spectrum colour

3.3.1.2 X-ray Absorption

This is similar to absorption method in other regions of electromagnetic spectra like UV-Visible/IR spectroscopy. It gives information about the absorbing material. In this method a beam of X-ray is passed through the sample and the fraction of X-ray photons absorbed is considered to be a measure of concentration of the sample. This method is least used as compared to other X-ray methods. It is used to detect imperfection in the internal structure, elemental analysis, thickness measurement etc.

3.3.1.3 X-ray Fluorescence

In this method X-rays are generated within the sample and by measuring the wavelength and intensity of the generated X-ray; analyst can perform qualitative as well as quantitative analysis.

All X-ray spectroscopic methods are non-destructive.

3.3.1.4 Theory

Bragg's law suggests that the crystal structure can be considered as an array of atom forming planes. The X-ray on striking an atom will scatter in same direction. The scattered X-ray can interfere constructively if they are in phase or destructively if they are out of phase. The path difference between the two X-rays scattering from the two planes can be easily seen to be $2d\sin\theta$, where d = interplanar spacing, θ = incident angle. For the two waves to interfere constructively, they should satisfy, the following relation $2d\sin\theta = n\lambda$ (λ = wavelength of X-ray). Now, if we consider the XRD graph for a crystalline material, we will get same intensity peaks in some material and for an amorphous material, no peaks will throw but we get a bump.

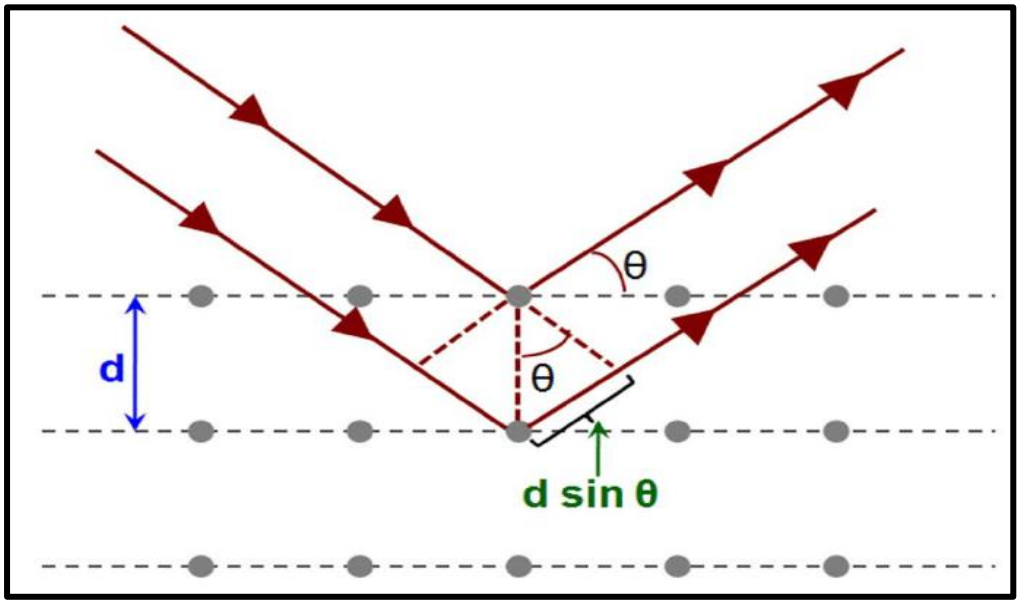

Fig. 3.6: Schematic diagram of the path difference between two "X" rays

Using JCPDS card, we can identify the material and by using Scherrer formula we can get size of the material from the XRD graph.

$D = k\lambda/\beta cos\ \theta$ (3.1)

Where,

D = size of particle of crystalline method,

k = dimensionless shape factor,

λ = wavelength of incident X-ray,

β = Line broadening at half of maximum intensity (FWHM), and

θ = Bragg's Angle.

3.3.1.5 Instrumentation

X-ray Tube

X-ray tube is a large vacuum tube containing a heated cathode of tungsten filament and a copper target metal anode. It is operated at a higher voltage up to 60 KV.

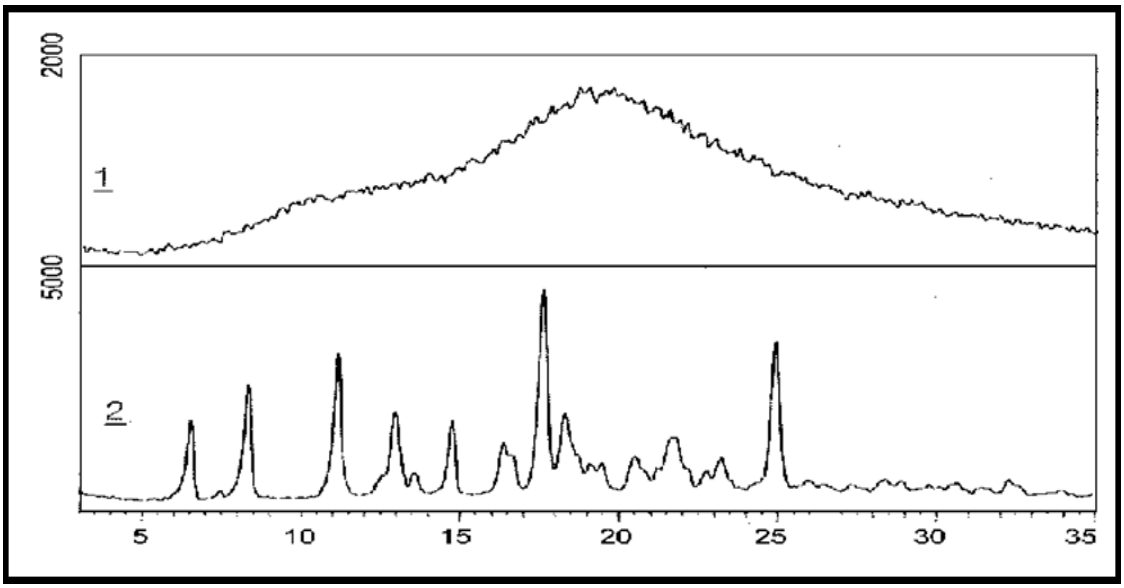

Fig. 3.7: XRD patterns for (1) Amorphous material, (2) Crystalline material

Collimator

To get a narrow beam of X-ray, they are passed through a collimator. It contains two closely packed metal plates, separated by a small gap.

Monochromator

(a) Filter: X-ray will be partly monochromatized. Filter absorbs undesirable radiations and passed required radiations.

(b) Crystal Monochromator: It is made up of suitable crystalline materials like Quartz.

Detector

A film is exposed and developed in X-rays passed through the sample and D value is determined by a densitometer.

$D = I_0/I$ (3.2)

Where,

I_0 = incident X-rays, and

I = transmitted X-rays.

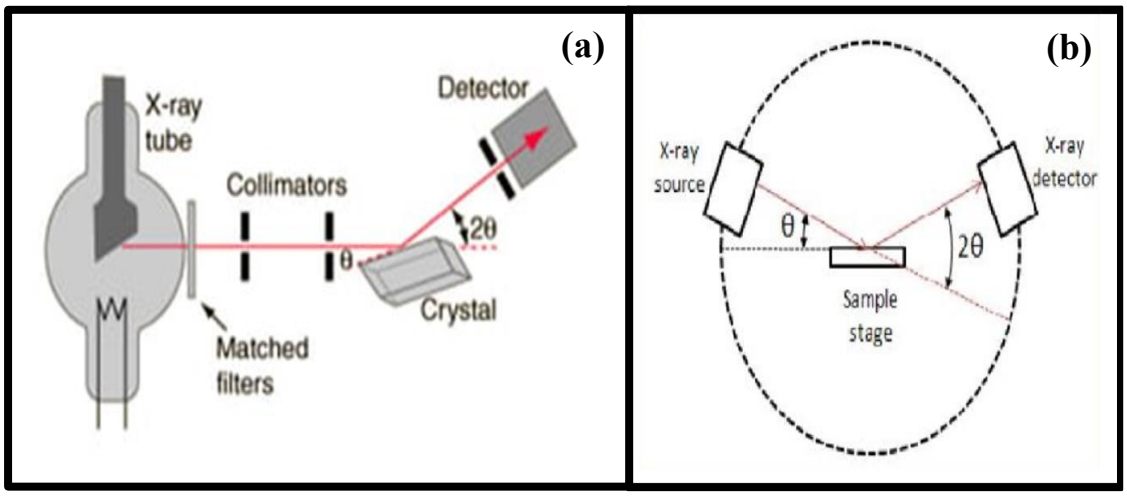

Fig. 3.8: The schematic diagram of Bragg's X-ray spectrometer (a) and the X-ray (b)

3.3.1.6 Procedure/Methodology

A simple X-ray diffraction experimental setup requires the following: a radiation source, a sample crystal and a detector. The source gives of X-rays that strike the crystal at some angle θ and the detector detects the scattered radiation at an angle of 2θ from the source. The X-rays heats the atom in the crystal plane and scatter in different direction. For diffraction to occur the scatter radiation must be coherent therefore the scattering must be elastic, the angular position of the source over the range of interest and correspondingly. The detector and the intensities of the scattered radiations are recorded and plotted versus 2θ. This plot of

intensity is called XRD pattern. The detector can be of several kinds. It requires a simple photographic plate or sophisticated.

Fig. 3.9: Experimental setup of X-Ray diffractometer

The intensity of the highest peak is set to 100 and the rest of the peaks are so called with respect to this. Thus, the peaks are mapped to a particular set of lattice planes given by the corresponding miller indices. This is done by calculating the interplanar spacing corresponding to a particular peak. And using a relationship between 'd' and the indices for different lattice types.

3.3.2 Fourier transform infrared spectroscopy (FTIR)

The vibration of molecules is the focus of FTIR spectroscopy, also known as Fourier-transform infrared spectroscopy. The sum of all the functional groups can be utilized to

identify a molecule because each functional group has a unique discrete vibrational energy. This makes FTIR microscopy perfect for sample identification, characterization of multilayer films, and particle analysis. The electromagnetic spectrum is divided into many sections that correspond to various energy (E), frequency, and wavelength ranges. The wavenumber (cm $^{-1}$), which is used to measure near, mid, and far-infrared light, is derived from the inverse relationship between wavelength and frequency.

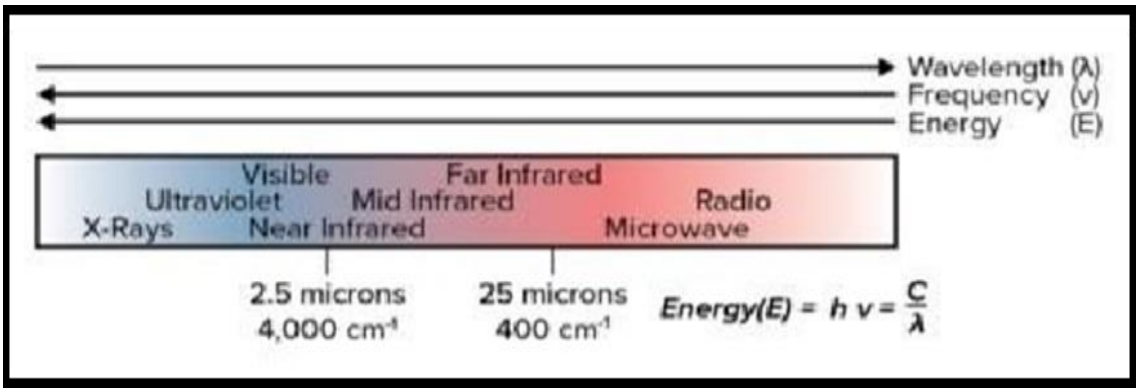

Fig 3.10: Electromagnetic spectrum showing near and far infrared regions

The IR light's ability to alter the dipole moments in molecules that are related to a particular vibrational energy is used by FTIR spectroscopy. Two variables—reduced mass (μ) and the bond spring constant (k)—relate to vibrational energy. We can examine C-C, C=C, and CC for the k constant, which reveal an increase of 800 cm $^{-1}$ across the period. A shift of 100 cm^{-1} results from replacing nitrogen and oxygen atoms in a C-C bond. It is clear from comparing the two series that bond strength affects wavenumbers more than mass. Every functional group has a unique vibration since each one is made up of distinct atoms and bonds with varied strengths (for instance, O-H and C-H stretches emerge at 3200 cm^{-1} and 2900 cm^{-1}, respectively). There is a correlation graph with different functional group vibrations. Since each molecule has a unique collection of vibrational energy bands for each of its functional groups, these peaks can be utilized to identify molecules via library searches of extensive sample libraries.

3.3.2.1 Working theory and different components of FTIR

The source, interferometer, and detector are the three main components of an FTIR. Typically, the source is a broad-spectrum emitter like a far-IR mercury lamp (10-700 cm $^{-1}$), a near-IR halogen lamp (2,200-25,000 cm $^{-1}$), or a mid-IR ceramic source (50-7,800 cm $^{-1}$). The interferometer, which can be seen in box, is the brain of FTIR and is made up of a beam-splitter, a stationary mirror, a moving mirror, and a timed laser. The beam-splitter divides a source of light into two channels, one leading to a stationary mirror and the other to a moving mirror. However, for high throughput applications, a low angle interferometer is favoured since the P and S polarizations converge near to the Brewster's Angle. In many FTIR systems, the beam-splitter is positioned at 45 degrees to the incident beam. For mid-IR, KBr (375 - 12,000 cm $^{-1}$), quartz (4,000 - 25,000 cm $^{-1}$), and far-IR, mylar (30 - 680 cm $^{-1}$), are common beam-splitter materials. At the beam-splitter, the beams from the fixed and moving mirrors are once again mixed and directed toward the sample.

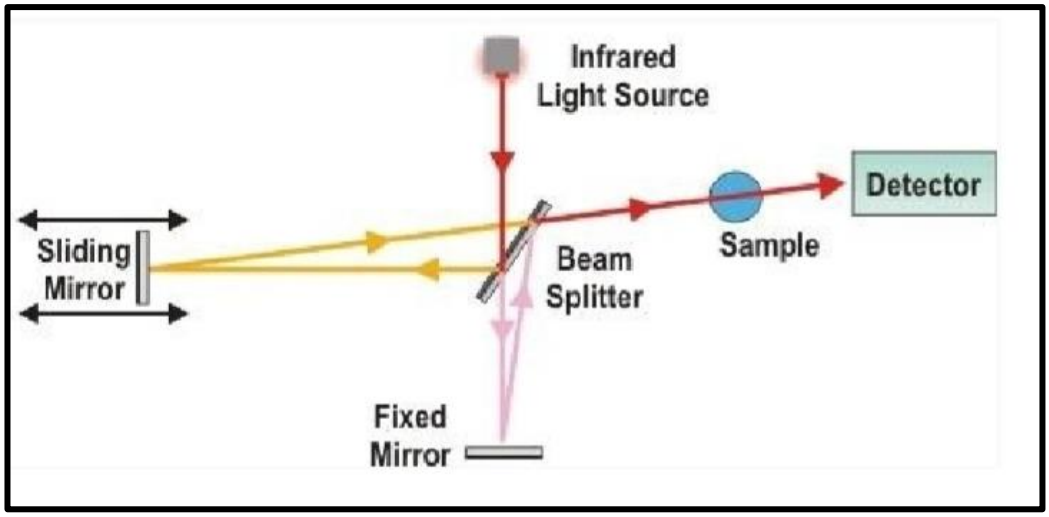

Fig. 3.11: Different parts and working of FTIR spectroscopy

Over the duration of the time, it takes for the moving mirror to make a pass; the difference in the paths of the mirrors generates both positive and negative interference. An interferogram plots the signal against the position of the mirrors (and subsequently, time). The precise known laser wavelength is utilized to calculate the location of the moving mirror. Due to its

superior wavelength stability as compared to solid-state or diode lasers, He-Ne lasers are the industry standard. Spectral additions, library searches, and other tasks requiring great wavenumber accuracy are made possible by this laser's steadiness.

3.3.2.2 Near Infrared

Between 4,000 and 12,800 cm^{-1} is where the Near-IR region of the electromagnetic spectrum is located. The simultaneous occurrence of two of the same vibrational modes, known as overtones, and two different vibrational modes, known as combinations, both occur in this region. The intensity of these modes is frequently extremely low because they are not strictly permitted by quantum mechanics. These spectra are frequently complicated, necessitating the employment of chemometric techniques like multivariate analysis. Despite these limitations, Near-IR spectroscopy has many advantages. First off, since the light's journey is long enough, bulk samples can be examined with little to no sample preparation. Second, unlike mid-IR, water has no impact on signal.

Fig. 3.12: Experimental set up of FTIR Spectrometer

3.3.2.3 Far infrared

The Far Infrared spectrum spans the wavelengths of 10 cm^{-1} and 700 cm^{-1}. 3+ atom functional groups, such as the bending of the -C-C-C- atom and lattice vibrations in crystalline materials, are the bonds that are visible in this region. Materials with the same chemical structure but distinct crystal structures may be differentiated using far-IR since they depend heavily on conformation or crystal structure.

3.3.3 UV-VIS Spectroscopy

Spectroscopy is the study of electromagnetic radiation's interaction with matter. In UV-VIS spectroscopy the range of spectrum is from UV to visible light range. Wavelength of electromagnetic radiation within this range is incident upon sample and the desired concentration of certain compound present in the sample is calculated by this method.

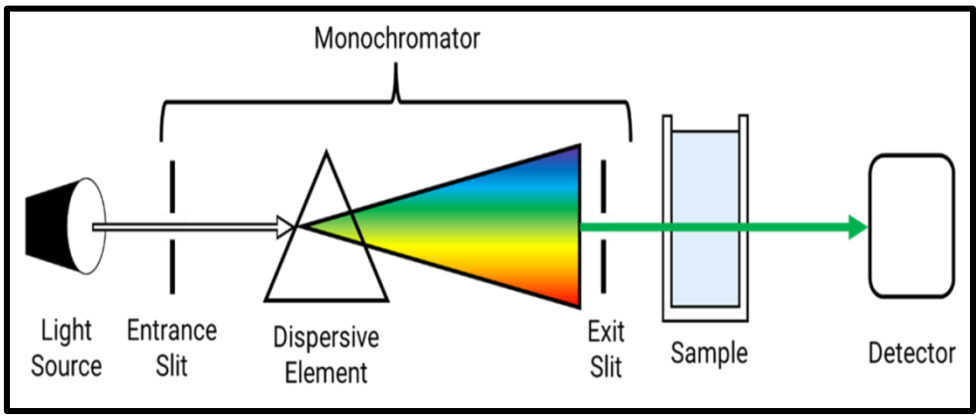

Fig. 3.13: Diagrammatic setup UV-VIS spectroscopy

3.3.3.1 Working principle

When light hits a molecule/compound/element, it excites the electrons which jump to a higher energy level indicating a certain amount of energy transfer. The light after passing through the sample a certain fraction is absorbed and certain fraction is transmitted. From Beer-Lambert's law we get the relation between absorbance and concentration. The concentration can be calculated with this method of an unknown sample.

I' = Incident light intensity,

I_0 = Intensity of light after passing through control (i.e. water),

I = Intensity of light after passing through test sample,

Transmittance (T) = I/I_0,

Percentage transmittance = T*100 = T %,

Absorbance (A) = -log T,

Transmittance (T) = 10^{-A},

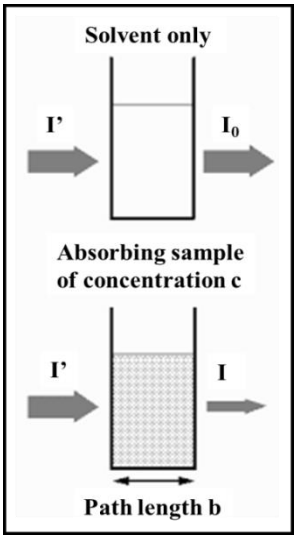

Fig. 3.14: Diagram for calculation of concentration

From Beer Lambert's law we get,

$A = \in Cl$,

$C = A/\in l$ (In terms of absorbance),

$C = -\log T/\in l$ (In terms of transmittance),

$C = (-\log I/I_0)/\in l$ (In terms of intensity).

3.3.3.2 Absorption Spectrum

It is the plot of absorbance vs wavelength of incident light.

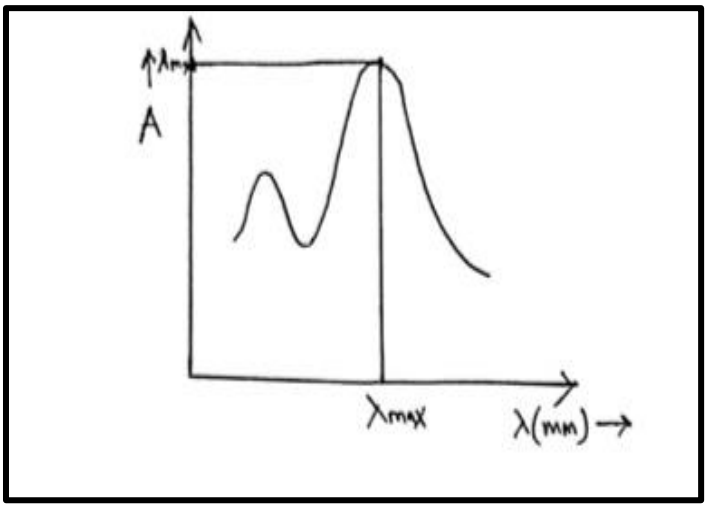

Fig. 3.15: Plot of absorbance versus wavelength

From this we can get the wavelength at which we can have maximum absorbance. And concentration value for maximum absorbance can be calculated. By using this UV-VIS method we can easily calculate the concentration of unknown sample and can also measure how much a chemical substance can absorb light.

3.3.3.3 Configuration of instrument

The transmittance or absorbance of a sample as a function of the wavelength of electromagnetic radiation is measured by a spectrophotometer. A spectrophotometer's essential elements are:

a. Source

b. Monochromator

c. Sample container

d. Detectors

a. Source

The ideal light source would have low noise, long-term stability, and a constant intensity across all wavelengths. However, there isn't a source like that. UV-visible spectrophotometers frequently use two sources. A continuous UV spectrum is produced when deuterium or hydrogen is electrically excited under low pressure. The mechanism entails the production of an excited molecular species, which disintegrates to produce two atomic species, an ultraviolet photon, and other by products. You can represent this as follows:

D2+ electrical energy→ D2* →D' + D'' + hv

Radiation from deuterium lamps is visible in the 160–375 nm range. These lamps must have quartz cuvettes and windows since glass absorbs light with wavelengths shorter than 350 nm. As a Visible source of light tungsten filament lamp is commonly used. This type of lamp is employed in the wavelength range of 350-2500 nm.

b. Monochromator

All monochromators have specific parts, including an exit slit, collimating mirrors, focusing mirrors, a dispersing device (often a prism or grating), and an input slit. Through the entrance slit, multi-wavelength polychromatic light enters the monochromator. After collimating, the beam strikes the dispersing component at an angle. The grating or prism divides the beam's wavelengths into their individual components. Only radiation of a specific wavelength exits the monochromator through the exit slit when the dispersing element or the exit slit are moved.

c. Sample container

The cuvettes used to hold the reference solution and sample solution must be transparent to the radiation that will flow through them. For UV spectroscopy, quartz or fused silica cuvettes are necessary.

d. Detector

An electrical signal is created from a light signal by a detector. Commonly employed in UV-VIS spectroscopy as a detector is the photomultiplier tube. A photo-emissive cathode, numerous dynodes, and an anode make up the device. A photo-emissive cathode produces electrons when photons of radiation strike it. A multichannel photon detector is a linear photodiode array, which is another type of detector. These detectors can concurrently measure every component of a scattered radiation beam. Photodiode arrays are intricate gadgets with exceptional durability due to their solid state construction.

Fig. 3.16: Experimental set up of UV-Visible spectrophotometer

3.3.4 Field Emission Scanning Electron Microscope (FESEM)

FESEM is the abbreviation of Field Emission Scanning Electron Microscope. A FESEM is used to visualize very small topographic details on the surface or entire or fractional objects. Researchers in biology, chemistry and physics apply this technique to observe structures that may be as small as few nanometres. Electrons are liberated from a field emission source and accelerated in a high electric field gradient, within the high vacuum column these so called, primary electrons are focussed and deflected by electric lenses to produce a narrow scan

beam electronic lenses that bombard the object. As a result, the secondary electrons are emitted from each spot on the object. The angle and velocity of this secondary electrons relates to the surface structure of the object. A detector catches the secondary electrons and produced and electronic signal. This signal is amplified and transformed to a video scan image that can be scanned and processed further. In a field emission (FE) scanning electron microscope no heating but so called, cold source is employed. An extremely thin and sharp tungsten needle (tip diameter 10^{-2} to 10^{-8} m) function as a cathode in front of primary and secondary anode. The voltage between cathode and anode is in the order of magnitude of 0.5-30 KV, because the electron beam produced by the FE source is about 1000 times smaller than in standard microscope, the image quality is marked better. As field emission necessitates an extreme vacuum (10^{-8} torr) in the column of microscope, a device is present that regularly decontaminates the electron source by a current flash. The tungsten filament last theoretically for a long time (i.e. life time) provided the vacuum is maintained stable.

The electron beam is formed by the electromagnetic lenses (conductor lenses, scan coil, stigmator coils and objective lens) and the apertures in the column to a tiny sharp spot.

- **Condenser lens**

  The current in the condenser lens determines the diameter of the beam, low current results in a small diameter, a higher current in a larger beam. A narrow beam has the advantage that the resolution is better but disadvantage is signal to noise ratio is high. The situation is reversed when the beam has large diameter. The condenser lens consists mostly of two parts.

- **Scan coils**

  The scan coils deflect the electron beam over the object according to a zigzag position. The formation of image on monitor occurs synchronously with the scan memory. The scan velocity determines the refreshing rate on the screen and the

amount of noise in the image. The smaller the scanned region on the object, the larger the magnification becomes at a constant window size.

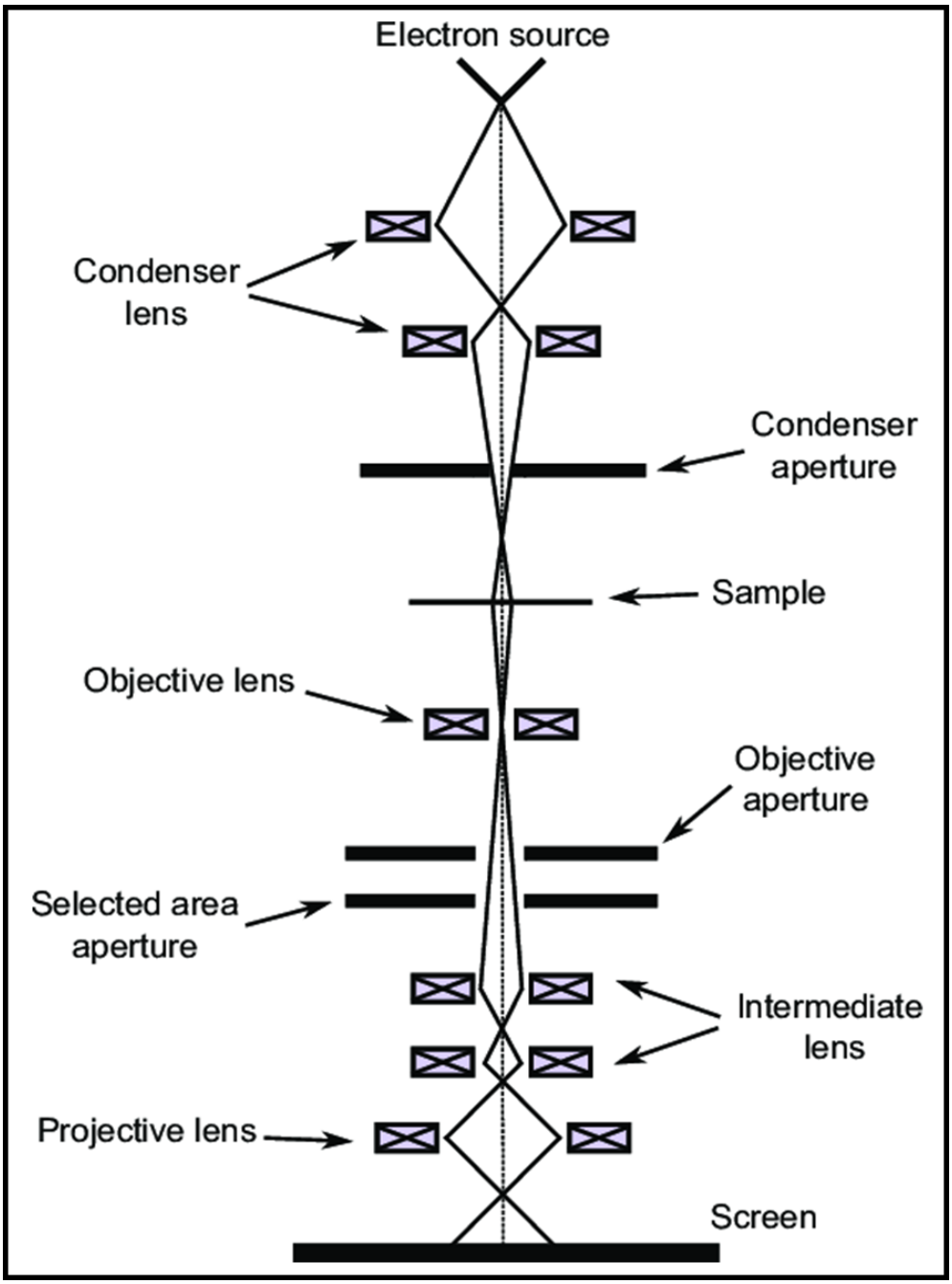

Fig 3.17: Schematic diagram of FESEM

- **Objective lens**

The objective lens is the lowest lens in the column. This lens focuses the electron beam on the object. At a short working distance, the objective lens needs to apply a

greater force to detect the electron beam. The shortest working distance produces the smallest beam diameter, the best resolution.

- **Stigmator coils**

  The stigmator coils are utilized to correct irregularities in the x and y reflector of the beam and thus to obtain a perfectly round shaped beam action of the beam, not circular, but ellipsoidal, the image looks blurred and stretched.

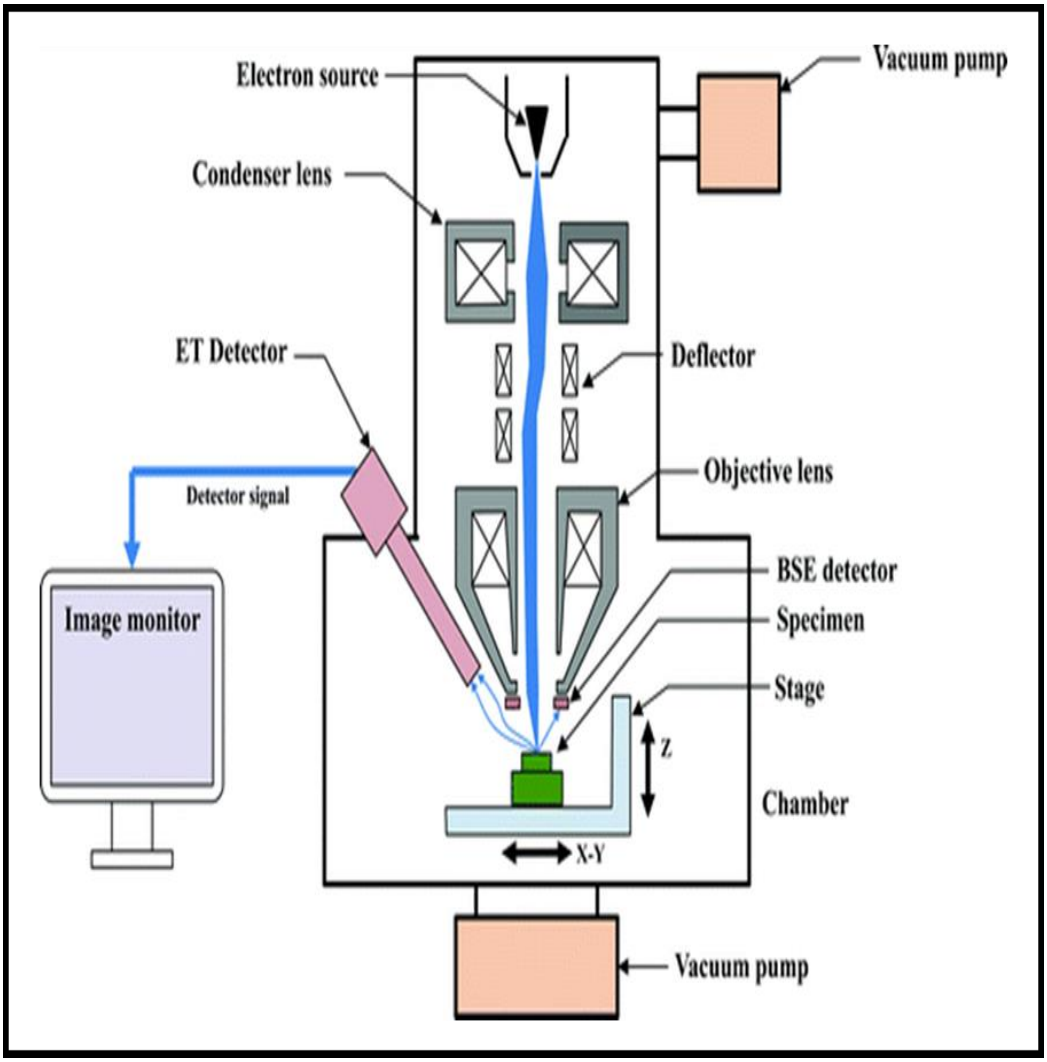

Fig. 3.18: Configuration of FESEM and its different components

- **Object chamber**

  After the object has been covered by a conductive layer it is mounted on to a special holder. The object is inserted through an exchange chamber into a high vacuum spot/part of a microscope and anchored on a moveable stage. In the virtual FESEM

the object can be moved in the horizontal as well as vertical direction on the screen by operating arrow in position box. The object can be repositioned in the chamber by means of a grey stick in a left right axis. The secondary electron emission detector is located at the rear end of the object holder in the chamber.

- **Image formation**

  When the primary probe bombards the object, secondary electrons are emitted from the object's surface at a certain velocity. This is determined by the levels and angles at the object's surface. The secondary electrons, which are attracted by corona, strike the scintillator that produces photons. The location and intensity of illumination of the mirror vary depending on properties of secondary electrons. The signal produced is amplified and the secondary electrons that is fed to a CRT. The contrast in the real time image that appears on the screen reflects the structure of surface on object. Parallel to analog image, a digital image is generated which can be further processed.

3.3.4.1 Magnification

Magnification is expressed by the distance travelled by the recording beam in a given time to the distance travelled by the beam on the specimen. In scanning electron microscope, the area is scanned in a sequence. So, if D_s &D_r are the sides of the square scanned on the specimen and on the recording unit in the image, then magnification: $M = D_r/D_s$.

Since resolution is clearly related to the size of the beam diameter, the size of the beam emitted from the electron gun must be sufficiently demagnified.

3.3.5 Photoluminescence Spectroscopy (PL)

Using photoluminescence (PL) spectroscopy is an easy, straightforward, non-destructive technique. The band gap, impurity concentration, defect detection, recombination

mechanism, surface structure, fluorescence characteristic, and excited states of a material can all be identified using this technique. In the non-contact mode, photoluminescence spectroscopy is carried out. It is a technique for non-destructively inspecting a material's electronic structure. It can be summed up as a device that communicates with both matter and light.

3.3.5.1 Basic Principle

Excess energy from the light that strikes a sample is absorbed by the substance. Photo-excitation is the term used to describe this. The sample can release this extra energy in a variety of ways, including light emission, commonly referred to as luminescence. Luminescence caused by photo-excitation is known as photoluminescence.

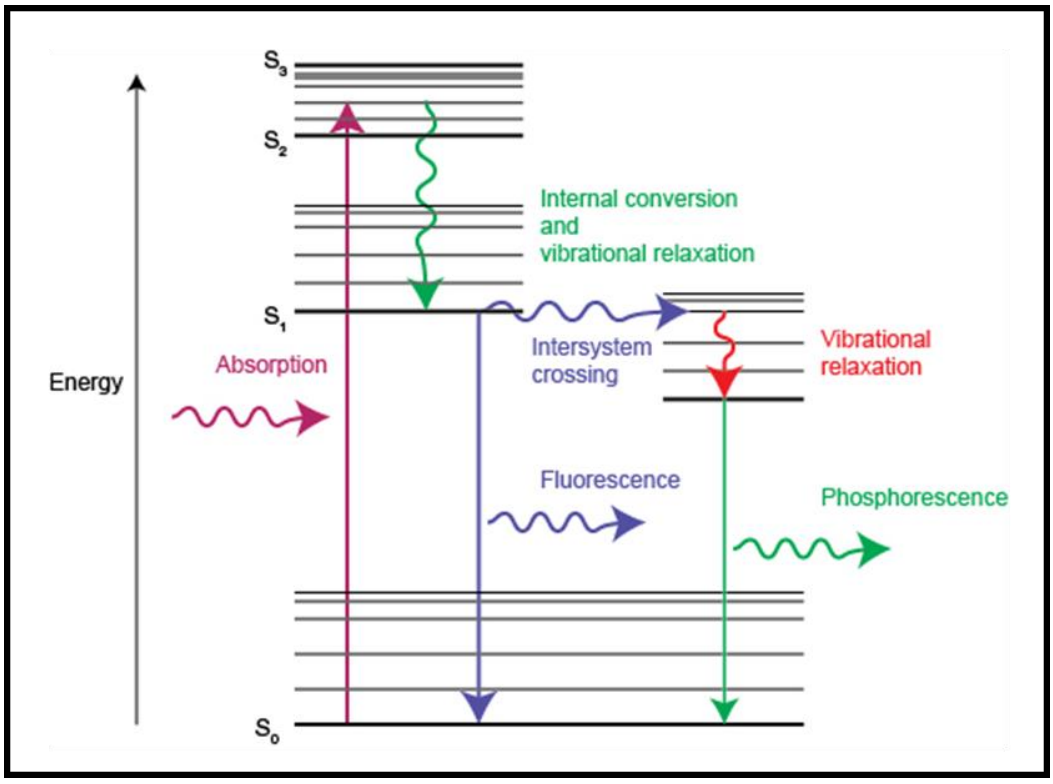

Fig. 3.19: Schematic diagram of spectrofluorometer instrument

When a substance is stimulated, its electrons reside the permitted excited states. These excited electrons release the excess energy in the form of light (radiative process) or any non-radiative process in order to return to their stable, i.e., equilibrium or ground state. The

energy of the emitted light (photoluminescence) is proportional to the energy difference between the two electronic states involved in the transition between excited and equilibrium states. The proportion of the radiative process controls how much light is released.

3.3.5.2 Photoluminescence Different Modes

a. Resonant radiation: In this process, a photon of a particular wavelength is absorbed, and an instantaneous emission of an equivalent photon follows. The time scales for this process are of the order of 10 nanoseconds, and there are no visible internal energy changes between absorption and emission.

b. Fluorescence: A specific joule of absorbed energy is released when the chemical substrate starts the internal energy transition by emitting photons before returning to its ground state, making the emitted light less energetic than the absorbed. Fluorescence is one of the recognized processes, having a lifespan of 10^{-8} to 10^{-4} s.

c. Phosphorescence: Intersystem crossover (ISC) is a radiation-based transition in which the absorbed energy moves through an electronic transition with numerous spin states. Fluorescence has a shorter lifetime than phosphorescence, which is commonly measured in the range of 10^{-4} to 10^{-2} s. As a result, phosphorescence happens less frequently than fluorescence because the triplet state of the molecule increases the likelihood of intersystem crossing to a lower energy state before phosphorescence.

3.3.5.3 Working Principle

The material's electrons can move into allowed excited states when light is focused on it. The excess energy is released when these electrons reach their equilibrium states, which may or may not result in the emission of light (a radiative process) (a non-radiative process). The difference in energy levels between the two electron states involved in the transition from the excited state to the equilibrium state (photoluminescence) determines the energy of the light

that is produced. The proportionate contribution of the radiative process determines how much light is released. The emitted light often has less energy since it has a longer wavelength than the radiation that was absorbed. One electron can absorb two photons when the electromagnetic radiation being absorbed is strong enough, which causes an emission of light with a shorter wavelength than the electromagnetic energy being absorbed. Resonance fluorescence happens when the emitted radiation has the same wavelength as the absorbed light. When radiation in the ultraviolet region of the spectrum—which is invisible to the human eye is absorbed and released as visible light, photoluminescence takes place.

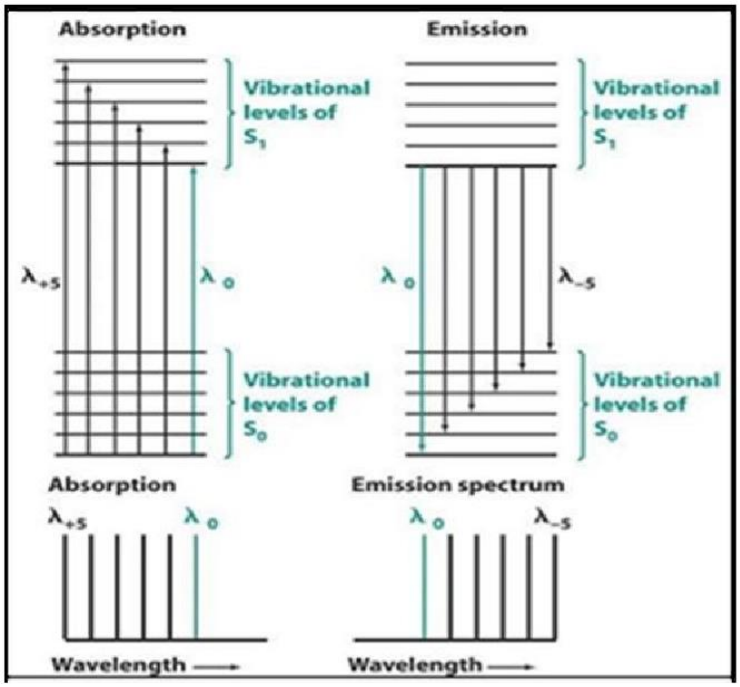

Fig. 3.20: Representing the energy level diagrams which mention why structure is seen in the absorption as well as emission spectrum and also why the spectra are roughly mirrored images of each other

A fluorophore's (a fluorescent molecule) ground state is S_0, and its first (electronically) excited state is S1. S1 is a molecule that has multiple ways of relaxing. It is capable of non-radiative relaxation, in which the excitation energy is converted to heat (vibrations) and transferred to the solvent. Organic molecules that have been excited can also relax by going from a triplet state to a secondary nonradiative relaxation phase, such as phosphorescence.

Interaction with a second molecule via fluorescence quenching can also cause an S1 state to relax. Due to its distinct triplet ground state, molecular oxygen (O_2) is a very powerful fluorescence quencher.

3.3.5.4 Instrumentation of Photoluminescence

A spectrofluorometer is a piece of analytical equipment that measures and records a sample's fluorescence. The excitation, emission, or both wavelengths may be scanned in order to capture the fluorescence. Using additional attachments, the analysis of signal deviation in relation to time, temperature, concentration, polarization, or other variables is explored.

The block diagram of the fluorescence spectrometer is displayed below. Monochromators (wavelength selectors), laser sources (sample illumination), detectors, and corrected spectra are all components of fluorescence spectrometers.

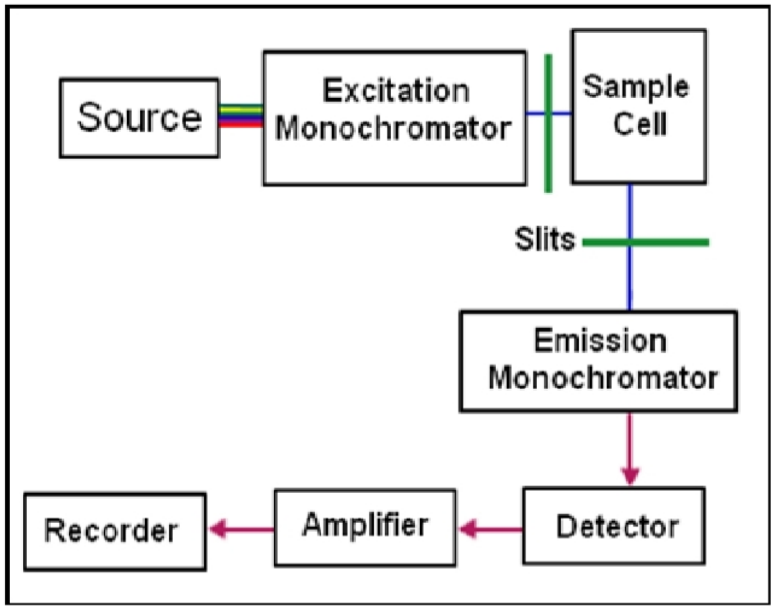

Fig. 3.21: Schematic diagram of photoluminescence

a. Source of Illumination

The light source is a continuous-type, 150 W, ozone-free xenon arc lamp. A diamond-turned elliptical-shaped mirror collects the light from the lamps, which is then directed into the entry slit of the excitation monochromators. The excitation monochromator is separated from the

lamp housing by a quartz-based window, which allows heat to escape the system and provides protection in the event of the lamp's infrequent failure. Spherical aberrations and re-diffraction are stretched and reduced when the complete spectrum can be resolve.

b. Monochromators

Excitation monochromators and emission monochromators are the two categories under which monochromators fall. It uses entire reflective optics to keep resolution high throughout the whole spectrum while also minimizing spherical aberrations and re-diffraction.

c. Gratings

Reflection The primary function of grating in a monochromator is to disperse striking (incident) light through vertically oriented grooves. By spinning gratings with 1200 grooves per millimetre and blazing them at 330 nm (excitation) and 500 nm (emission), spectra can be obtained. MgF_2 has been used as a protective coating to the grating to prevent oxidation.

d. Slits

Very flexible slits are used at the entrance and exit points of the monochromator. The excitation monochromator's slit width determines the incident light's bandpass, whereas the emission monochromator's slits govern the fluorescence intensity signal, which is then measured by the signal detector.

The trade-off between signal strength and spectral resolution affects slit width. Because more light hits both the sample and the detector when the slit width is larger, the resolution suffers; nevertheless, when narrower slits are used, the resolution improves but at the expense of the signal.

e. Shutters

Under the excitation monochromator's exit slit, an excitation shutter is put in place to shield the sample from photobleaching or photodegradation brought on by extended exposure to

light. A detector is protected from the bright light by an emission shutter that is placed shortly before the emission monochromator enters the system.

f. Sample compartment

The sample compartment has a number of additional attachments and fibre optic bundles for transferring the excitation beam to the distant sample and returning the emission beam to the emission monochromator.

Fig. 3.22: Photoluminescence analysis carried out by Horiba Jobin Yvon Fluromax

g. Detectors

Signal detectors and reference detectors are the two different categories of detectors. An R928P photomultiplier tube serves as the photon counting signal detector and sends the signal to a photon counting module. The reference detector's job is to keep an eye on the xenon lamp's adjustment for wavelength- and time-dependent output. This detector works by increasing the silicon photodiode, which is placed right before the sample chamber, using UV light.

3.3.5.5 Applications

- Determination of Band gap,
- Identification of level of Impurity as well as a defect,

- Recombination phenomena, and
- Surface structure and excited states.

3.3.6. Photocatalytic Measurements

3.3.6.1. Experimental set-up

Photocatalytic activity of the as-synthesized samples was measured at ambient temperature at a pH of 7. In order to maintain the temperature of the catalytic reactor system at a constant value, a double-walled glass beaker was used with continuous flow of cold water in-between the two walls. To measure the photocatalytic activity of the as-prepared samples, 30 mg of the catalysts were dispersed in 40 mL of 10^{-5} mol/L RhB dye solution. The catalyst dispersed solution was vigorously stirred for 1 hour under complete dark condition to ensure proper adsorption-desorption equilibrium of the dye on the catalyst surface. After this, the system was placed under a 400 W high pressure mercury lamp (Phillips-HPL-N G/74/2, MBF-400W, 200-250V) covering the complete range from 365 to 679 nm which was used as a visible-light source. A UV cut off filter ($\lambda > 400$ nm) was employed to negate the UV emission. 3 mL of the reaction solution was withdrawn from the suspension at regular time intervals which was immediately centrifuged to remove the catalyst; and the concentration of the RhB dye was monitored by using an UV−Vis absorption spectrophotometer. Also, the degradation efficiency (η) of the as-synthesized samples can be calculated from C_t/C_0 vs. t plot using the equation,

$$\eta = (C_0 - C_t)/C_0 \times 100\ \% \qquad (3.3)$$

Where,

C_0 and C_t are the concentrations of RhB at time t = 0 (initial RHB concentration) and t = t (final RhB concentration).

Chapter 4

Synthesis Process

4.1 Synthesis of orthorhombic hydrated tungsten tri-oxide (O-$WO_3.0.33H_2O$)

- For the hydrothermal synthesis of orthorhombic hydrated tungsten tri-oxide, Sodium Chloride (0.15 g) was added to 25 mL of deionized Water. Then sonicate it was sonicated for 5 minutes.
- Then Sodium tungstate dihydrate (0.4 g) was dissolved in the above sodium chloride solution and sonicated for 5 minutes.
- The above solution is placed on a magnetic stirrer for one and half hour.
- Then hydrochloric acid was added dropwise by 1000T pipette to the above solution until the pH value of the solution becomes 1 and again stirred for 30 minutes.
- Then transfer the solution to a PTFE chamber, set inside a stainless-steel autoclave and installed in the oven.
- The synthesis conditions were set at 180 ℃ for 3 hours and was let cooling down at room temperature inside the oven.
- The synthesized product was collected and centrifuged at 4500 rpm for 5 minutes with deionized water and ethanol until its pH becomes 7.
- The resultant powder was finally dried overnight in oven at 60 ℃ [1].

4.2 Synthesis of tungsten tri-oxide nanoparticles (WO_3)

- In the preparation of tungsten tri-oxide nanoparticles tungsten hexachloride was used as a precursor.
- The reaction took place by dissolving 0.05 M of tungsten hexachloride and 0.05 M of urea in 40 mL ethanol solution.
- The solution was stirred until it was converted to dark blue in colour.

- Then the solution was transferred to a PTFE chamber, set inside a stainless-steel autoclave and installed in the oven.
- The synthesis conditions were set at 180 ℃ for 12 hours and was let cooling down at room temperature inside the oven.
- The resultant powder was washed and rinsed several times to remove the untreated species.
- Finally, the synthesized product was dried in an oven at 60 ℃ overnight and collected.
- The obtained product was annealed at 500 ℃ for 3 hours to obtain pristine tungsten tri-oxide nanoparticles. [2,3,4]

4.3 Synthesis of graphitic carbon nitride (g-C_3N_4)

The bulk g-C_3N_4 was synthesized by thermal treatment of urea in a muffle furnace at 600 ℃ in air for 4 hours at 5 ℃/min heating rate. The light yellow coloured sample was obtained. After that for exfoliation following stapes were followed:

- Acetone was poured in a round bottom flask and synthesized g-C_3N_4 was added in the round bottom flask.
- The above solution was sonicated for 16 hours for proper exfoliation of graphitic carbon nitride.
- Then the above product was filtered with deionized water several times.
- Whitish yellow precipitate was collected.
- Then it was dried at 60 ℃ over night to obtain the product.

4.4 Synthesis of WO_3/g-C_3N_4 (Before annealing) and WO_3/g-C_3N_4 (After annealing)

- The reaction took place by dissolving 0.05 M of tungsten hexachloride and 0.05 M of urea in 40 mL ethanol solution.

- The solution was stirred until it was converted to dark blue in colour.

  Then 200 mg of g-C_3N_4 was added to the above solution and stirred for 5 hours.
- Then the solution was transferred to a PTFE chamber, set inside a stainless-steel autoclave and installed in the oven.
- The synthesis conditions were set at 180 ℃ for 12 hours and was let cooling down at room temperature inside the oven.
- The resultant powder was washed and rinsed several times with deionized water and ethanol to remove the untreated species.
- Finally, the synthesized product was dried in an oven at 60 ℃ overnight and collected as (WO_3/g-C_3N_4 (Before annealing))
- Some portion of the product was not annealed and some portion was annealed at 500℃ for three hours to obtain WO_3/g-C_3N_4 (Annealed).

4.5 Synthesis of WO_3/Exfoliated g-C_3N_4 (Before annealing) and WO_3/Exfoliated g-C_3N_4 (After annealing)

- The reaction took place by dissolving 0.05 M of tungsten hexachloride and 0.05 M of urea in 40 mL ethanol solution.
- The solution was stirred until it was converted to dark blue in colour.
- Then 200 mg of Exfoliated g-C_3N_4 [5] was added to the above solution and stirred for 5 hours.
- Then the solution was transferred to a PTFE chamber, set inside a stainless-steel autoclave and installed in the oven.
- The synthesis conditions were set at 180 ℃ for 12 hours and was let cooling down at room temperature inside the oven.

- The resultant powder was washed and rinsed several times with deionized water and ethanol to remove the untreated species.
- Finally, the synthesized product was dried in an oven at 60 ℃ overnight and collected as (WO_3/Exfoliated g-C_3N_4 (Before annealing))
- Some portion of the product was not annealed and some portion was annealed at 500 ℃ for three hours to obtain WO_3/Exfoliated g-C_3N_4 (Annealed).

4.6 References

1. Santos, L., Silveira, C.M., Elangovan, E., Neto, J.P., Nunes, D., Pereira, L., Martins, R., Viegas, J., Moura, J.J., Todorovic, S. and Almeida, M.G., 2016. Synthesis of WO_3 nanoparticles for biosensing applications. *Sensors and Actuators B: Chemical*, *223*, 186-194.

2. Jeevitha, G., Abhinayaa, R., Mangalaraj, D. and Ponpandian, N., 2018. Tungsten oxide-graphene oxide (WO_3-GO) nanocomposite as an efficient photocatalyst, antibacterial and anticancer agent. *Journal of Physics and Chemistry of Solids*, *116*, 137-147.

3. Shanmugam, M., Alsalme, A., Alghamdi, A. and Jayavel, R., 2015. Enhanced photocatalytic performance of the graphene-V_2O_5 nanocomposite in the degradation of methylene blue dye under direct sunlight. *ACS applied materials & interfaces*, *7*(27), 14905-14911.

4. Hara, K., Zhao, Z.G., Cui, Y., Miyauchi, M., Miyashita, M. and Mori, S., 2011. Nanocrystalline electrodes based on nanoporous-walled WO_3 nanotubes for organic-dye-sensitized solar cells. *Langmuir*, *27*(20), 12730-12736.

5. Singh, J., Arora, A. and Basu, S., 2019. Synthesis of coral like WO_3/g-C_3N_4 nanocomposites for the removal of hazardous dyes under visible light. *Journal of Alloys and Compounds*, *808*, 151734.

Chapter 5

Results & Discussion

5.1 Structural Analysis

5.1.1 Powder X-ray Diffraction (PXRD)

The as prepared samples were subjected to PXRD (Powder X-ray Diffraction). The powder X-ray diffraction was recorded from D8 Bruker advanced X-ray diffractometer with a radiation source of Cu Kα (λ = 1.54 angstrom) and at a scanning rate of 5 degree/minute for proper identification of the sample.

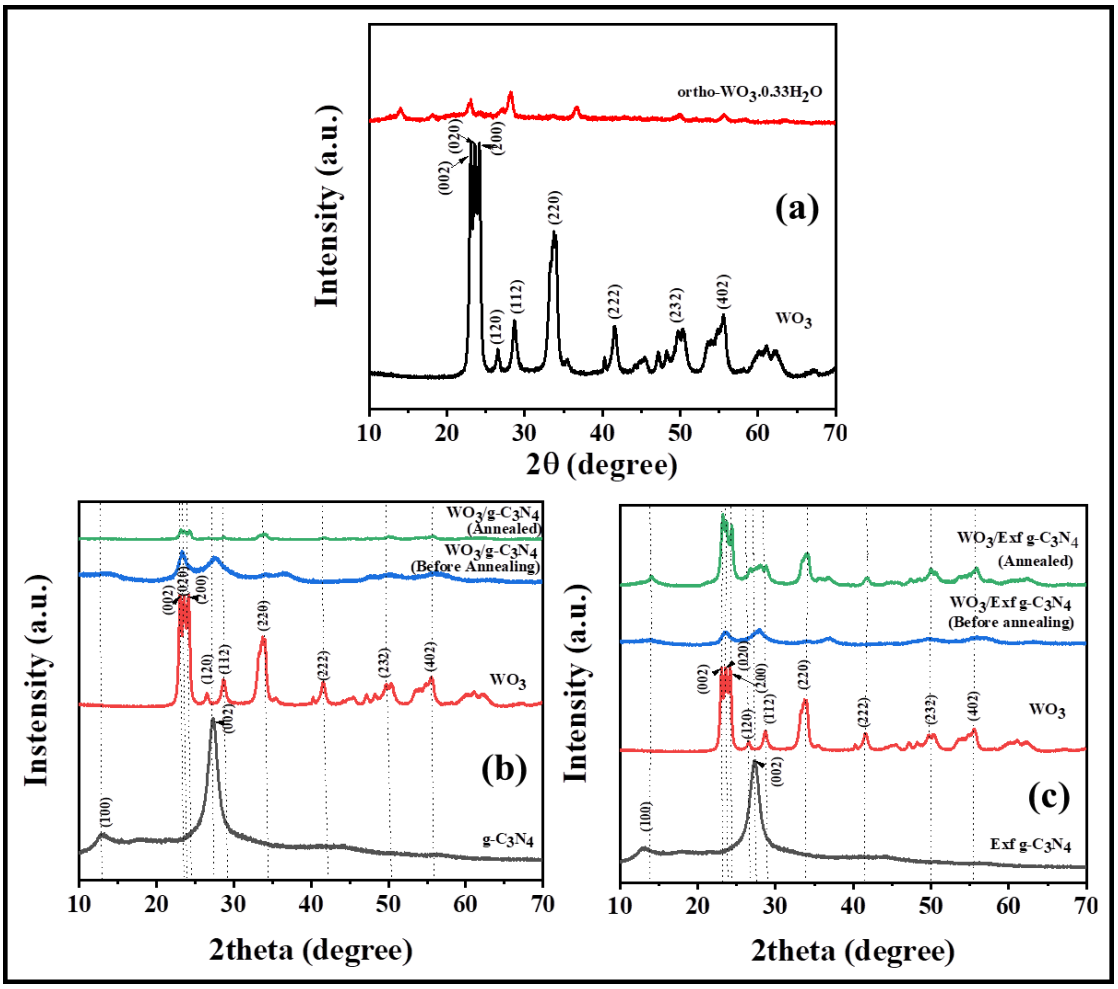

Fig. 5.1: The PXRD pattern of all synthesized sample

Fig. 5.1 displays the PXRD pattern of g-C_3N_4, WO_3 nanoparticles and various nanocomposites of WO_3/g-C_3N_4. Pure g-C_3N_4 had two characteristic diffraction peaks at 13.0 and 27.7 ° corresponding to (100) and (002) planes which was attributed to the interlayer tri-s-triazine structural packing and the interplanar stacking of conjugated aromatic systems,

respectively [1-4]. An annealing at 500 ℃ for 3 hours was used to obtain the desired PXRD pattern of WO_3. Has major peaks at 23.08, 23.56, 24.35, 26.54, 28.70, 34.13, 41.6, 49.90 and 55.8 ° and consequently the corresponding planes are (002), (020), (200), (120), (112), (220), (222), (232) and (402) which ensure the formation of monoclinic phase of WO_3 nanoparticles and they well matched with the JCPDS card no 89-4476. Most of the major peaks are sharp, which represents the high crystallinity of WO_3 nanoparticles [5-6]. Moreover, it could be noticed that the various PXRD patterns of WO_3/g-C_3N_4 (annealed) nanocomposites and WO_3/exfoliated g-C_3N_4 (annealed) nanocomposite were composed of diffraction peaks WO_3 nanoparticles and g-C_3N_4. It could be further noticed from the PXRD pattern that the intensity of WO_3 peaks in the synthesized composites decreases and also the graphitic carbon nitride peak arises in the PXRD pattern of the nanocomposites.

5.2 Compositional Analysis

5.2.1 Fourier transform infrared spectroscopy (FTIR) analysis

In order to gain a better understanding of how bonds are formed, FTIR spectroscopy of synthesized samples was conducted (Shimadzu FTIR-8400S). FTIR spectra of g-C_3N_4, WO_3, WO_3/g-C_3N_4 (annealed) and WO_3/g-C_3N_4 (before annealing) are presented in Fig. 5.2(a) and the spectra of exfoliated g-C_3N_4, WO_3, WO_3/exfoliated g-C_3N_4 (annealed) and WO_3/Exfoliated g-C_3N_4 (before annealing) are presented in Fig. 5.2(b). From both the spectra, that can observe for the pure g-C_3N_4 and exfoliated g-C_3N_4 the bands are in the region ranging from 1206 to 1639 cm^{-1} corresponds to C-N stretching vibration modes of heterocycles [7]. The peak appearing at 810 cm^{-1} was attributed to the stretching peaks of s-triazine units [8]. The broad absorption peaks at <1000 cm^{-1} indicated the presence of pure WO_3. The peaks at 824 and 774 cm^{-1} are assigned to the stretching vibration modes of O-W-O bonds [9]. The composites were composed of peaks of both g-C_3N_4 and WO_3 nanoparticles which generally signifies that both the materials are present in the composite. Furthermore, it

can see a slight shift in in g-C_3N_4 peak at 810 cm^{-1} in the nanocomposite that signifies strong interaction between WO_3 nanoparticles and s-triazine units of g-C_3N_4.

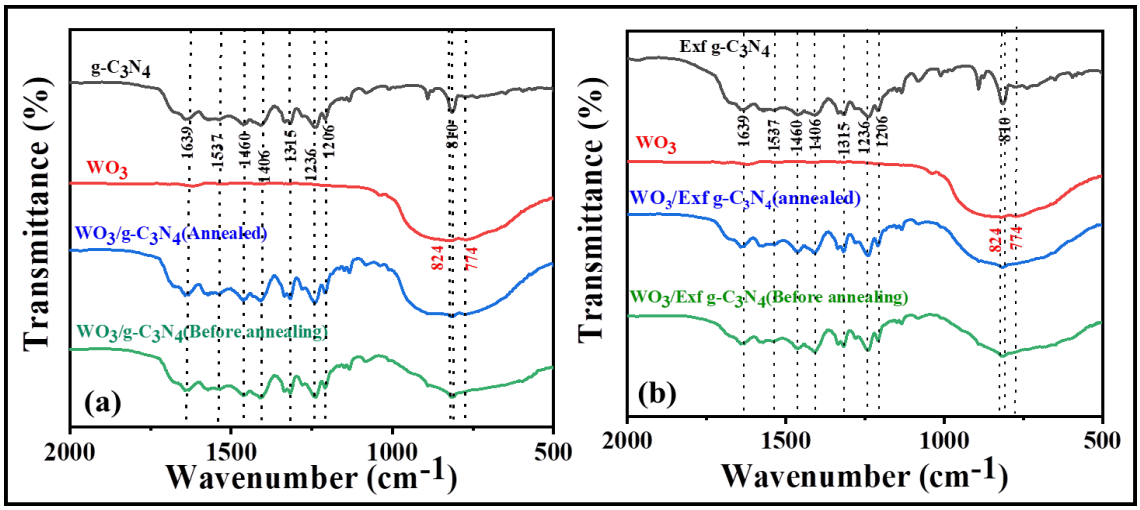

Fig. 5.2: The FTIR spectra of all synthesized sample

It could also be noticed that there is a faint decrease in peak appearing at 810 cm^{-1} in the nanocomposites as compared to pure and exfoliated g-C_3N_4 which might be due to the presence of WO_3 nanoparticles over the exfoliated graphitic carbon nitride layers.

5.3 Optical Analysis

5.3.1 UV-VIS DRS Analysis

In diffuse reflectance spectroscopy the plot is between reflectance (%) and wavelength (nm) in Fig. 5.3(a) the DRS analysis of WO_3 and O-WO_3.0.33H_2O is shown from which can infer that there is a fall in the reflectance spectra occurring at 481 and 453 nm respectively. The indirect band gap of the as synthesized samples, have been calculated from diffuse reflectance spectra by employing Kubelka-Munk method and the corresponding plots of Kubelka-Munk function vs. the photonic energy. The indirect band gap of WO_3 and O-WO_3.0.33H_2O was calculated as 2.56 and 3.08 eV respectively displayed in Fig. 5.3(d). From Fig. 5.3(b) can infer the fall of the reflectance spectra of WO_3/g-C_3N_4 (annealed) and WO_3/g-C_3N_4 (before annealing) which are at 469 and 443 nm respectively. The indirect band gap of

the nanocomposite after and before annealing was calculated from the plot of Kubelka-Munk function vs. photonic energy which comes out to be 2.35 and 2.53 eV respectively presented in Fig. 5.3(e).

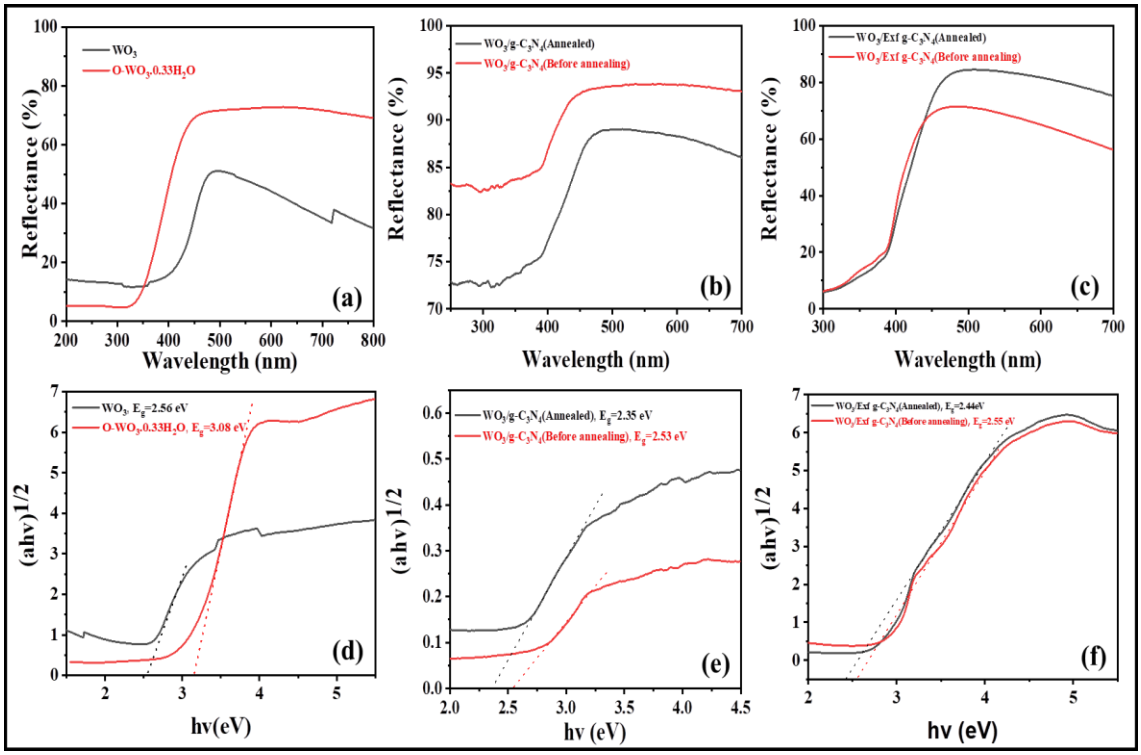

Fig. 5.3: The diffuse reflectance spectra of all synthesized sample (a-c) and inset: Kubelka-Munk plots for calculation of indirect band gaps

Similarly from Fig. 5.3(c) it can observe the fall of reflectance spectra of the tungsten trioxide nanocomposite wrapped with exfoliated graphitic carbon nitride after and before annealing is at 473 and 450 nm respectively and the indirect band gap of the synthesized samples was calculated from the plot of Kubelka-Munk function vs. photonic energy which comes out to be 2.44 and 2.55 eV respectively demonstrated in Fig. 5.3(f). Thus, pristine tungsten trioxide and its nanocomposite have band gap which are in accordance with the visible range.

5.3.2 Photoluminescence (PL) Analysis

The PL analysis (Photoluminescence) spectra were employed to further investigate the transport and the separation of the photogenerated carriers. Fig. 5.4(a), 5.4(b) and 5.4(c)

shows the PL spectra of tungsten trioxide and its nanocomposites formed with bulk and exfoliated graphitic carbon nitride before and after annealing. From Fig. 5.4(a) we can notice that the intensity emission peaks of tungsten trioxide, tungsten trioxide/graphitic carbon nitride (before annealing and after annealing) in decreasing order which signifies that the recombination rate of photogenerated electron-hole pairs is faster in case of tungsten trioxide but the recombination of electron-hole pairs is blocked effectively in case of the nanocomposite which leads to the enhancement of its photocatalytic activity.

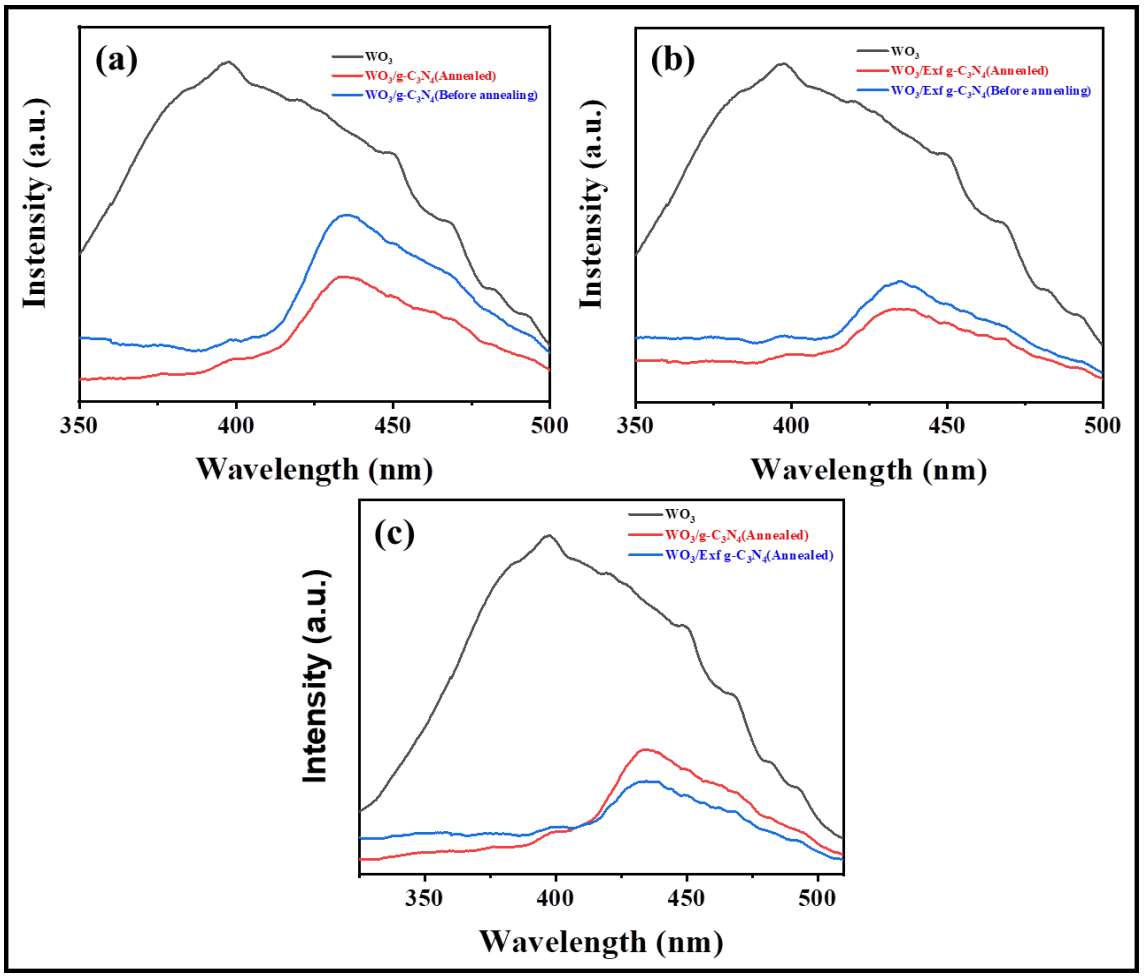

Fig. 5.4: The photoluminescence emission spectra of all synthesized sample

From Fig. 5.4(b) can notice the intensity emission peaks of tungsten trioxide, tungsten trioxide/exfoliated graphitic carbon nitride (before annealing and after annealing) in decreasing order which similarly signifies that the nanocomposites have much slower

recombination rate of photogenerated carriers which leads to the enhancement of its photocatalytic activity in comparison to that of the pristine tungsten trioxide catalyst.

From Fig. 5.4(c) the PL emission spectra of tungsten trioxide, tungsten trioxide/graphitic carbon nitride (annealed) and tungsten trioxide/exfoliated graphitic carbon nitride (annealed) are shown. It can infer from the spectra that the nanocomposite of WO_3/exfoliated g-C_3N_4 have much slower recombination rate of photogenerated electron-hole pairs that that of WO_3/g-C_3N_4 nanocomposite which is justified by the intensity of the emission peak of the PL spectra thus WO_3/exfoliated g-C_3N_4 have enhanced photocatalytic activity as compared to that of the tungsten trioxide nanocomposite formed with bulk graphitic carbon nitride.

5.4 Morphological Analysis

5.4.1 Field Emission Scanning Electron Microscopy (FESEM)

The morphology of the all samples is evident from the field emission scanning electron microscopy (FESEM) in Fig. 5.5 respectively. All samples exhibited two-dimensional morphology. The nature of the all samples was nanoparticle like morphology. The pure WO_3 and ortho $WO_3.0.33H_2O$ hydrothermal synthesized samples were displayed in Fig. 5.5(a-b). The ortho WO_3 sample presented flower like morphology that assembled by self WO_3 sheets. The WO_3 nanoparticle uniformly distributed on the GCN sheets on the annealed or non-annealed samples, and it's demonstrated in the Fig. 5.5 (c-f). The FESEM images of GCN(X) in Fig. 5.5(g), was a bulk sheet-like structure remain stacked in clusters. As exfoliated GCN(Y) breaks down these bulk clusters through exfoliation, smaller sheets are formed as a result, which was displayed in Fig. 5.5(h).

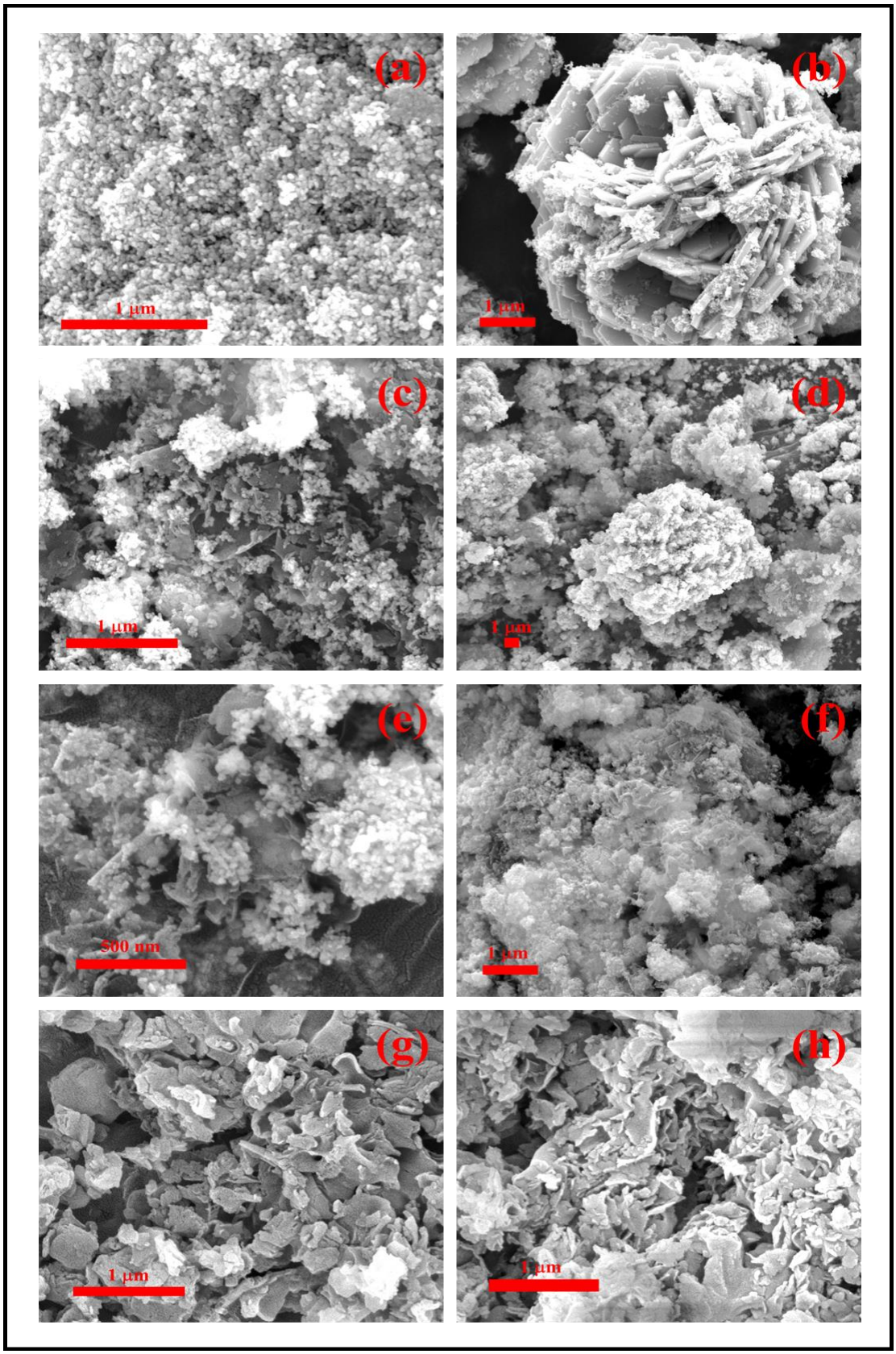

Fig. 5.5: (a)W1-WO_3, (b) W2-Ortho WO_3.0.33H2O, (c) W5-WO_3/GCN (annealed), (d) W7-WO_3/GCN (before annealing), (e) W8-WO_3/exfoliated GCN (annealed), (f) W9-WO_3/exfoliated GCN (before annealing), (g) X-GCN, (h) Y-Exfoliated GCN.

5.5 Photocatalytic Activity

By observing the degradation activity of a $^{10\text{-}5}$ M concentration of an aqueous solution of the organic textile dye Rhodamine B (RhB) under ambient conditions, in the presence of visible light irradiation, and at a neutral pH value (pH 7). It was possible to record the photocatalytic dye degradation property of the synthesized samples. The as-synthesized samples were subjected to a photocatalytic testing technique in a specially designed double-walled glass beaker with continuous water flow in between the two walls. In this system, 40 mL of an aqueous dye (RhB) solution contained 30 mg of the catalyst in its prepared form. The adsorption-desorption equilibrium condition was then achieved by constantly dark stirring the appropriate dye solution for 1 hour. After that, the entire setup was moved beneath an Hg lamp with a UV cut-off filter acting as a visible light source. 4 mL of the aqueous solution was collected at certain intervals of time and immediately centrifuged to separate the catalyst material from the dye solution. The dye solution's absorbance spectra were then assessed using a UV-Vis spectrophotometer [10].

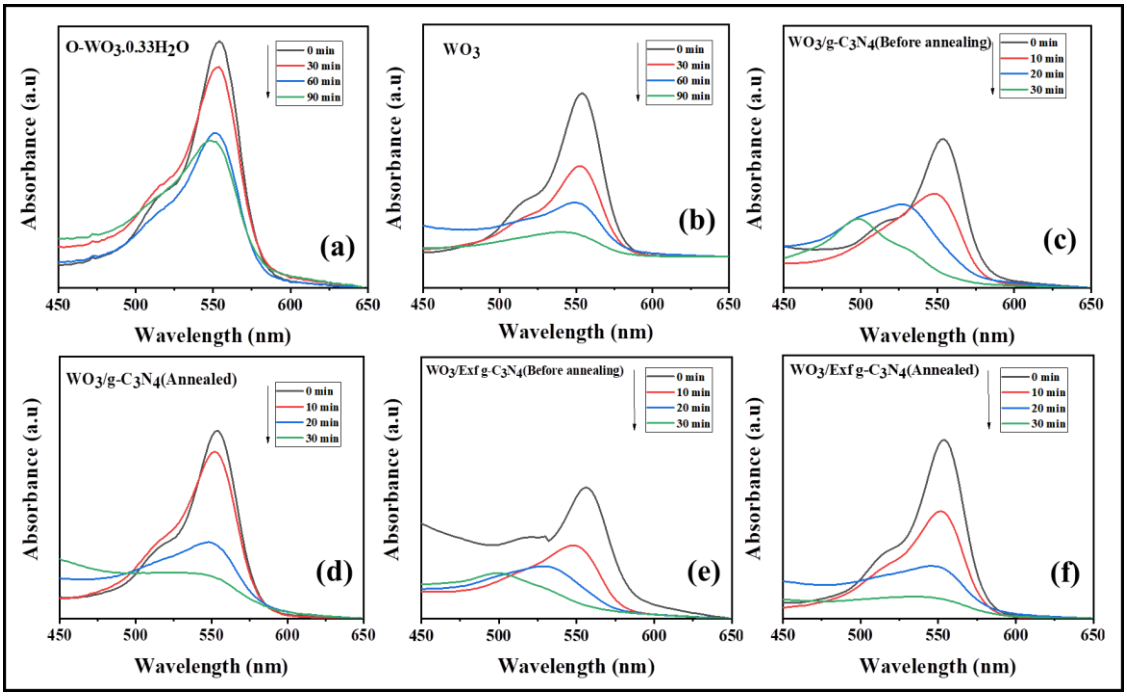

Fig. 5.6: Absorbance spectra of (a) O-WO_3.0.33H_2O, (b) WO_3, (c) WO_3/GCN (before annealing), (d) WO_3/GCN (annealed), (e) WO_3/exfoliated GCN (before annealing), and (f) WO_3/exfoliated GCN (annealed) samples

5.5.1 Photocatalytic Performance Analysis

By observing the degradation, the active photocatalytic performances of both pristine materials were studied by efficiently degrading RhB dye under visible light irradiation. RhB dye absorbance pattern is shown in Fig 5.6(a-b) after catalytic reactions in the synthesized samples: O-WO_3.0.33H_2O, WO_3. Pure catalyst materials degrade after about 90 minutes of visible light irradiation. The figure 5.6 (c-f) illustrates the optimal absorbance pattern of RhB dye following catalytic reactions with WO_3/g-C_3N_4 (before and after annealing) and WO_3/exfoliated g-C_3N_4 (before and after annealing). Catalytic materials degrade after 30 minutes of visible light irradiation. Figs. 5.7(a) and 5.7(c) show the C/C_0 vs. irradiation time (t) plot, and Fig. 5.7(b) and Fig. 5.7(d) shows the ln(C_0/C) vs. irradiation time (t) plot.

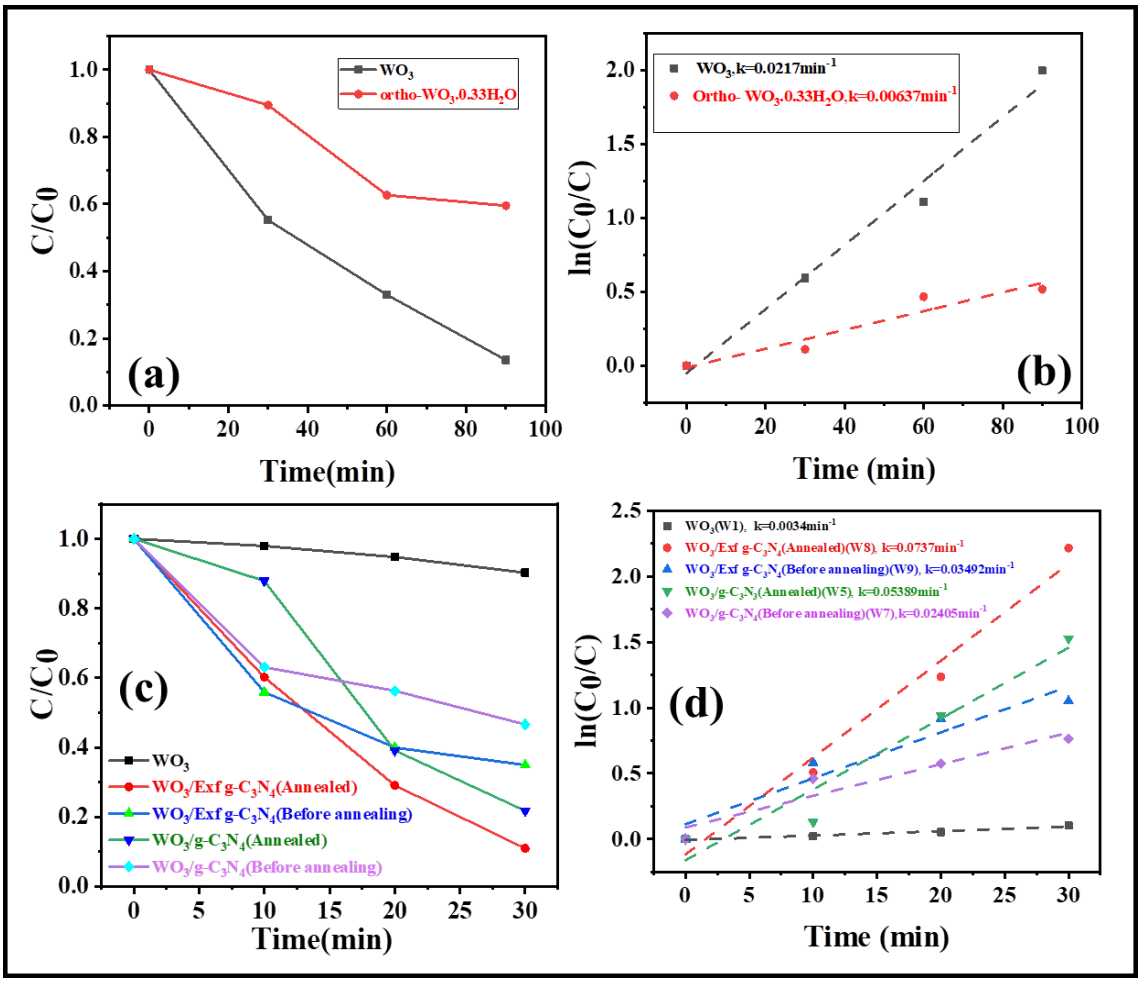

Fig. 5.7: The C/C_0 vs. irradiation time (t) plots (a,c), and the ln(C_0/C) vs. irradiation time (t) plots (b,d) for the pure and composite materials

This plot is also known as the 1st-order rate kinetics plot of materials. The linear fitting of the plot of ln(C_0/C) vs. irradiation time (t) gave the rate constant values from the slope. The corresponding bar graph showing the rate constant values for the samples is presented in Figs. 5.8(a) and 5.8(c).

$$\ln(C_0/C) = k_{app}*t \qquad (5.1)$$

where, C_0 = initial concentration of aqueous Rhodamine B dye,

C = final concentration of aqueous RhB dye and catalyst solution at time 't',

k_{app} = apparent first order kinetics rate constant, and

t = irritation time.

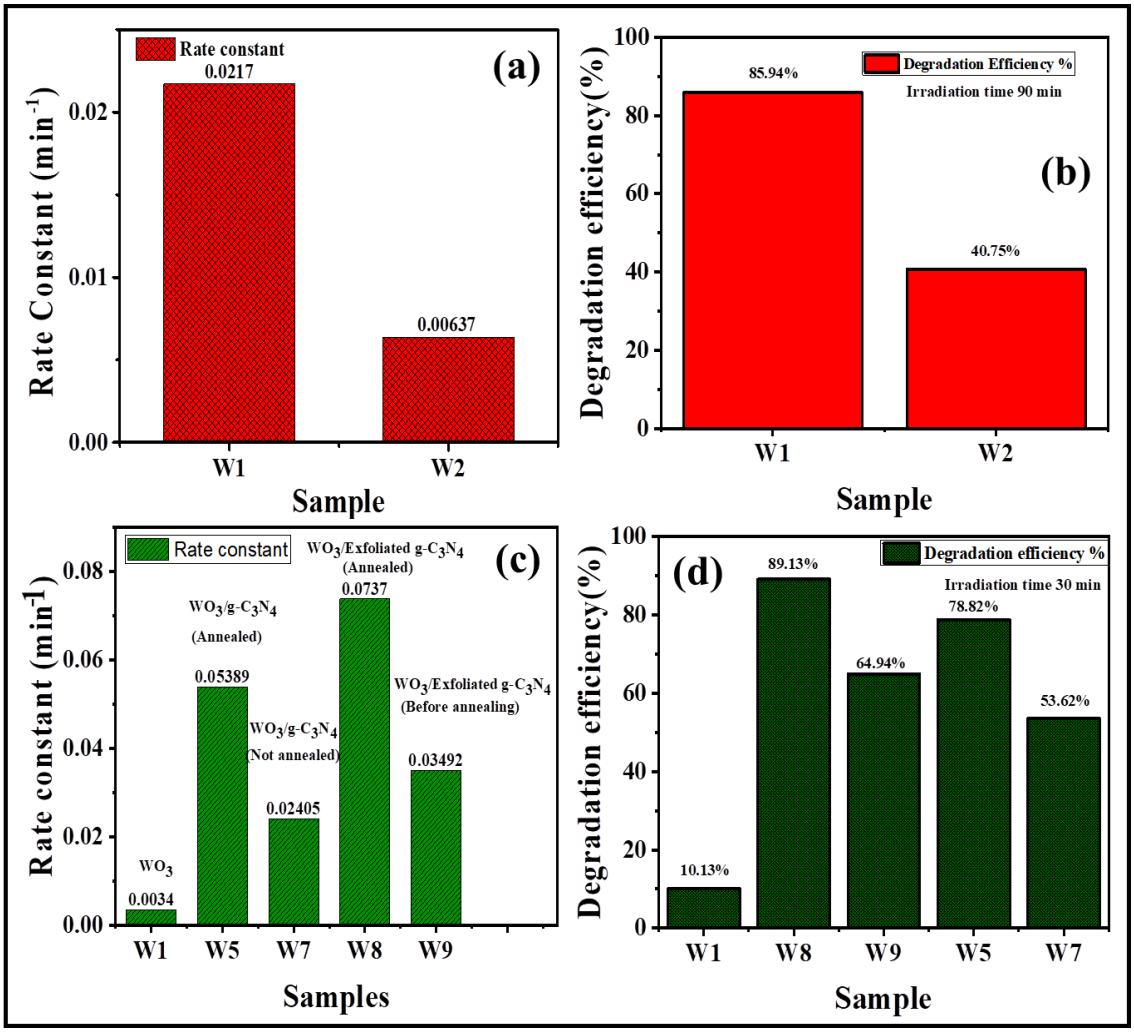

Fig. 5.8: The bar plots of 1st order rate constant (a, c) and the photodegradation efficiency (b, d) for the pure and composite materials

The photodegradation efficiency can be seen from the bar plot Fig. 5.8(b, d), that the pristine WO_3 degrade the RhB dye at an efficiency of 85.94 % which is much higher than the photodegradation efficiency of ortho-hydrated tungsten trioxide (40.75 %). The photodegradation efficiency was calculated by equation:

$$\eta\ \% = \frac{(\eta 0 - \eta t)}{\eta 0} * 100 \qquad (5.2)$$

where, η % = photodegradation efficiency of the photocatalyst,

η0 = initial absorbance of aqueous Rhodamine B dye solution, and

ηt = final absorbance of aqueous RhB dye and catalyst solution at the time 't'.

The photodegradation efficiency of the composite samples can be observed from the bar plot in Fig. 5.8(d). The WO_3/exfoliated g-C_3N_4 after annealing sample was displayed the high photodegradation efficiency about 89.13 % at 30 minutes under visible light irradiations.

5.5.2 Proposed Mechanism

The band gap energy values of g-C_3N_4 and WO_3 are obtained from the calculation of Kubelka-Munk function plot as 2.71 and 2.56 eV respectively. From review of the past work the electronegativity values of g-C_3N_4 and WO_3 are 4.64 and 6.59 eV respectively [11-12]. Therefore, from Mulliken's electronegativity theory,

$$E_{CB} = X_{semiconductor} - E^e - 0.5E_g \qquad (5.3)$$

Where, E_{CB} = conduction band edge potential, E^e = the energy of free electron of hydrogen scale (c.a. 4.5 eV) and E_g = band gap energy of the semiconductor [12].

The conduction band potential of g-C_3N_4 and WO_3 can be calculated as -1.22 and 0.81 eV respectively. As seen in the formula

$E_{CB} = E_{VB} - E_g$ (5.4)

From the valence band potential of g-C_3N_4 and WO_3 can be calculated to be 1.495 and 3.37 eV respectively.

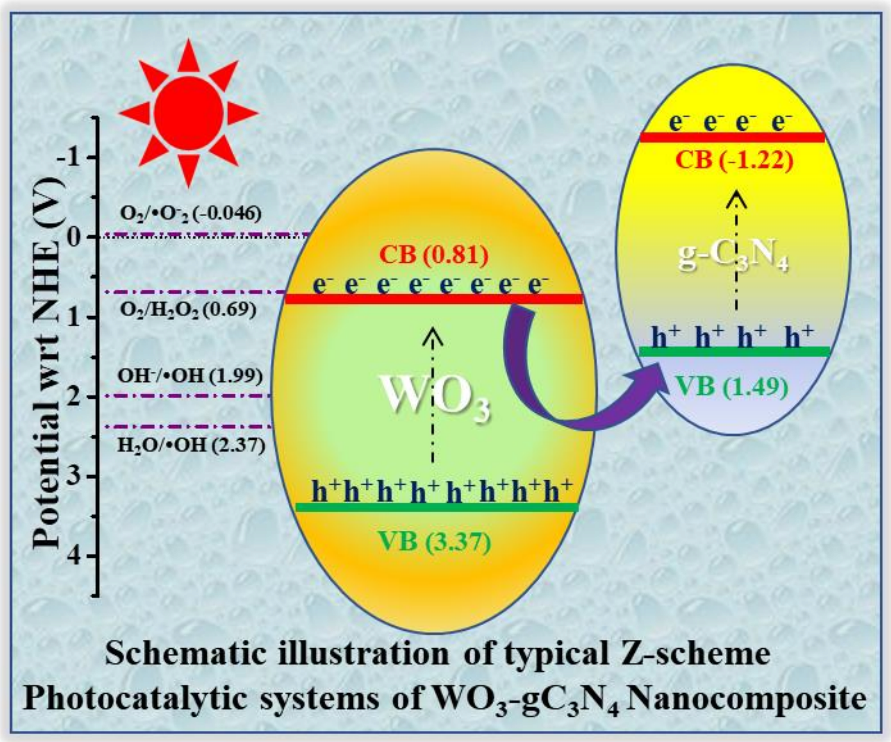

Scheme 5.1: A schematic illustration of typical Z-scheme photocatalysis mechanism of WO_3-gC_3N_4 materials upon visible light exposure

On the basic of the experimental results, the possible Z scheme photocatalytic mechanism for the WO_3/g-C_3N_4 with enhanced photocatalytic activity has been proposed. Generally, both graphitic carbon nitride and tungsten trioxide are excited by irradiation with visible light to generate photogenerated electron-hole pairs in the conduction band and valence band of the semiconductors. After that the photogenerated electrons from the conduction band of tungsten trioxide can quickly recombine with the photogenerated holes from the valence band of graphitic carbon nitride because of the narrow distance between the bands. The photogenerated electron and holes in the conduction band of g-C_3N_4 and the valence band of WO_3 respectively, are left behind which lead to the enhancement of the separation efficiency

of electron hole pairs, which in turn increases the photocatalytic activity of the composite material, and it was an increased efficiency towards the degradation of RhB dye.

5.6 References

1. Deng, S., Yang, Z., Lv, G., Zhu, Y., Li, H., Wang, F. and Zhang, X., 2019. WO_3 nanosheets/g-C_3N_4 nanosheets' nanocomposite as an effective photocatalyst for degradation of rhodamine B. *Applied Physics A*, *125*, 1-11.

2. Huang, L., Xu, H., Li, Y., Li, H., Cheng, X., Xia, J., Xu, Y. and Cai, G., 2013. Visible-light-induced WO_3/g-C_3N_4 composites with enhanced photocatalytic activity. *Dalton Transactions*, *42*(24), 8606-8616.

3. Li, M., Chen, C., Xu, L., Jia, Y., Liu, Y. and Liu, X., 2021. Surface defect-rich ceria quantum dots anchored on sulfur-doped carbon nitride nanotubes with enhanced charge separation for solar hydrogen production. *Journal of Energy Chemistry*, *52*, 51-59.

4. Zhao, Z., Ma, Y., Fan, J., Xue, Y., Chang, H., Masubuchi, Y. and Yin, S., 2018. Synthesis of graphitic carbon nitride from different precursors by fractional thermal polymerization method and their visible light induced photocatalytic activities. *Journal of Alloys and Compounds*, *735*, 1297-1305.

5. Jeevitha, G., Abhinayaa, R., Mangalaraj, D. and Ponpandian, N., 2018. Tungsten oxide-graphene oxide (WO_3-GO) nanocomposite as an efficient photocatalyst, antibacterial and anticancer agent. *Journal of Physics and Chemistry of Solids*, *116*, 137-147.

6. Ragunathan, A., Krishnan, R. and Kamaludeen, B.A., 2015. Stability of tungsten oxide nanoparticles in different media. *Journal of Chemical Research*, *39*(11), 622-626.

7. Feng, J., Chen, T., Liu, S., Zhou, Q., Ren, Y., Lv, Y. and Fan, Z., 2016. Improvement of g-C_3N_4 photocatalytic properties using the Hummers method. *Journal of colloid and interface science*, *479*, 1-6.

8. Niu, P., Zhang, L., Liu, G. and Cheng, H.M., 2012. Graphene-like carbon nitride nanosheets for improved photocatalytic activities. *Advanced Functional Materials*, *22*(22), 4763-4770.

9. Huang, L., Xu, H., Li, Y., Li, H., Cheng, X., Xia, J., Xu, Y. and Cai, G., 2013. Visible-light-induced WO_3/g-C_3N_4 composites with enhanced photocatalytic activity. *Dalton Transactions*, *42*(24), 8606-8616.

10. Sarkar, R., Das, D., Chanda, K., Das, B., Sarkar, S. and Chattopadhyay, K.K., 2022. Hydrothermal synthesis of GO wrapped BiOCl nanosheet and its application in visible light assited catalytic degradation of Rhodamine B dye. *Materials Chemistry and Physics*, *279*, 125796.

11. Praus, P., 2021. On electronegativity of graphitic carbon nitride. *Carbon*, *172*, 729-732.

12. Székely, I., Kedves, E.Z., Pap, Z. and Baia, M., 2021. Synthesis Design of Electronegativity Dependent WO_3 and $WO_3 \cdot 0.33\ H_2O$ Materials for a Better Understanding of TiO_2/WO_3 Composites' Photocatalytic Activity. *Catalysts*, *11*(7), 779.

Chapter 6

Conclusion
&
Scope for future works

6.1 Conclusions

In conclusion, we were able to successfully synthesize tungsten trioxide, ortho hydrated tungsten trioxide, tungsten trioxide/graphitic carbon nitride composite (before and after annealing) and tungsten trioxide/exfoliated graphitic carbon nitride composite (before and after annealing) by hydrothermal method and the structural and optical analysis were efficiently done by sophisticated techniques like PXRD, FTIR, UV-VIS DRS, PL and FESEM. The degradation efficiency of the nanocomposites is significantly better than that of pristine tungsten trioxide. In addition, the photodegradation efficiency of tungsten trioxide/exfoliated graphitic carbon nitride (89.13 %) is higher than that of tungsten trioxide/graphitic carbon nitride (78.82 %). The annealed nanocomposites had higher photodegradation efficiency than their counterparts which are not annealed. Rhodamine B dye, a hazardous organic pollutant, was effectively photodegraded by the nanocomposites in a short period of time assisted by visible light irradiation. The increased degradation efficiency of the nanocomposite in comparison to the pure tungsten trioxide was likewise explained by a feasible mechanism. In this way, the catalyst effectively removes hazardous contaminants from the aquatic ecosystem during waste water treatment.

6.2 Scope for future works

Future research on nanocomposites made of tungsten trioxide (WO_3) and exfoliated graphitic carbon nitride (g-C_3N_4) offers great promise in a number of scientific and technological fields. The unique qualities of both components are combined in this hybrid material, improving performance and enabling multiple uses. WO_3/g-C_3N_4 nanocomposites can be investigated as effective catalysts for electrochemical reactions, such as oxygen reduction and evolution reactions in fuel cells and metal-air batteries, in the field of energy storage and conversion. The interaction between WO_3 and g-C_3N_4 can enhance the stability and kinetics of reactions, hence improving the overall performance of energy devices. Photocatalysis and

environmental remediation are two more potential applications. Since WO_3 and g-C_3N_4 have similar qualities, such as high surface area, tunable bandgaps, and potent light absorption, they are good prospects for effective contaminant degradation, water splitting, and solar fuel production. To increase catalytic efficiency and stability, future study can concentrate on tailoring the nanocomposite's composition, structure, and fabrication processes. Additionally, WO_3/g-C_3N_4 nanocomposites have promising applications in optoelectronics, electronics, and sensors. Gas sensors, photodetectors, and solar cells can all benefit from the addition of exfoliated g-C_3N_4 to WO_3 matrices since it improves the electrical conductivity, charge carrier mobility, and light absorption characteristics. The research on WO_3/exfoliated g-C_3N_4 nanocomposites in the future needs to focus on sophisticated synthesis methods, in-depth characterisation, and systematic studies on their performance in diverse applications. Researchers can create unique functional nanocomposites with increased efficiency and enhance energy, environmental, and electronic technologies by taking advantage of the synergistic properties of these materials.